ISSN 0280–5316
ISRN LUTFD2/TFRT--5629--SE

Modelling of Two-Phase Flows with Modelica™

Olaf Bauer

Department of Automatic Control
Lund Institute of Technology
November 1999

Department of Automatic Control
Lund Institute of Technology
Box 118
SE-221 00 Lund Sweden

Document name
MASTER THESIS

Date of issue
November 1999

Document Number
ISRN LUTFD2/TFRT--5629--SE

Author(s)
Olaf Bauer

Supervisor
H. Tummescheit, A. Jakobsen, J. Fredsted and N. Pettit

Sponsoring organisation

Title and subtitle
Modelling of Two-Phase Flows with Modelica-TM. (Modellering av två-fas flöden med Modelica-TM.)

Abstract

Modelica-TM is an object-oriented language for modeling physical systems that was designed in the last years with the goal to become a standardized multi-domain modeling language. This paper describes a robust model for homogeneous and inhomogeneous two phase flows with dynamic or static slip correlation. It was developed in the context of developing a Modelica base library for thermo-hydraulic applications. The model describes the transient behavior of a fluid moving through a pipe during a phase change caused by heat transfer or pressure changes. Measurements from a refrigeration cycle were used to validate the model. Physical approaches were taken to model friction and momentum exchange between the phases. Spezialized thermodynamic equations of state were developed in order to improve the simulation speed. The model also includes the one-phase flow of liquid or vapor as limiting cases in order to make the simulation of a complete phase-transition possible. The model is numerically robust in all flow regions. Modelica's language features are used to structure the code for reusability in different contexts. These features make the model well suited for a reusable model library.

Key words

Classification system and/or index terms (if any)

Supplementary bibliographical information

ISSN and key title
0280–5316

ISBN

Language
English

Number of pages
100

Recipient's notes

Security classification

Contents

List of Figures

Nomenclature

Symbol	Unit	Physical Meaning
a, b, c		thermodynamic property
a	m/s	velocity of sound
A	m^2	surface area
b		coefficient
c	J/(kgK)	specific heat capacity
$\tilde{c}$	J/(kgK)	limiting value of c
C	–	constant
D	m	diameter
e	J/kg	specific energy
$\boldsymbol{e}$	–	unit vector
E	J	energy
f	J/kg	specific free energy
F	N	axial force
$\boldsymbol{F}$	N	force vector
g	J/kg	specific free enthalpy
$\boldsymbol{g}$	m/s^2	acceleration due to gravity vector
G	$kg/(m^2s)$	mass velocity
h	J/kg	specific enthalpy
$\dot{H}$	J/s	enthalpy flux
i	–	counter
I	kgm/s	axial momentum
$\dot{I}$	kgm/s^2	axial momentum flux
$\boldsymbol{I}$	kgm/s	momentum vector
J		Jacobian matrix
k		correction factor
L	m	length
$\dot{m}$	kg/s	mass flow rate
M	kg	mass
M	kg/kmol	molecular weight
n	–	number of cells
$\boldsymbol{n}$	–	unit normal vector
p	Pa	pressure
P	W	power
$\dot{\boldsymbol{q}}$	J/m^2s	specific heat flux vector
$\dot{Q}$	J/s	heat flux
R	m	radius of curvature
s	J/(kgK)	specific entropy
S	(m/s)/(m/s)	slip ratio
t	s	time
$\boldsymbol{t}$	–	unit tangential vector
T	K	temperature
T	N/m^2	stress tensor
u	J/kg	specific internal energy
U	J	internal energy
v	m^3/kg	specific volume
V	m^3	volume

w	m/s	axial velocity
$\boldsymbol{w}$	m/s	velocity vector
W	Nm	work
x, y		independent variables
x	kg/kg	quality
$\dot{x}$	(kg/s)/(kg/s)	flow quality
z	m	axial position
$\boldsymbol{z}$	m	position vector

Greek Letters

α	$\mathrm{W/(m^2K)}$	heat transfer coefficient
β		thermodynamic property
γ	$\mathrm{m^2/m^2}$	void fraction
δ	–	indicator function or weight factor
δ	m	thickness
ε	N/N	fraction of acceleration force shared by the vapour phase
ζ	–	interfacial friction factor
ζ^*	–	$\zeta A_{int}/A_w$
η	Pa s	dynamic viscosity
κ	$\mathrm{m^2/m^2}$	specific surface area
λ	W/mK	thermal conductivity
μ	$\mathrm{kg/(m^2s)}$	mass velocity through a moving interface
ν	$\mathrm{kg/(m^2s)}$	$\dot{m}_{int}/A$
ξ	–	friction factor
ρ	$\mathrm{kg/m^3}$	density
σ	N/m	surface tension
τ	$\mathrm{N/m^2}$	shear stress
Φ	–	two-phase multiplier
ϕ		function
φ		angle between $\boldsymbol{g}$ and $\boldsymbol{e}_z$
Ψ		quantity of state
ψ		specific quantity of state
$\hat{\psi}$		specific quantity of state between two control volumes

Subscripts

1	inlet
2	outlet
A	surface
C_2H_6O	ethanol
c	condenser
$corr$	correction
$evap$	evaporation
ext	external
f	fluid

g	gravity
H_2O	water
i	counter, room coordinate
in	inlet
int	phase interface, internal
j	counter, room coordinate
p	pressure, isobaric
kin	kinetic
out	outlet
ref	reference
sat	saturation
τ	friction
th	theoretical
v	isochoric
w	wall
z	axial component

Subscripts are also used to denote partial derivatives

Superscripts

$'$	liquid
$''$	vapour

Dimensionless Numbers

Fr	$w^2/(gD)$	Froude number
Nu	$\alpha D/\lambda$	Nusselt number
Pr	$\eta c_p/\lambda$	Prandtl number
Re	$\rho w D/\eta$	Reynolds number
We	$\rho w^2 D/\sigma$	Weber number

Operators

Δ	difference
d	total differential
∂	partial differential
det	determinant
div	divergence
!	factorial function

1. Introduction

A mathematical model for one-component two-phase flows is developed for the simulation of evaporators and condensers in refrigeration cycles. Since the refrigerant undergoes a complete phase transition, the model has to include one-phase flows as a limiting case. Due to the on/off control strategy commonly applied to refrigerators, the resulting process is dominated by transient phenomena. As simulations of refrigerant evaporators show [1], the accuracy of a two-phase flow model in a transient process depends on the modelling detail of the hydrodynamic behaviour of liquid and vapour.

The most simple approach is to define average properties and utilize the model equations for one-phase flows. This approach is, however, restricted to homogeneous flows, which in any case is a simplifying assumption that is justified when one phase is dispersed within the other, i.e. as tiny drops or bubbles. Otherwise a spatial separation of the phases occurs, especially in horizontal pipes. For a given pressure gradient, the velocity of the vapour is, due to its low density and viscosity, higher than the velocity of the liquid.

The homogeneous model can be derived from the physical principles of the conservation of mass, momentum and energy. Considering the actual heterogeneity requires an additional equation to determine the velocity difference. Empirical correlations are available, but a heterogeneous model can also be obtained from separate momentum balances for each phase. The latter approach provides more physical relevance, but contains the difficulty of predicting friction and momentum exchange between the phases, which will be attempted within this thesis

The model is implemented in the object-oriented programming language **Modelica** and to become a part of a thermohydraulic model library. Refrigerant properties can be computed from the NIST REFPROP library, but simple equations of state will be developed to minimize the computation time. For evaluation of the model, the simulation environment **Dymola** is used, which contains algorithms for integration of ordinary differential equations over the time. To account for the spatial distribution of the properties of the flow, the model equations have to be discretized. Simulation results will be compared with measurement data from a refrigeration test plant at Danfoss, Denmark.

2. Balance Equations

2.1 Quantities of State

The thermodynamic state of a fluid particle can be described by the infinitesimal quantities of volume dV, mass dM, momentum $d\boldsymbol{I}$ and energy dE. It is more common to use specific variables, representing a quantity $d\Psi$ per unit mass

$$\psi = \frac{d\Psi}{dM} \tag{2.1}$$

The specific values of volume, momentum and energy are therefore

$$v = \frac{dV}{dM} \qquad \boldsymbol{w} = \frac{d\boldsymbol{I}}{dM} \qquad e = \frac{dE}{dM} \tag{2.2}$$

where $\boldsymbol{w}$ is the velocity of the fluid. The reciprocal value of the specific volume is known as the density

$$\rho = \frac{1}{v} = \frac{dM}{dV} \tag{2.3}$$

The energy dE may be split up into internal and kinetic energy

$$dE = dU + dE_{kin} \tag{2.4}$$

which gives two more specific values

$$u = \frac{dU}{dM} \qquad e_{kin} = \frac{|\boldsymbol{w}|^2}{2} \tag{2.5}$$

where u quantifies the mechanical energy of the molecules in a motionless fluid. The overall specific energy becomes

$$e = u + e_{kin} \tag{2.6}$$

A potential energy is not declared; the related quantity will be considered as the work of the gravitational field.

2.2 Balance Equations

Integration over the infinitesimal values $d\Psi$ yields the overall quantity Ψ

$$\Psi = \int d\Psi = \int_M \psi dM = \int_V \rho\psi dV \tag{2.7}$$

The rate of change of a quantity is formally written as

$$\frac{d\Psi}{dt} = \frac{d}{dt}\int_V \rho\psi \, dV \tag{2.8}$$

Application of the Leibnitz rule [7] yields

$$\frac{d\Psi}{dt} = \int_V \frac{\partial(\rho\psi)}{\partial t} \, dV + \int_A \rho\psi \boldsymbol{w}_A \boldsymbol{n} \, dA \tag{2.9}$$

The first term on the right hand side represents the rate of change of a quantity Ψ for a control volume keeping its shape; the derivative operator can thus be put under the integral. The second term accounts for the rate of change of Ψ due to a displacement of the volumes' surface A. Therein, $\boldsymbol{w}_A$ denotes the local velocity of surface displacement, while $\boldsymbol{n}$ is the unit normal vector of the surface (outward direction is positive). The scalar product $\boldsymbol{w}_A\boldsymbol{n}$ yields the component of $\boldsymbol{w}_A$ normal to the surface, fig. 2.1.

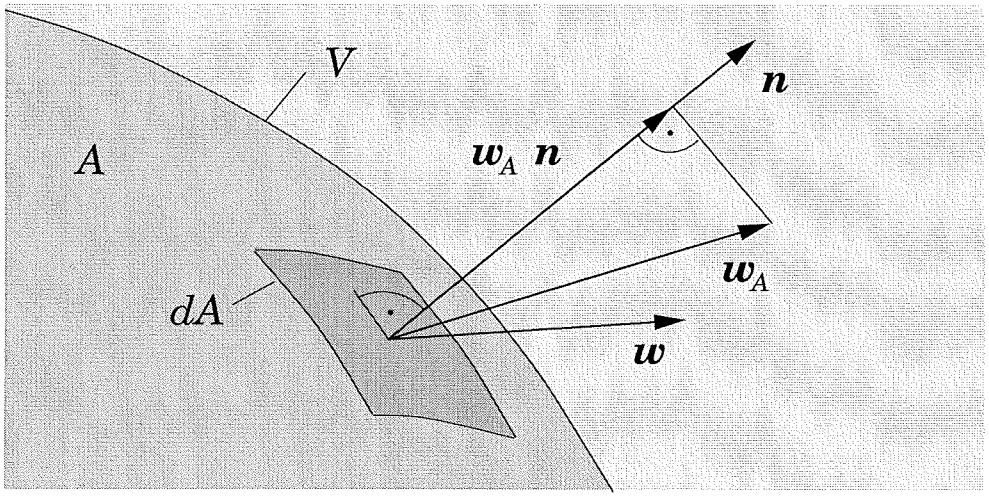

Figure 2.1 Velocities on a surface element

The influence of the second term becomes obvious when inserting $\psi = v$, which gives the rate of change of volume

$$\frac{dV}{dt} = \int_A \boldsymbol{w}_A \boldsymbol{n} \, dA \tag{2.10}$$

The Leibnitz rule serves to switch between different approaches of balancing: In an Eulerian approach, the control volume is considered as fixed, $\boldsymbol{w}_A = 0$, and the second term in eq. (2.9) disappears. In a Lagrangian approach, the surface velocity equals the velocity of the fluid particles on the surface, $\boldsymbol{w}_A = \boldsymbol{w}$; in that case no particle enters or leaves the control volume, which therefore contains permanently the same particles. Besides these two approaches, $\boldsymbol{w}_A$ may be defined in any appropriate way.

The Leibnitz rule will now be applied to the quantities mass, momentum and energy, leading to the basic balance equations.

Mass Balance

For $\psi = 1$ the Leibnitz rule eq. (2.9) yields the derivative of mass

$$\frac{dM}{dt} = \int_V \frac{\partial \rho}{\partial t}\, dV + \int_A \rho \boldsymbol{w}_A \boldsymbol{n}\, dA \tag{2.11}$$

In a Lagrangian approach, $\boldsymbol{w}_A = \boldsymbol{w}$, the control volume contains a constant mass, thus

$$\int_V \frac{\partial \rho}{\partial t}\, dV + \int_A \rho \boldsymbol{w} \boldsymbol{n}\, dA = 0 \tag{2.12}$$

which essentially describes the conservation of mass and is also known as the continuity equation. Solving this equation for the first term and inserting it into eq. (2.11) gives

$$\frac{dM}{dt} = \int_A \rho(\boldsymbol{w}_A - \boldsymbol{w})\boldsymbol{n}\, dA \tag{2.13}$$

Since no mass is created or destroyed, the term on the right hand side represents the flow of mass through the surface of the control volume, i.e. the mass flow rate

$$\dot{m} := \int_A \rho(\boldsymbol{w}_A - \boldsymbol{w})\boldsymbol{n}\, dA \tag{2.14}$$

which, in this definition, is positive for a flow of mass into the control volume.

Momentum Balance

The Leibnitz rule, eq. (2.9), evaluated for $\psi = \boldsymbol{w}$, yields the derivative of momentum

$$\frac{d\boldsymbol{I}}{dt} = \int_V \frac{\partial(\rho \boldsymbol{w})}{\partial t}\, dV + \int_A \rho \boldsymbol{w}(\boldsymbol{w}_A \boldsymbol{n})\, dA \tag{2.15}$$

According to Newton's second law, the momentum of a constant mass ($\boldsymbol{w}_A = \boldsymbol{w}$) increases due to the applied forces

$$\int_V \frac{\partial(\rho \boldsymbol{w})}{\partial t}\, dV + \int_A \rho \boldsymbol{w}(\boldsymbol{w}\boldsymbol{n})\, dA = \sum \boldsymbol{F} \tag{2.16}$$

It is common to distinguish between body forces and surface forces. If gravity is the only body force present, the force on a mass dM becomes $d\boldsymbol{F}_g = \boldsymbol{g} dM$, where $\boldsymbol{g}$ is the vector of the acceleration due to gravity, which is constant. Integration yields the overall gravity force

$$\boldsymbol{F}_g = \int_V \rho \boldsymbol{g}\, dV = M\boldsymbol{g} \tag{2.17}$$

The surface forces are usually split up into the pressure force and the friction force. The pressure force acts opposite to the unit normal vector, $d\boldsymbol{F}_p = -p\boldsymbol{n}dA$, causing an overall force on the surface of an amount

$$\boldsymbol{F}_p = -\int_A p\boldsymbol{n}\, dA \tag{2.18}$$

The friction force of an infinitesimal small element, caused by viscous and turbulent forces, is expressed by use of a stress tensor

$$\mathsf{T} = \begin{pmatrix} \tau_{11} & \tau_{21} & \tau_{31} \\ \tau_{12} & \tau_{22} & \tau_{32} \\ \tau_{13} & \tau_{23} & \tau_{33} \end{pmatrix} \tag{2.19}$$

where $1, 2, 3$ are the room coordinates and τ_{ji} denotes the shear stress in direction of i on a surface j = const. Multiplication with the unit normal vector $\boldsymbol{n}$ yields the stress force vector on a surface element, $d\boldsymbol{F}_\tau = \mathsf{T}\boldsymbol{n}dA$. Integration gives

$$\boldsymbol{F}_\tau = \int_A \mathsf{T}\boldsymbol{n}\, dA = \int_A \sum_{i,j} \tau_{ji}(\boldsymbol{n}\boldsymbol{e}_j)\boldsymbol{e}_i\, dA \tag{2.20}$$

where $\boldsymbol{e}_i$ is the unit vector in direction of i. Pressure and friction forces are also present inside the volume, but cancel themselves out and thus have no influence on the momentum of the control volume as a whole. Solving eq. (2.16) for the first term and inserting it into eq. (2.15) yields

$$\frac{d\boldsymbol{I}}{dt} = \int_A \rho\boldsymbol{w}(\boldsymbol{w}_A - \boldsymbol{w})\boldsymbol{n}\, dA + \boldsymbol{F}_g + \boldsymbol{F}_p + \boldsymbol{F}_\tau \tag{2.21}$$

The first term on the right hand side accounts for the convective transport of momentum.

Energy Balance

Applying the Leibnitz rule eq. (2.9) with $\psi = e$ yields the rate of change of energy

$$\frac{dE}{dt} = \int_V \frac{\partial(\rho e)}{\partial t}\, dV + \int_A \rho e\boldsymbol{w}_A\boldsymbol{n}\, dA \tag{2.22}$$

The energy of a closed system ($\boldsymbol{w}_A = \boldsymbol{w}$) is, according to the first law of thermodynamics, increased only by an addition of heat and work. If $\dot{Q}$ denotes the heat flux and P denotes the power, this gives

$$\int_V \frac{\partial(\rho e)}{\partial t}\, dV + \int_A \rho e\boldsymbol{w}\boldsymbol{n}\, dA = \sum P + \dot{Q} \tag{2.23}$$

The power P is the integral of the local power dP, which is the local work per unit time $dP = dW/dt$. The work results from the movement of a particle

along a line $d\boldsymbol{z}$, caused by a force $d\boldsymbol{F}$ attacking on the particle. The work is the component of the force in direction of the movement times the length, i.e. the scalar product $dW = d\boldsymbol{F}d\boldsymbol{z}$. The quotient of $d\boldsymbol{z}$ and time dt is the flow velocity vector $\boldsymbol{w}$, thus

$$P = \int dP = \int \frac{dW}{dt} = \int \frac{d\boldsymbol{F}d\boldsymbol{z}}{dt} = \int \boldsymbol{w}d\boldsymbol{F} \tag{2.24}$$

Inserting the forces introduced in the previous section yields

$$P_g = \int_V \rho \boldsymbol{g}\boldsymbol{w}\, dV \tag{2.25}$$

$$P_p = -\int_A p\boldsymbol{w}\boldsymbol{n}\, dA \tag{2.26}$$

$$P_\tau = \int_A \mathbf{T}\boldsymbol{w}\boldsymbol{n}\, dA \tag{2.27}$$

When solving eq. (2.23) for the first term and inserting it into eq. (2.22) one obtains

$$\frac{dE}{dt} = \int_A \rho e(\boldsymbol{w}_A - \boldsymbol{w})\boldsymbol{n}\, dA + P_g + P_p + P_\tau + \dot{Q} \tag{2.28}$$

where the first term on the right hand side quantifies the convective transport of energy.

In chapter 4 the equations derived here will be applied to the two-phase flow in a pipe. The variables to be used for that purpose will be presented in the next chapter.

3. State Variables for Two-Phase Flow

3.1 Extensive Quantities of State

Specific Quantities of State

Contrary to a mixture of gases, a liquid-vapour mixture does not form a continuum. The phases are separated from each other by an interface. A local specific quantity of state $\psi = d\Psi/dM$, e.g.

$$\psi = v, \boldsymbol{w}, u, e, ... \tag{3.1}$$

may therefore be expressed as

$$\psi = \delta\psi'' + (1-\delta)\psi' \tag{3.2}$$

where δ is an indicator function, denoting the phase present

$$\delta = \begin{cases} 0 & \text{liquid} \\ 1 & \text{vapour} \end{cases} \tag{3.3}$$

while ψ'' and ψ' are the the specific quantities of vapour and liquid, respectively.

Overall Quantities of State

The overall quantity of state Ψ of a control volume containing liquid and vapour fractions is obtained from an integration similar to eq. (2.7)

$$\Psi = \int_M \psi \, dM = \int_M \left[\delta\psi'' + (1-\delta)\psi'\right] \, dM \tag{3.4}$$

The indicator function can be eliminated by integrating separately over each phase and then summing up. With $\delta = 0$ in the liquid phase and $\delta = 1$ in the vapour phase we find

$$\Psi = \int_{M''} \psi'' \, dM + \int_{M'} \psi' \, dM \tag{3.5}$$

Replacing the mass with $dM = \rho dV$ in each phase yields

$$\Psi = \int_{V''} \rho''\psi'' \, dV + \int_{V'} \rho'\psi' \, dV \tag{3.6}$$

The terms on the right hand side of eq. (3.5) and eq. (3.6) represent the overall quantities of state of vapour Ψ'' and liquid Ψ', thus

$$\Psi = \Psi'' + \Psi' \tag{3.7}$$

Average Quantities of State

The average specific quantity is defined analogously to the local specific quantity. It is defined for each phase separately and for the control volume as a whole

$$\psi := \frac{\Psi}{M} \qquad \psi'' := \frac{\Psi''}{M''} \qquad \psi' := \frac{\Psi'}{M'} \tag{3.8}$$

This definition has the advantage that an overall quantity Ψ can be expressed as a product of the average specific quantity and the average density, $\Psi = \rho\psi V$. Inserting the equations above into eq. (3.7) gives

$$\psi M = \psi'' M'' + \psi' M' \tag{3.9}$$

Division by $M = M'' + M'$ yields

$$\psi = x\psi'' + (1 - x)\psi' \tag{3.10}$$

where x is the quality

$$x := \frac{M''}{M'' + M'} \tag{3.11}$$

In eq. (3.9) the masses may be replaced by $M = \rho V$

$$\rho\psi V = \rho''\psi''V'' + \rho'\psi'V' \tag{3.12}$$

division by $V = V'' + V'$ yields

$$\rho\psi = \gamma\rho''\psi'' + (1 - \gamma)\rho'\psi' \tag{3.13}$$

where the void fraction γ has been used

$$\gamma := \frac{V''}{V'' + V'} \tag{3.14}$$

If the control volume reduces to an area, the void fraction becomes

$$\gamma \rightarrow \frac{A''}{A'' + A'} \tag{3.15}$$

The quantities $\gamma\rho''$ and $(1-\gamma)\rho'$ in eq. (3.13) are the partial densities of vapour and liquid respectively. Comparison of eq. (3.13) and eq. (3.10) shows

$$\gamma\rho'' = x\rho \qquad (1 - \gamma)\rho' = (1 - x)\rho \tag{3.16}$$

From the two equivalent definitions eq. (3.10) and eq. (3.13) various average variables may be derived. The ones needed in this thesis are in terms of the void fraction

$$\rho = \gamma\rho'' + (1-\gamma)\rho' \tag{3.17}$$
$$\rho w = \gamma\rho''w'' + (1-\gamma)\rho'w' \tag{3.18}$$

and in terms of the quality

$$v = xv'' + (1-x)v' \tag{3.19}$$
$$u = xu'' + (1-x)u' \tag{3.20}$$
$$h = xh'' + (1-x)h' \tag{3.21}$$
$$w = xw'' + (1-x)w' \tag{3.22}$$

where h denotes the enthalpy, defined for each phase (and as an overall average quantity in case of equal pressures, $p' = p''$) by

$$h := u + \frac{p}{\rho} \tag{3.23}$$

and w denotes the axial component of the average velocity

$$w := \boldsymbol{w}\boldsymbol{e}_z \tag{3.24}$$

The averageing process described above is only applicable to extensive quantities. Average intensive quantities, such as pressure and temperature, must be defined in a different way.

3.2 Thermodynamic State

In a one-component one-phase fluid, two independent thermodynamic properties determine the thermodynamic state. If pressure p and temperature T are used as independent variables, internal energy and density can be expressed as follows

$$\begin{aligned} \rho &= \rho(p,T) \\ u &= u(p,T) \end{aligned} \tag{3.25}$$

These dependencies are usually obtained from measurements and then implemented into an algebraic equation of state. Such an equation is only locally valid, but will, for simplicity, also be applied to the average values of ρ and u. Eq. (3.25) thus implicitly defines the average pressure and temperature.

In a one-component two-phase fluid, the average values of ρ and u may in each phase be computed from an equation of state

$$\rho'' = \rho''(p'',T'') \qquad \rho' = \rho'(p',T') \tag{3.26}$$
$$u'' = u''(p'',T'') \qquad u' = u'(p',T') \tag{3.27}$$

which implies, that vapour and liquid may have different (average) pressures and temperatures. The difference in each case is, at least close to the interface, negligibly small. The interface itself is in state of equilibrium.

Equilibrium Properties

In the exceptional case of thermal, mechanical and chemical equilibrium, temperature, pressure and specific free enthalpy of both phase are in each case equal[1]

$$\begin{aligned} T &= T' = T'' \\ p &= p' = p'' \\ g &= g' = g'' \end{aligned} \tag{3.28}$$

Since g itself is determined by T and p, only one parameter among these three can be varied independently. This implies, that the temperature is determined by the pressure

$$T = T_{sat}(p) \tag{3.29}$$

which is known as the saturation temperature. As a result, the specific quantities of each phase are functions of the pressure only

$$\rho'' = \rho''(p) \qquad \rho' = \rho'(p) \tag{3.30}$$

$$u'' = u''(p) \qquad u' = u'(p) \tag{3.31}$$

The average overall density and internal energy can then be computed from eq. (3.19) and eq. (3.20). Apart from the pressure, only the quality x remains as the second independent parameter. Since x provides non-trivial information only in the two-phase region, it is not applicable to the one-phase region. A couple of independent variables that can be used in both regions of state is, for example, pressure and enthalpy. In the two-phase region, the quality is then obtained from eq. (3.21)

$$x = \frac{h - h'(p)}{h''(p) - h'(p)} \tag{3.32}$$

Thus p and h determine the equilibrium thermodynamic state in both regions of state. They will be used as independent variables in this thesis.

Non-equilibrium Properties

If the equilibrium conditions eq. (3.28) were skipped, each phase would maintain its own dependency on two independent variables and may achieve a metastable state. The equilibrium conditions, however, would have to be imposed upon the system as tendencies, to make sure that equilibrium is reached

[1] It should be noted, that mechanical equilibrium does not necessarily imply equal pressures. As shown in section 4.2 this is only true for a planar phase interface and the absence of mass transfer over the interface.

when external influences are removed. This leads to the complex task of determination of the heat and mass transfer between the phases. The related transfer coefficients as well as the shape and movement of the interface would have to be described. The resulting equations then replace the ideal assumptions made in eq. (3.28).

In small control volumes with relatively slow changes of pressure any deviation from equilibrium is almost instantly achieved, compared to the transport of heat and mass over its surface. For a control volume less than 1 m^3 the assumption of equilibrium is justified for pressure changes slower than 10 bar/s [10]. The processes studied in this thesis are restricted to control volumes of less then 10^{-3} m^3, and the maximum speed of pressure changes is about 0.5 bar/s, which is clearly within the limits. Hence there is no need to include non-equilibrium effects.

3.3 Hydrodynamic State

The mass flow rate through a surface has, most generally, been defined in eq. (3.18). In a cross-section of a pipe the unit normal vector $\boldsymbol{n}$ is in the direction of the axial unit vector $\boldsymbol{e}_z$. The mass flow rate will be defined positive in direction of $\boldsymbol{e}_z$. For a fixed cross-section ($\boldsymbol{w}_A = 0$) this gives

$$\dot{m} := \int_A \rho \boldsymbol{w} \boldsymbol{e}_z \, dA = \int_A \rho w \, dA = \rho w A \tag{3.33}$$

where ρw inside the integral is the local axial mass velocity G, while in the last term it stands for the average value of G, which, due to the definition of average values made in section 3.1, equals the product of average density and average velocity.

The mass flow rate can be resolved into the vapour and liquid fractions by multiplication of eq. (3.18) with A, which gives

$$\dot{m} = \dot{m}'' + \dot{m}' \tag{3.34}$$

where the vapour and liquid mass flow rates are

$$\dot{m}'' = \gamma \rho'' w'' A \tag{3.35}$$

$$\dot{m}' = (1 - \gamma) \rho' w' A \tag{3.36}$$

and γ is the void fraction in a cross-sectional area, eq. (3.15). In a stratified flow, the above relations are also obtained from a geometrical consideration, fig. 3.1.

The stratified flow is a special case among several flow regimes that occur in a horizontal heated pipe [2]. We will not consider these in detail, but distinguish only between dispersed flow (bubble and spray flow) and separated flow (stratified and annular flow). This distinction is roughly related to the distinction between homogeneous and heterogeneous flow.

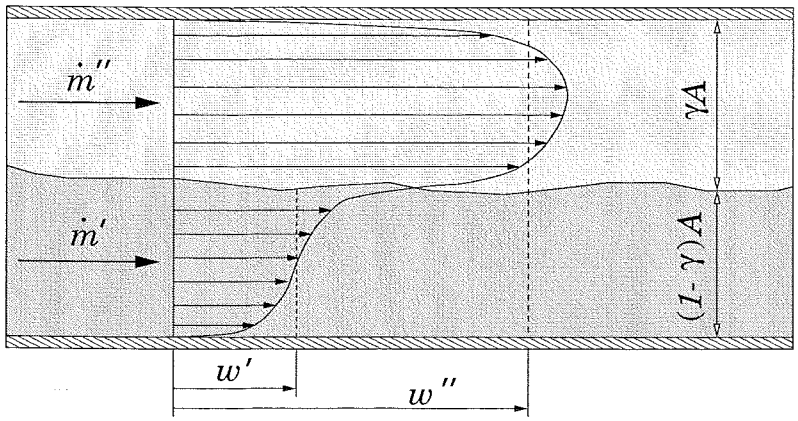

Figure 3.1 Stratified two-phase flow

Homogeneous Flow

Following the pattern of the conditions of thermodynamic equilibrium, which gave $T'' = T'$ and $p'' = p'$, one might assume an equality of vapour and liquid velocities $w = w'' = w'$. Eq. (3.35) and eq. (3.36) then become

$$\dot{m}'' = \gamma \rho'' w A \tag{3.37}$$
$$\dot{m}' = (1-\gamma)\rho' w A \tag{3.38}$$

Substitution of the partial densities with the quality from eq. (3.16) gives

$$\dot{m}'' = x\dot{m} \tag{3.39}$$
$$\dot{m}' = (1-x)\dot{m} \tag{3.40}$$

Thus, the quality x determines the partition of the mass flow rate into its vapour and liquid fractions. This simple relation between thermodynamic and hydrodynamic properties is, however, only applicable to homogeneous flows, e.g. in dispersed flows, where a particle of the distributed phase is entirely surrounded by particles of the continuous phase. In that case, the interfacial friction will almost equalise the velocities.

Heterogeneous Flow

In a separated flow, the interfacial friction equalises the velocities at the interface, but barely affects the average velocity of each phase, fig. 3.1. A considerable difference of the average velocities occurs, which is often expressed in terms of the slip ratio S

$$S := \frac{w''}{w'} \tag{3.41}$$

Due to the low density and viscosity of the vapour, its average velocity is usually higher than the average liquid velocity. In technical applications S is in the range [10]

$$1 \leq S \leq \sqrt{\frac{\rho'}{\rho''}} \tag{3.42}$$

Since (for pressures below the critical point) $\rho' \gg \rho''$ the velocity difference cannot be neglected. The mass flow rate of each phase must therefore be computed from eq. (3.35) and eq. (3.36) and summed up to obtain the overall mass flow rate. Similar to the quality eq. (3.11) a vapour mass flow ratio can be defined

$$\dot{x} := \frac{\dot{m}''}{\dot{m}'' + \dot{m}'} \tag{3.43}$$

which will be called the flow quality. Insertion of eq. (3.35) and eq. (3.36) gives

$$\dot{x} = \frac{\gamma\rho''w''}{\gamma\rho''w'' + (1-\gamma)\rho'w'} \tag{3.44}$$

For $w'' = w'$ the velocities can be cancelled down and eq. (3.44) turns to eq. (3.16), thus $\dot{x} = x$. Using the flow quality in the case when vapour and liquid have the same mass flow rates, but different flow directions, results in a division by zero singularity. The slip ratio S causes a similar problem for a vapour flow over motionless liquid. For that reason, the velocity difference

$$\Delta w := w'' - w' \tag{3.45}$$

will be used as a characteristic variable in this thesis, when computational problems are likely to occur for S and $\dot{x}$. From eq. (3.22) the velocity of each phase can be written in terms of the velocity difference and the average velocity

$$w'' = w + (1-x)\Delta w \tag{3.46}$$
$$w' = w - x\Delta w \tag{3.47}$$

Inserting this into eq. (3.35) and eq. (3.36) and using eq. (3.16) gives

$$\dot{m}'' = x\dot{m} + \dot{m}_{corr} \tag{3.48}$$
$$\dot{m}' = (1-x)\dot{m} - \dot{m}_{corr} \tag{3.49}$$

with a correction mass flow rate

$$\dot{m}_{corr} = x(1-x)\rho\Delta wA \tag{3.50}$$

Division of eq. (3.48) by $\dot{m}$ yields a relation between the flow quality and the quality

$$\dot{x} = x + x(1-x)\frac{\Delta w}{w} \tag{3.51}$$

When compared to the homogeneous model, eq. (3.48) and eq. (3.49) reveal the influence of the velocity difference on the mass flow distribution: For a given quality, the vapour mass flow rate is increased by an amount of $\dot{m}_{corr}$ on the cost of the liquid mass flow rate.

A second interpretation of $\dot{m}_{corr}$ is obtained from the point of view of an observer moving at average velocity w: The relative velocities are then $w''-w = (1-x)\Delta w$ for the vapour and $w'-w = -x\Delta w$ for the liquid. The related mass flow rates are $\gamma\rho''(1-x)\Delta wA$ and $-(1-\gamma)\rho' x\Delta wA$. Application of eq. (3.16) shows that both phases have the same mass flow rate $\dot{m}_{corr}$, but opposite flow directions (see also fig. 6.4 on page 43).

4. One-Dimensional Two-Phase Flow

The balance equations derived in chapter 2 will now be applied to a fixed segment of a pipe with constant diameter containing liquid and vapour fractions of a pure fluid, fig. 4.1. The surface integrals are resolved into the ones for inlet A_1, outlet A_2 and wall A_w. Due to friction, the fluid particles adhere at the wall; the fluid velocity is thus $\boldsymbol{w} = 0$ in the integrals over the wall area. Since the pipe does not move, the velocity of the surface displacement is $\boldsymbol{w}_A = 0$.

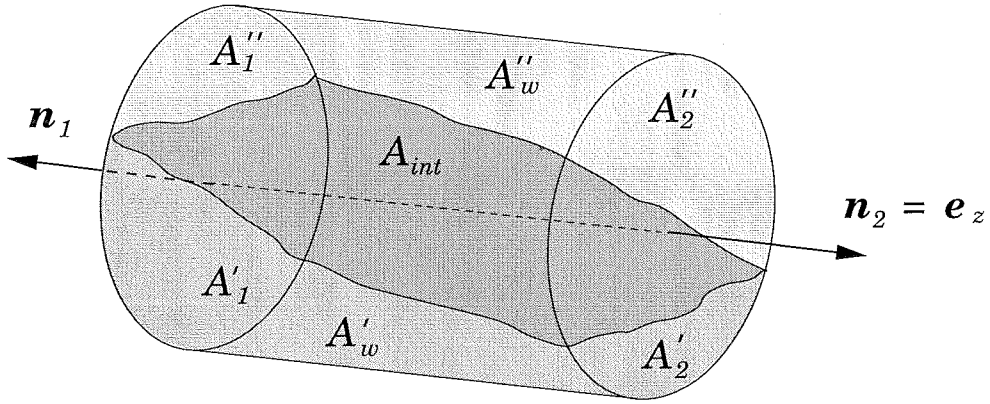

Figure 4.1 Areas in a two-phase pipe flow

The balance equations for mass and momentum will also be applied to each phase separately. The surface of the vapour phase is formed by fractions of inlet A''_1, outlet A''_2 and wall A''_w plus the entire interfacial area between the phases A_{int}. Similarly, the liquid contacts the areas A'_1, A'_2, A'_w and A_{int}. At the interface both phases may have different velocities $\boldsymbol{w}''_{int}$, $\boldsymbol{w}'_{int}$. The interface itself moves with the velocity $\boldsymbol{w}_{int}$.

4.1 Mass Balance

Overall Mass Balance

With $\boldsymbol{w} = 0$ at the wall and $\boldsymbol{w}_A = 0$ eq. (2.13) simplifies to

$$\frac{dM}{dt} = -\int_{A_{1,2}} \rho \boldsymbol{w} \boldsymbol{n} \, dA \tag{4.1}$$

where the right hand side represents the entering and leaving mass. Since $\boldsymbol{n}_1 = -\boldsymbol{e}_z$ and $\boldsymbol{n}_2 = \boldsymbol{e}_z$ we obtain, considering the definition of the mass flow rate in eq. (3.33),

$$\frac{dM}{dt} = \dot{m}_1 - \dot{m}_2 \tag{4.2}$$

or, since $\dot{m} = \dot{m}'' + \dot{m}'$,

$$\frac{dM}{dt} = \dot{m}_1'' - \dot{m}_2'' + \dot{m}_1' - \dot{m}_2' \tag{4.3}$$

Separate Mass Balances

The general mass balance equation eq. (2.13), evaluated for vapour and liquid separately, yields

$$\frac{dM''}{dt} = -\int_{A_{1,2}''} \rho'' \boldsymbol{w}'' \boldsymbol{n} \, dA + \int_{A_{int}} \rho''(\boldsymbol{w}_{int} - \boldsymbol{w}_{int}'')\boldsymbol{n}_{int}'' \, dA \tag{4.4}$$

$$\frac{dM'}{dt} = -\int_{A_{1,2}'} \rho' \boldsymbol{w}' \boldsymbol{n} \, dA + \int_{A_{int}} \rho'(\boldsymbol{w}_{int} - \boldsymbol{w}_{int}')\boldsymbol{n}_{int}' \, dA \tag{4.5}$$

In each equation the first term on the right hand side represents the entering and leaving mass flow rate of the phase considered. The second term quantifies the mass flow over the interface due to phase change. Therein, $\boldsymbol{n}_{int}''$ and $\boldsymbol{n}_{int}'$ are the unit normal vectors of the interfacial area, which are directed opposite to each other, fig. 4.2,

$$\boldsymbol{n}_{int}'' = -\boldsymbol{n}_{int}' \tag{4.6}$$

By use of the (relative) interfacial mass velocities,

$$\mu'' := \rho''(\boldsymbol{w}_{int} - \boldsymbol{w}_{int}'')\boldsymbol{n}_{int}'' \tag{4.7}$$

$$\mu' := \rho'(\boldsymbol{w}_{int} - \boldsymbol{w}_{int}')\boldsymbol{n}_{int}' \tag{4.8}$$

the two mass balances can also be written as follows

$$\frac{dM''}{dt} = \dot{m}_1'' - \dot{m}_2'' + \int_{A_{int}} \mu'' \, dA \tag{4.9}$$

$$\frac{dM'}{dt} = \dot{m}_1' - \dot{m}_2' + \int_{A_{int}} \mu' \, dA \tag{4.10}$$

Interfacial Mass Balance

Adding up the separate mass balances and subtracting the result from the overall mass balance eq. (4.3) yields

$$\int_{A_{int}} \mu'' \, dA + \int_{A_{int}} \mu' \, dA = 0 \tag{4.11}$$

which can be regarded as the mass balance for the interface: Since it contains (arguably) no mass, just as much mass enters as leaves the interface. This must also hold for a single point on the interface, thus

$$\mu'' + \mu' = 0 \tag{4.12}$$

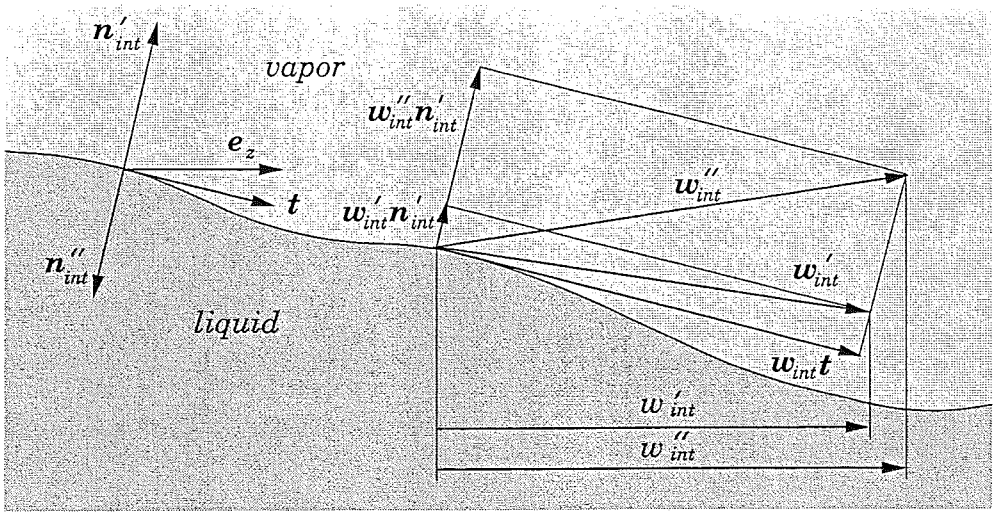

Figure 4.2 Velocities at the phase interface

To show the influence of the interfacial mass flow on the velocities at the interface, eq. (4.7) and eq. (4.8) are multiplied with the unit normal vectors and then solved for w_{int}

$$w_{int} = w''_{int} + \frac{\mu''}{\rho''} n''_{int} \tag{4.13}$$

$$w_{int} = w'_{int} + \frac{\mu'}{\rho'} n'_{int} \tag{4.14}$$

Subtraction of eq. (4.14) from eq. (4.13) gives, together with eq. (4.12), and eq. (4.6)

$$(w''_{int} - w'_{int}) = \left[\frac{1}{\rho''} - \frac{1}{\rho'}\right] \mu'' n'_{int} \tag{4.15}$$

which proves that the vapour and liquid velocities normal to the interface must differ locally, in case a phase transition takes place. Multiplication of eq. (4.15) and eq. (4.13) with the tangential unit vector t gives, since $nt = 0$,

$$w''_{int}t = w'_{int}t = w_{int}t \tag{4.16}$$

the equality of tangential velocities. If the mass flow over the interface is primarily perpendicular to the flow direction, which can be assumed in a duct with small diameter, the tangential velocities are approximately equal to the axial velocities, fig. 4.2. Eq. (4.16) then leads to

$$w''_{int} \approx w'_{int} \approx w_{int} \tag{4.17}$$

4.2 Momentum Balance

Overall Momentum Balance

Three-Dimensional Equation Considering the adhesion condition $w = 0$

at the wall, the general momentum balance eq. (2.21) evaluated for a fixed segment of a pipe, $\boldsymbol{w}_A = 0$, gives

$$\frac{d\boldsymbol{I}}{dt} = -\int_{A_{1,2}} \rho \boldsymbol{w}(\boldsymbol{w}\boldsymbol{n})\, dA + \boldsymbol{F}_g + \boldsymbol{F}_p + \boldsymbol{F}_\tau \tag{4.18}$$

The first term represents the momentum transfer due to convection through in- and outlet. The forces are

$$\boldsymbol{F}_g = \int_V \rho \boldsymbol{g}\, dV = M\boldsymbol{g} \tag{4.19}$$

$$\boldsymbol{F}_p = -\int_{A_{1,2}} p\boldsymbol{n}\, dA - \int_{A_w} p\boldsymbol{n}\, dA \tag{4.20}$$

$$\boldsymbol{F}_\tau = \int_{A_{1,2}} \mathbf{T}\boldsymbol{n}\, dA + \int_{A_w} \mathbf{T}\boldsymbol{n}\, dA \tag{4.21}$$

One-Dimensional Equation The axial component of the equation is obtained from multiplication with the axial unit vector $\boldsymbol{e}_z$. Using $w = \boldsymbol{w}\boldsymbol{e}_z$ we get

$$\frac{dI}{dt} = -\int_{A_{1,2}} w\rho\boldsymbol{w}\boldsymbol{n}\, dA + F_g + F_p + F_\tau \tag{4.22}$$

where I, w, F are the axial components of $\boldsymbol{I}, \boldsymbol{w}, \boldsymbol{F}$. The axial gravity force is

$$F_g = \int_V \rho g \boldsymbol{e}_z\, dV = Mg\boldsymbol{e}_z \tag{4.23}$$

Since $\boldsymbol{n}_1\boldsymbol{e}_z = -1$, $\boldsymbol{n}_1\boldsymbol{e}_z = 1$ and $\boldsymbol{n}_w\boldsymbol{e}_z = 0$, the axial pressure force becomes

$$F_p = \int_{A_1} p\, dA - \int_{A_2} p\, dA = (p_1 - p_2)\, A \tag{4.24}$$

where p_1 and p_2 are the average pressures at in- and outlet. In the friction force term, the axial component of $\mathbf{T}\boldsymbol{n}$ at in- and outlet equals the normal shear stress τ_{zz} which is usually negligible compared to the pressure. The only considerable axial contribution is the wall friction

$$F_\tau \approx F_w = \int_{A_w} (\mathbf{T}\boldsymbol{n}_w)\, \boldsymbol{e}_z = \int_{A_w} \tau_z\, dA = \tau_w A_w \tag{4.25}$$

where τ_z is the local axial shear stress and τ_w denotes its average value.

Eq. (4.22) can be expressed as

$$\frac{dI}{dt} = \dot{I}_1 - \dot{I}_2 + F_g + F_p + F_\tau \tag{4.26}$$

where $\dot{I}$ is the flow of momentum in direction of the axial position vector

$$\dot{I} = \int_A w\rho\boldsymbol{w}\boldsymbol{e}_z\, dA \tag{4.27}$$

If liquid and vapour have different velocities, the integral must be split up to be evaluated

$$\dot{I} = \int_{A''} w''\rho''\boldsymbol{w}''\boldsymbol{e}_z \, dA + \int_{A'} w'\rho'\boldsymbol{w}'\boldsymbol{e}_z \, dA \tag{4.28}$$

These terms will be approximated as follows

$$\dot{I} \approx \dot{m}''w'' + \dot{m}'w' \tag{4.29}$$

Replacing $\dot{m}''$ and $\dot{m}'$ with eq. (3.48) and eq. (3.49) yields

$$\dot{I} \approx \dot{m}w + \dot{m}_{corr}\left(w'' - w'\right) \tag{4.30}$$

where w and $\dot{m}_{corr}$ are defined in eq. (3.22), and eq. (3.50), respectively.

Separate Momentum Balances

Three-Dimensional Equation Applied to the vapour phase separately, the momentum balance takes the form

$$\frac{d\boldsymbol{I}''}{dt} = -\int_{A''_{1,2}} \rho''\boldsymbol{w}''(\boldsymbol{w}''\boldsymbol{n}) \, dA + \int_{A_{int}} \mu''\boldsymbol{w}''_{int} \, dA + \boldsymbol{F}''_g + \boldsymbol{F}''_p + \boldsymbol{F}''_\tau \tag{4.31}$$

where the interfacial mass velocity μ'', defined in eq. (4.7) has been employed. The forces are

$$\boldsymbol{F}''_g = \int_{V''} \rho\boldsymbol{g} \, dV \tag{4.32}$$

$$\boldsymbol{F}''_p = -\int_{A''_{1,2}} p\boldsymbol{n} \, dA - \int_{A''_w} p\boldsymbol{n} \, dA - \int_{A_{int}} p''\boldsymbol{n}''_{int} \, dA \tag{4.33}$$

$$\boldsymbol{F}''_\tau = \int_{A''_w} \mathbf{T}\boldsymbol{n}_w \, dA + \int_{A_{int}} \mathbf{T}''\boldsymbol{n}''_{int} \, dA \tag{4.34}$$

The normal shear stresses in $\boldsymbol{F}''_\tau$ have been neglected.

One-Dimensional Equation Multiplication of eq. (4.31) with $\boldsymbol{e}_z$ yields the axial component of the momentum balance

$$\frac{dI''}{dt} = \dot{I}''_1 - \dot{I}''_2 + \int_{A_{int}} \mu''w''_{int} \, dA + F''_g + F''_p + F''_\tau \tag{4.35}$$

where $w''_{int} = \boldsymbol{w}''_{int}\boldsymbol{e}_z$ denotes the axial vapour velocity at the interface. The axial vapour momentum flow will be approximated by

$$\dot{I}'' = \int_{A''} w''\rho''\boldsymbol{w}''\boldsymbol{e}_z \, dA \approx \dot{m}''w'' \tag{4.36}$$

The gravity and pressure forces are

$$F_g'' = M'' g e_z \tag{4.37}$$

$$F_p'' = p_1'' A_1'' - p_2'' A_2'' - \int_{A_{int}''} p n_{int}'' e_z \, dA \tag{4.38}$$

The friction force is resolved into wall friction and interfacial friction

$$F_\tau'' = F_w'' + F_{int}'' \tag{4.39}$$

with

$$F_w'' = \int_{A_w''} (\mathbf{T} n_w) \, e_z \, dA = \int_{A_w''} \tau_z'' \, dA \tag{4.40}$$

$$F_{int}'' = \int_{A_{int}} (\mathbf{T}'' \boldsymbol{n}_{int}'') \, e_z \, dA = \int_{A_{int}} \tau_{int}'' \, dA \tag{4.41}$$

where τ_z'' and τ_{int}'' denote the axial components of the wall shear stress and interfacial shear stress respectively. The axial vapour momentum balance now takes the form

$$\frac{dI''}{dt} = \dot{m}_1'' w_1'' - \dot{m}_2'' w_2'' + \int_{A_{int}} \mu'' w_{int}'' \, dA + F_g'' + F_p'' + F_w'' + F_{int}'' \tag{4.42}$$

The liquid momentum balance is obtained by replacing the superscripts $''$ with $'$.

Interfacial Momentum Balance

When forming the three-dimensional liquid momentum balance similar to eq. (4.31), then adding up both separate momentum balances and finally subtracting the result from the overall momentum balance eq. (4.18), we arrive at the momentum balance for the interface

$$\int_{A_{int}} \left[p' \boldsymbol{n}_{int}' + p'' \boldsymbol{n}_{int}'' \right] dA = \int_{A_{int}} \left[\mu'' \boldsymbol{w}_{int}'' + \mu' \boldsymbol{w}_{int}' + \mathbf{T}'' \boldsymbol{n}_{int}'' + \mathbf{T}' \boldsymbol{n}_{int}' \right] dA \tag{4.43}$$

Evaluated locally with $\mu'' = -\mu'$ and $\boldsymbol{n}_{int}'' = -\boldsymbol{n}_{int}'$ it gets

$$(p' - p'') \boldsymbol{n}_{int}' = \mu''(\boldsymbol{w}_{int}'' - \boldsymbol{w}_{int}') + \mathbf{T}'' \boldsymbol{n}_{int}'' + \mathbf{T}' \boldsymbol{n}_{int}' \tag{4.44}$$

Normal Component The component of eq. (4.44) normal to the interface is obtained from a multiplication with $\boldsymbol{n}_{int}'$

$$p' - p'' = \mu''(\boldsymbol{w}_{int}'' - \boldsymbol{w}_{int}') \boldsymbol{n}_{int}' + (\mathbf{T}'' \boldsymbol{n}_{int}'') \boldsymbol{n}_{int}' + (\mathbf{T}' \boldsymbol{n}_{int}') \boldsymbol{n}_{int}' \tag{4.45}$$

Shear stresses normal to the interface are caused by the surface tension σ. Applying the Laplace law yields [4]

$$p' - p'' = \mu''(\boldsymbol{w}_{int}'' - \boldsymbol{w}_{int}') \boldsymbol{n}_{int}' \pm \sigma \left[\frac{1}{R_1} + \frac{1}{R_2} \right] \tag{4.46}$$

where R_1 and R_2 are the radii of curvature of the interface. The positive sign is valid, if the centre of curvature is located in the liquid phase. The equation can further be simplified by replacing the velocity difference with eq. (4.15) [7]

$$p' - p'' = (\mu'')^2 \left[\frac{1}{\rho''} - \frac{1}{\rho'}\right] \pm \sigma \left[\frac{1}{R_1} + \frac{1}{R_2}\right] \tag{4.47}$$

If the interface is planar, $R_1, R_2 \to \infty$, the mass transfer causes a higher pressure in the liquid, regardless of the direction of the interfacial mass flow, evaporation ($\mu'' > 0$) or condensation ($\mu'' < 0$). The influence of μ is negligible for small drops or bubbles $R_1, R_2 \to 0$. In the case of bubbles, the negative sign is valid; the pressure in the bubble is thus higher than in the surrounding liquid. The determination of the average pressures from this equation will not be attempted, instead, a zero pressure difference will be assumed.

Tangential Component A scalar multiplication of eq. (4.44) with the tangential vector $\boldsymbol{t}$ leads us to the tangential component of the interfacial momentum balance. Since $\boldsymbol{nt} = 0$ the pressure term vanishes

$$0 = \mu''(\boldsymbol{w}''_{int} - \boldsymbol{w}'_{int})\boldsymbol{t} + (\mathbf{T}''\boldsymbol{n}''_{int})\boldsymbol{t} + (\mathbf{T}'\boldsymbol{n}'_{int})\boldsymbol{t} \tag{4.48}$$

Due to the equality of tangential velocities, eq. (4.16), the first term on the right hand side is zero and the equation simplifies to an equilibrium of tangential stresses

$$0 = (\mathbf{T}''\boldsymbol{n}''_{int})\boldsymbol{t} + (\mathbf{T}'\boldsymbol{n}'_{int})\boldsymbol{t} \tag{4.49}$$

As fig. 4.2 illustrates, in a stratified or annular flow the axial unit vector $\boldsymbol{e}_z$ is approximately in the direction of $\boldsymbol{t}$, thus

$$0 \approx \tau''_{int} + \tau'_{int} \tag{4.50}$$

4.3 Energy Balance

The overall energy balance eq. (2.28), evaluated for a fixed straight pipe with $\boldsymbol{w} = 0$ at the wall, yields

$$\frac{dE}{dt} = -\int_{A_{1,2}} \rho e \boldsymbol{w}\boldsymbol{n}\, dA + P_g + P_p + P_\tau + \dot{Q} \tag{4.51}$$

With $dV = dAdz$ and $dz = dz\boldsymbol{e}_z$ the power due to gravity forces can be written as follows

$$P_g = \int_V \rho g \boldsymbol{w}\, dV = \int_V \rho g \boldsymbol{w}\, dAdz\boldsymbol{e}_z = \int_{\Delta z}\int_A \rho w \boldsymbol{e}_z\, dAgdz = \int_{\Delta z} \dot{m} g dz \tag{4.52}$$

Since the pipe wall is fixed, the surface forces which apply at the wall perform no work. The remaining terms for in- and outlet are

$$P_p = -\int_{A_{1,2}} p\boldsymbol{w}\boldsymbol{n}\, dA \tag{4.53}$$

$$P_\tau = \int_{A_{1,2}} \mathsf{T}\boldsymbol{w}\boldsymbol{n}\, dA \approx 0 \tag{4.54}$$

where P_τ is the work of the normal shear stresses, which are negligible. P_τ must not be mistaken for the power due to friction, which does not appear in the overall energy balance. Friction does not affect the overall energy, but causes a transformation of kinetic energy to internal energy within the fluid. In eq. (4.51) these energy forms may be written explicitly

$$\frac{dU}{dt} + \frac{dE_{kin}}{dt} = -\int_{A_{1,2}} \rho u \boldsymbol{w}\boldsymbol{n}\, dA - \int_{A_{1,2}} \rho\frac{\boldsymbol{w}^2}{2}\boldsymbol{w}\boldsymbol{n}\, dA + P_g + P_p + P_\tau + \dot{Q} \tag{4.55}$$

Resolving this equation into one equation for each energy derivative is difficult. In appendix A the following equations are derived from integration of balance equations for an infinitesimal small fluid particle (Navier-Stokes equations):

$$\frac{dE_{kin}}{dt} = -\int_{A_{1,2}} \rho\frac{\boldsymbol{w}^2}{2}\boldsymbol{w}\boldsymbol{n}\, dA + P_g - \int_V w_i\frac{\partial p}{\partial z_i}\, dV + \int_V w_i\frac{\partial \tau_{ji}}{\partial z_j}\, dV \tag{4.56}$$

$$\frac{dU}{dt} = -\int_{A_{1,2}} \rho u \boldsymbol{w}\boldsymbol{n}\, dA + \dot{Q} - \int_V p\frac{\partial w_i}{\partial z_i}\, dV + \int_V \tau_{ji}\frac{\partial w_i}{\partial z_j}\, dV \tag{4.57}$$

The last two terms in eq. (4.56) quantify the rate of change of kinetic energy due to surface forces. The related terms in eq. (4.57) cause a deformation of the fluid particles. The deformation work cannot be stored as potential energy, but is irreversibly transformed into heat, and thus increases the internal energy [6]. Eq. (4.57) is equivalent to

$$\frac{dU}{dt} = -\int_{A_{1,2}} \rho u \boldsymbol{w}\boldsymbol{n}\, dA + \dot{Q} + P_p + \int_V w_i\frac{\partial p}{\partial z_i}\, dV + \int_V \tau_{ji}\frac{\partial w_i}{\partial z_j}\, dV \tag{4.58}$$

The last term therein is positive – otherwise internal energy would be transformed into kinetic energy, which violates the second law of thermodynamics. The pressure integral is negative, since a negative pressure gradient is required to overcome the friction. It will be assumed that both integrals sum up to approximately zero

$$\int_V w_i\frac{\partial p}{\partial z_i}\, dV + \int_V \tau_{ji}\frac{\partial w_i}{\partial z_j}\, dV \approx 0 \tag{4.59}$$

In the remaining internal energy balance the pressure work and the convective term can be combined

$$\frac{dU}{dt} = -\int_{A_{1,2}} [\rho u + p]\, \boldsymbol{w}\boldsymbol{n}\, dA + \dot{Q} \tag{4.60}$$

Since $h = u + p/\rho$ the integral represents the flow of enthalpy

$$\dot{H} = \int_A \rho h \boldsymbol{w}\boldsymbol{n}\, dA \tag{4.61}$$

The integral may be resolved into the flow of enthalpy of each phase

$$\dot{H} = \int_{A''} \rho'' h'' \boldsymbol{w}''\boldsymbol{n}\, dA + \int_{A'} \rho' h' \boldsymbol{w}'\boldsymbol{n}\, dA \tag{4.62}$$

which will be approximated by

$$\dot{H} \approx \dot{m}'' h'' + \dot{m}' h' \tag{4.63}$$

The right hand side can, in analogy to eq. (4.30), also be expressed in terms of the correction mass flow rate, eq. (3.50)

$$\dot{H} \approx \dot{m} h + \dot{m}_{corr} \left(h'' - h'\right) \tag{4.64}$$

where h is the average enthalpy, defined in eq. (3.21). The energy equation to be used reads

$$\frac{dU}{dt} = \dot{H}_1 - \dot{H}_2 + \dot{Q} \tag{4.65}$$

5. Thermodynamic Model

Two thermodynamic variables must be known to determine the thermodynamic state of a pure fluid. The objective of this chapter is to provide appropriate differential equations from the balance equations derived in the previous chapter. The convective terms appearing therein will be modelled in the next chapter.

5.1 Differential Equations

Differential equations for ρ and u are obtained from balance equations for mass and internal energy. The resulting primary equations can be transformed into secondary forms providing improved stability and performance in dynamic simulations.

Primary Equations

A differentiation of $M = \rho V$ and $U = uM$ for a constant volume yields

$$V\frac{d\rho}{dt} = \frac{dM}{dt} \tag{5.1}$$

$$M\frac{du}{dt} = \frac{dU}{dt} - u\frac{dM}{dt} \tag{5.2}$$

Equations for the rate of change of mass and internal energy have been derived in chapter 4

$$\frac{dM}{dt} = \dot{m}_1 - \dot{m}_2 \tag{5.3}$$

$$\frac{dU}{dt} = \dot{H}_1 - \dot{H}_2 + \dot{Q} \tag{5.4}$$

The flow of enthalpy has been expressed as follows

$$\dot{H} = \dot{m}h + \dot{m}_{corr}\left(h'' - h'\right) \tag{5.5}$$

with a correction mass flow rate

$$\dot{m}_{corr} = x(1-x)\rho\Delta wA \tag{5.6}$$

The heat flux is commonly written in terms of a heat transfer coefficient α

$$\dot{Q} = \alpha A_w(T_w - T) \tag{5.7}$$

where A_w and T_w denote the wall area and its average temperature. Empirical correlations for the heat transfer coefficient α in the one- and two-phase region are listed in appendix B.

(Numerical) integration of eq. (5.1) and eq. (5.2) yields values for ρ and u. Experience shows, that the differential equation for the density eq. (5.1) causes numerical stiffness in the liquid area, where, due to the low compressibility, minimal changes of the density, caused by the numerical algorithm, lead to large, unrealistic changes of the pressure. It is thus desirable to transform the system of differential equations into a numerically more stable secondary form.

Secondary Equations

From eq. (5.1) and eq. (5.2) differential equations for any combination of two state variables can easily be derived. In general, the independent parameters of the available equation of state should be chosen. The equation of state used within the NIST REFPROP library is, however, a (fundamental) equation for the free enthalpy $f(T, \rho)$ containing the density, which cannot be used for the reasons described above.

The NIST REFPROP library contains external functions for other combinations of independent parameters, i.e. (T, p), (p, h) and (p, s), which, however, apply time-consuming numerical methods to solve the fundamental equation for its independent parameters. Moreover, all combinations, including (T, ρ), use numerical methods to compute the saturation properties from the equilibrium conditions eq. (3.28).

To keep the computation time low, the NIST REFPROP library will not be used directly during the simulation. Instead, fast approximation functions will be created, whose independent variables can then be chosen as appropriate. In this thesis, pressure and enthalpy, common variables for a description of refrigeration cycles, will be used.

To transform eq. (5.1) and eq. (5.2) into differential equations for p and h, the general correlations $\rho = \rho(p, h)$ and $u = u(p, h)$ are differentiated by the time. Application of the chain rule yields

$$\frac{d\rho}{dt} = \left.\frac{\partial \rho}{\partial p}\right|_h \frac{dp}{dt} + \left.\frac{\partial \rho}{\partial h}\right|_p \frac{dh}{dt} \tag{5.8}$$

$$\frac{du}{dt} = \left.\frac{\partial u}{\partial p}\right|_h \frac{dp}{dt} + \left.\frac{\partial u}{\partial h}\right|_p \frac{dh}{dt} \tag{5.9}$$

These equations can also be written in vector notation

$$\frac{d}{dt}\begin{pmatrix} \rho \\ u \end{pmatrix} = \mathbf{J}\frac{d}{dt}\begin{pmatrix} p \\ h \end{pmatrix} \tag{5.10}$$

where $\mathbf{J}$ is the Jacobian matrix, containing the partial derivatives

$$\mathbf{J} = \begin{pmatrix} \left.\frac{\partial \rho}{\partial p}\right|_h & \left.\frac{\partial \rho}{\partial h}\right|_p \\ \left.\frac{\partial u}{\partial p}\right|_h & \left.\frac{\partial u}{\partial h}\right|_p \end{pmatrix} \tag{5.11}$$

To obtain differential equations for pressure and enthalpy eq. (5.10) must be

solved for the derivative of (p, h)

$$\frac{d}{dt}\begin{pmatrix} p \\ h \end{pmatrix} = \mathbf{J}^{-1}\frac{d}{dt}\begin{pmatrix} \rho \\ u \end{pmatrix} \tag{5.12}$$

The inverse of the Jacobian is computed as follows [3]

$$\mathbf{J}^{-1} = \frac{1}{\det \mathbf{J}}\begin{pmatrix} \frac{\partial u}{\partial h}\Big|_p & -\frac{\partial \rho}{\partial h}\Big|_p \\ -\frac{\partial u}{\partial p}\Big|_h & \frac{\partial \rho}{\partial p}\Big|_h \end{pmatrix} \tag{5.13}$$

with the determinant

$$\det \mathbf{J} = \frac{\partial \rho}{\partial p}\Big|_h \frac{\partial u}{\partial h}\Big|_p - \frac{\partial \rho}{\partial h}\Big|_p \frac{\partial u}{\partial p}\Big|_h \tag{5.14}$$

The partial derivatives of u can be reduced to the ones of ρ. From $u = h - p/\rho$ we obtain

$$\frac{\partial u}{\partial h}\Big|_p = 1 + \frac{p}{\rho^2}\frac{\partial \rho}{\partial h}\Big|_p \qquad \frac{\partial u}{\partial p}\Big|_h = -\frac{1}{\rho} + \frac{p}{\rho^2}\frac{\partial \rho}{\partial p}\Big|_h \tag{5.15}$$

Therefore

$$\det \mathbf{J} = \frac{\partial \rho}{\partial p}\Big|_h + \frac{1}{\rho}\frac{\partial \rho}{\partial h}\Big|_p = \frac{1}{a^2} \tag{5.16}$$

where a is, as shown in appendix C.2, the velocity of sound. The inverse of the Jacobian becomes

$$\mathbf{J}^{-1} = a^2\begin{pmatrix} 1 + \frac{p}{\rho^2}\frac{\partial \rho}{\partial h}\Big|_p & -\frac{\partial \rho}{\partial h}\Big|_p \\ \frac{1}{\rho} - \frac{p}{\rho^2}\frac{\partial \rho}{\partial p}\Big|_h & \frac{\partial \rho}{\partial p}\Big|_h \end{pmatrix} \tag{5.17}$$

and the new system of differential equations, multiplied with the mass $M = \rho V$ reads

$$V\frac{\rho}{a^2}\frac{dp}{dt} = \left(\rho + \frac{p}{\rho}\frac{\partial \rho}{\partial h}\Big|_p\right) V\frac{d\rho}{dt} - \frac{\partial \rho}{\partial h}\Big|_p M\frac{du}{dt} \tag{5.18}$$

$$V\frac{\rho}{a^2}\frac{dh}{dt} = \left(1 - \frac{p}{\rho}\frac{\partial \rho}{\partial p}\Big|_h\right) V\frac{d\rho}{dt} + \frac{\partial \rho}{\partial p}\Big|_h M\frac{du}{dt} \tag{5.19}$$

Inserting eq. (5.1) and eq. (5.2) and substituting the internal energy with $u = h - p/\rho$ gives

$$V\frac{\rho}{a^2}\frac{dp}{dt} = \left(\rho + h\frac{\partial \rho}{\partial h}\Big|_p\right)\frac{dM}{dt} - \frac{\partial \rho}{\partial h}\Big|_p\frac{dU}{dt} \tag{5.20}$$

$$V\frac{\rho}{a^2}\frac{dh}{dt} = \left(1 - h\frac{\partial \rho}{\partial p}\Big|_h\right)\frac{dM}{dt} + \frac{\partial \rho}{\partial p}\Big|_h\frac{dU}{dt} \tag{5.21}$$

Integration of these equations yields values for p and h. The next task is to provide equations of state based on these two variables, that enable a fast computation of other properties during a simulation run.

5.2 Equation of State

The properties to be computed from (p, h) are the temperature T, which determines the heat flux in eq. (5.7), and the density ρ, as well as its derivatives $\partial\rho/\partial p|_h$ and $\partial\rho/\partial h|_p$, which appear in the equations above. The medium used in the refrigeration test plant is R22. Fig. 5.1 shows the $\log p, h$-diagram of R22 including lines of constant temperatures and densities. It was created on the basis of subroutines from the NIST REFPROP library. The library was extended by C-routines computing certain first and second partial derivatives of properties from the derivatives of the fundamental equation, using correlations derived in appendix C.

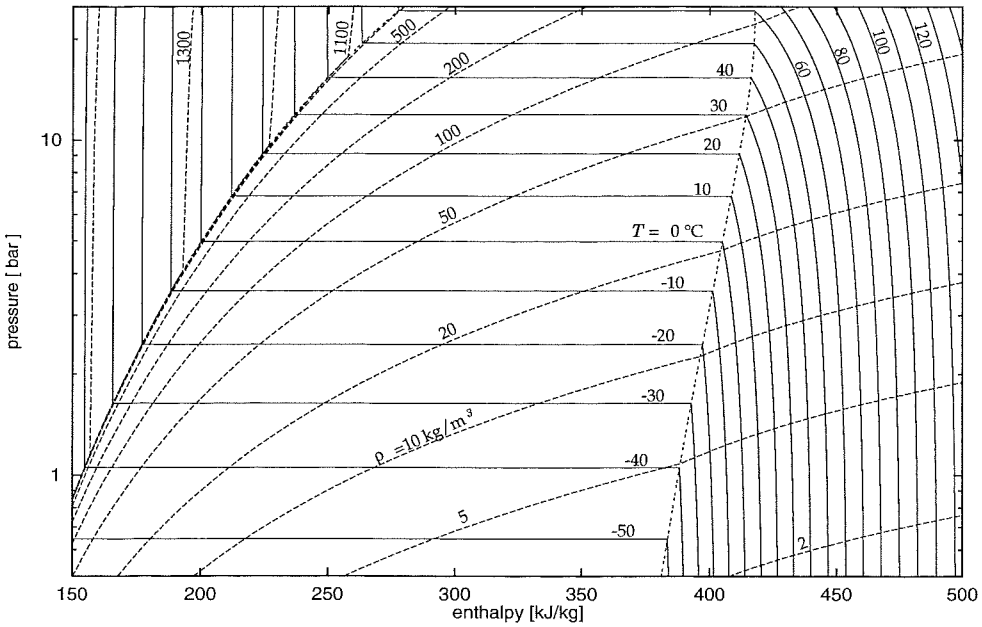

Figure 5.1 $\log p$,h-diagram of R22

The determination of the region of state of a given point (p, h) is obtained from a comparison of the enthalpy with the equilibrium liquid and vapour enthalpy

$$\begin{array}{ll} h < h'(p) & \text{liquid} \\ h'(p) \leq h \leq h''(p) & \text{two-phase} \\ h''(p) < h & \text{vapour} \end{array} \tag{5.22}$$

To obtain algebraic equations of states for theses regions, Taylor expansions on the dew and boiling point are used. This approach has the advantage that a continuous transition of the temperature and density functions on the phase boundaries is achieved. The density derivatives are not continuous, as can be seen from fig. 5.1.

Properties and derivatives on the saturation curves are calculated from the NIST REFPROP library and then approximated by polynomials (least squares fit) using the pressure as independent variable. For numerical reasons the pressure and/or the property was in some cases replaced by a function. The order of the polynomial was not adapted to the individual case, but chosen as constant, $n = 5$. For $h'(p)$ a different approach was taken (see below).

The relative error for T_{sat}, h'', h' and ρ' is less than 0.03% in a pressure range 1..20 bar of R22. For ρ'' the maximum error is 0.5%, which is due to its low values at low pressures. The relative error of the other polynomial functions is of secondary interest, since they are only used within the Taylor expansions. The error of the Taylor expansions for T, ρ, $\partial\rho/\partial p|_h$ and $\partial\rho/\partial h|_p$, is presented in section 5.2.

Vapour Region

As fig. 5.1 shows, a wide region of state can be covered with a Taylor expansion for isobars starting at $h = h''(p)$. The related Taylor series is

$$\psi(p,h) = \sum_i \left.\frac{\partial^i \psi}{\partial h^i}\right|''_p (p) \frac{(h - h''(p))^i}{i!} \tag{5.23}$$

Using a subscript notation for partial derivatives

$$\psi_p = \left.\frac{\partial \psi}{\partial p}\right|_h \qquad \psi_h = \left.\frac{\partial \psi}{\partial h}\right|_p \tag{5.24}$$

and the abbreviation

$$\Delta h = h - h''(p) \tag{5.25}$$

eq. (5.23) becomes

$$\psi(p,h) = \psi''(p) + \psi''_h(p)\Delta h + \psi''_{hh}(p)\frac{\Delta h^2}{2} + .. \tag{5.26}$$

For the temperature in the vapour region a linear approach is made

$$T = T_{sat}(p) + T''_h(p)\Delta h \tag{5.27}$$

Taylor expansions of second or third order provide an increased accuracy close to the dew point. However, as fig. 5.2 shows, they yield qualitatively wrong approximations for superheated vapour. This is due to a change of the curvature of an isobar close to the dew point.

Instead of the density, the specific volume is written in expansion form, because, compared to an isobar in a $\rho(h)$ diagram, the same line is almost linear in a $v(h)$ diagram, fig. 5.3. A second order expansion is chosen

$$v = v''(p) + v''_h(p)\Delta h + \frac{1}{2}v''_{hh}(p)\Delta h^2 \tag{5.28}$$

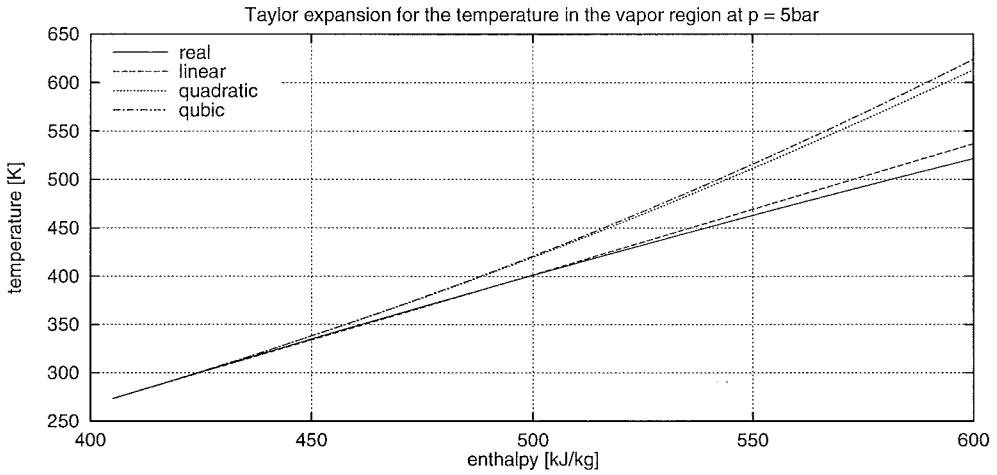

Figure 5.2 Taylor expansions for T in the vapour region

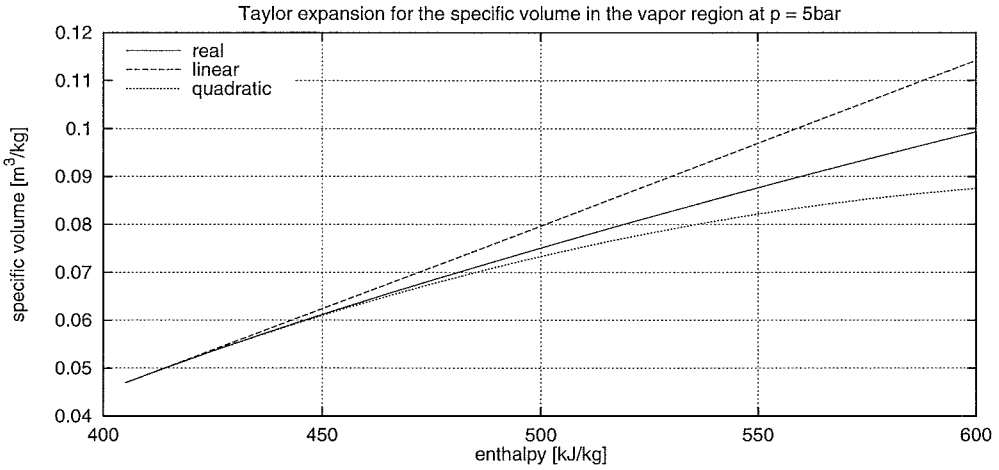

Figure 5.3 Taylor expansions for v in the vapour region

Consequently, the derivatives of v were used for a linear expansion

$$v_h = v'_h(p) + v''_{hh}(p)\Delta h \tag{5.29}$$
$$v_p = v'_p(p) + v''_{ph}(p)\Delta h \tag{5.30}$$

The density and its derivatives are then obtained from

$$\rho = v^{-1} \tag{5.31}$$
$$\rho_h = \frac{d\rho}{dv} v_h = -v^{-2} v_h = -\rho^2 v_h \tag{5.32}$$
$$\rho_p = \frac{d\rho}{dv} v_p = -v^{-2} v_p = -\rho^2 v_p \tag{5.33}$$

The properties on the dew point, denoted with a superscript $''$, as well as $T_{sat}(p)$ are approximated by polynomial functions, as explained in the previous subsection.

Liquid Region

As fig. 5.1 shows, temperature and density in the liquid region are almost independent of the pressure. Therefore, extrapolations along lines of constant enthalpies yield highly accurate approximations. The Taylor series is evolved as follows

$$\psi(p,h) = \sum_i \left.\frac{\partial^i \psi}{\partial p^i}\right|_h' (p'(h)) \frac{(p-p'(h))^i}{i!} \tag{5.34}$$

where $p'(h)$ is the inverse function of $h'(p)$, which is needed for identification of the phase region. Both functions should be completely consistent to avoid discontinuities. The following function was used

$$p'(h) = \left[b_0 + b_1 h + b_2 h^2\right]^6 \tag{5.35}$$

For a given pressure this function can be solved for $h = h'(p)$

$$h'(p) = -\frac{b_1}{2b_2} - \sqrt{\left(\frac{b_1}{2b_2}\right)^2 + \frac{\sqrt[6]{p} - b_0}{b_2}} \tag{5.36}$$

As mentioned above, the relative error of $h'(p)$ is less than 0.03% in a range $p = 1..20$ bar of R22.

Using the abbreviation

$$\Delta p = p - p'(h) \tag{5.37}$$

and subscripts to denote partial derivatives, eq. (5.34) gets

$$\psi(p,h) = \psi'(p') + \psi'_p(p')\Delta p + \psi'_{pp}(p')\frac{\Delta p^2}{2} + .. \tag{5.38}$$

Linear expansions are completely sufficient. The relative error of T and ρ in the region of interest is less than 0.1%.

$$T = T_{sat}(p') + T'_p(p')\Delta p \tag{5.39}$$
$$\rho = \rho'(p') + \rho'_p(p')\Delta p \tag{5.40}$$
$$\rho_h = \rho'_h(p') + \rho'_{hp}(p')\Delta p \tag{5.41}$$
$$\rho_p = \rho'_p(p') + \rho'_{pp}(p')\Delta p \tag{5.42}$$

The functions $\psi(p')$ are polynomials, except for the second derivatives of the densities, which were not suitable for an approximating polynomial. Instead, the related derivatives of the specific volume, v'_{hp} and v'_{pp} were used. From these, the second derivatives of the density are computed as follows

$$\rho'_{hp} = (-\rho^2 v_h)'_p = -2\rho' v'_h \rho'_p - \rho'^2 v'_{ph} = \frac{2}{\rho'}\rho'_h \rho'_p - \rho'^2 v'_{hp} \tag{5.43}$$

$$\rho'_{pp} = (-\rho^2 v_p)'_p = -2\rho' v'_p \rho'_p - \rho'^2 v'_{pp} = \frac{2}{\rho'}\rho'^2_p - \rho'^2 v'_{pp} \tag{5.44}$$

Fig. 5.4 demonstrates the accuracy of the Taylor expansion. The deviation on the extrapolation point at $p = 5\,\text{bar}$ is due to the error of the polynomial function $\rho'(p)$. It does not cause a discontinuity, because the same function $\rho'(p)$ is used in the two-phase region.

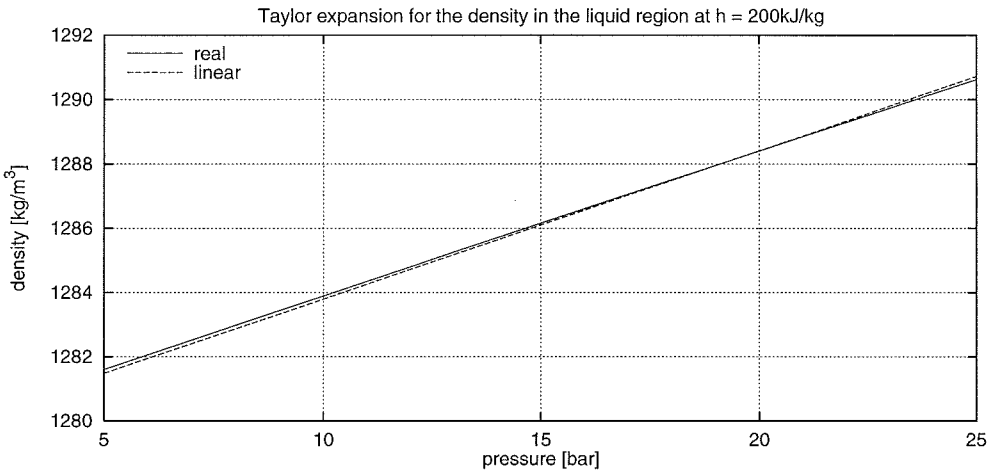

Figure 5.4 Taylor expansion for ρ in the liquid region

Two-Phase Region

In the two-phase region, the properties can be computed from the properties on the dew and boiling point. Taylor expansions are not needed. For a known enthalpy the quality is obtained from eq. (3.21), which gives

$$x = \frac{h - h'(p)}{h''(p) - h'(p)} \tag{5.45}$$

The enthalpy on the boiling point $h'(p)$ is computed from eq. (5.36). On the dew point a polynomial function is used. Since the specific volume is calculated from eq. (3.19) the two-phase density gets

$$\rho = \frac{1}{v} = \frac{1}{xv''(p) + (1-x)v'(p)} = \frac{1}{x/\rho''(p) + (1-x)/\rho'(p)} \tag{5.46}$$

where the functions for the liquid and vapour densities have already been used within the Taylor series for liquid and vapour. Now the void fraction can be computed. Eq. (3.17) gives

$$\gamma = \frac{\rho - \rho'(p)}{\rho''(p) - \rho'(p)} \tag{5.47}$$

The temperature equals the saturation temperature

$$T = T_{sat}(p) \tag{5.48}$$

which is a polynomial fit. As shown in appendix C.3, the density derivatives in the two-phase region can be expressed as follows

$$\left.\frac{\partial\rho}{\partial h}\right|_p = -\frac{\rho^2}{T}\frac{dT}{dp} \tag{5.49}$$

$$\left.\frac{\partial\rho}{\partial p}\right|_h = \frac{c_v\rho^2}{T}\left(\frac{dT}{dp}\right)^2 + \frac{\rho}{T}\frac{dT}{dp} \tag{5.50}$$

where the symbolic derivative of the function $T_{sat}(p)$ was used to obtain a function for its derivative dT/dp.[1] The specific isochoric heat capacity in the two-phase region can be written as

$$c_v = x\tilde{c}_v'' + (1-x)\tilde{c}_v' \tag{5.51}$$

The limiting isochoric heat capacities $\tilde{c}_v$ (which must not be mistaken for c_v of boiling liquid or dewing vapour) are written as polynomials. The formula for $\tilde{c}_v$ is derived in appendix C.3

Accuracy of the Equation of State

The accuracy achieved by the approximation functions is documented in the diagrams below. In the vapour region the relative error increases with the distance from the dew line, which is due to the extrapolation form chosen. The relative error of $\partial\rho/\partial p|_h$ and $\partial\rho/\partial h|_p$ is larger by a factor up to 5 compared to the one of the density, which is a result of the linear approach and the low values of the derivatives at low pressures. The objective to provide good approximations close to the two-phase region is obviously fulfilled.

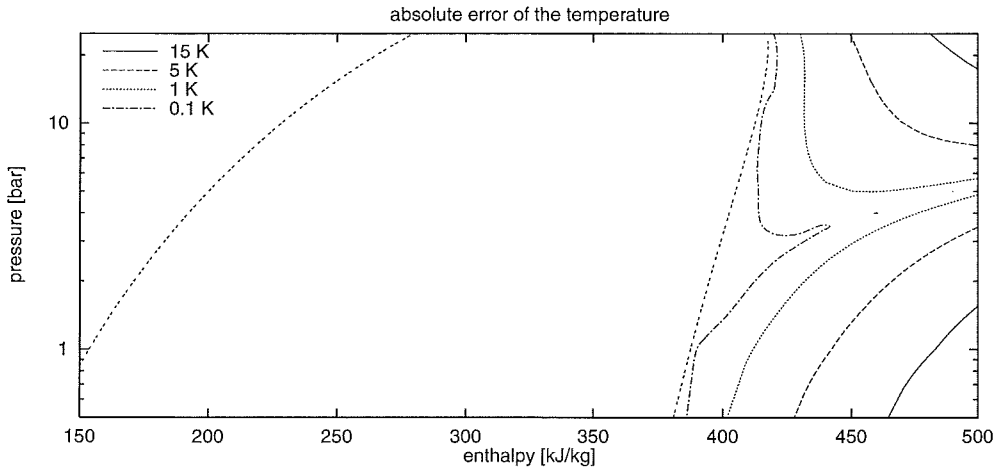

Figure 5.5 Absolute error of the approximation function for T

[1] This appears natural, but the derivative of a polynomial is often not usable in this way. In this case the result was, however, particularly accurate.

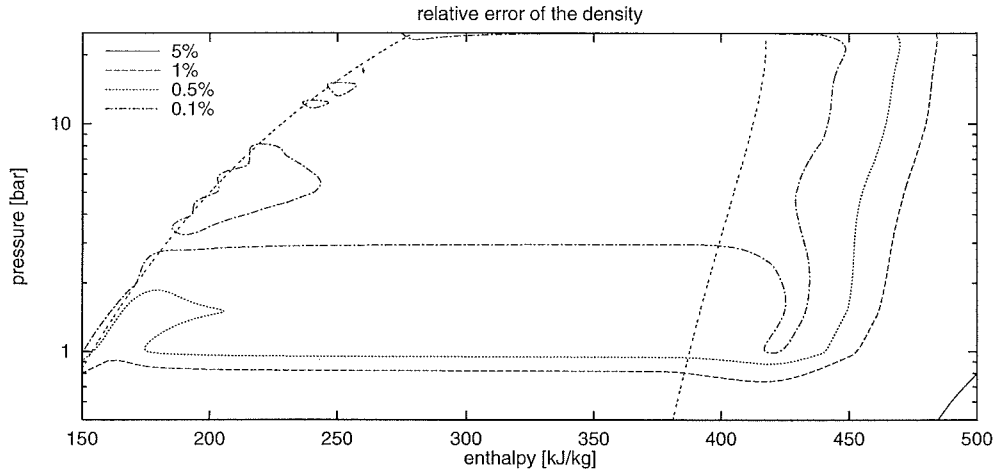

Figure 5.6 Relative error of the approximation function for ρ

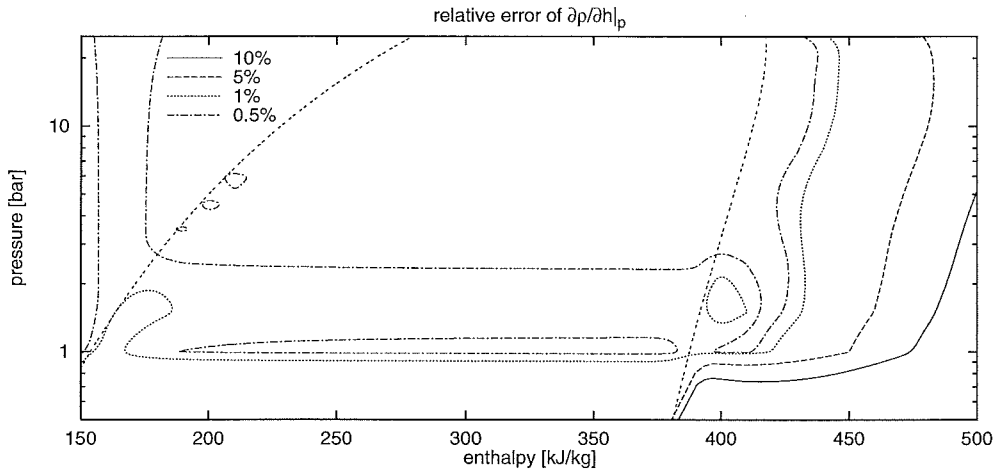

Figure 5.7 Relative error of the approximation function for $\partial\rho/\partial p|_h$

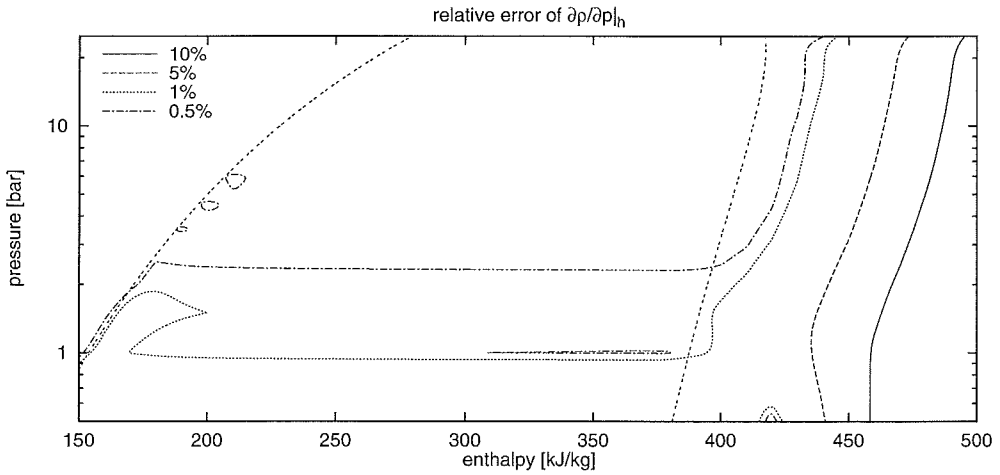

Figure 5.8 Relative error of the approximation function for $\partial\rho/\partial h|_p$

6. Hydrodynamic Model

The convective terms in the equations eq. (5.3) and eq. (5.4), i.e. the mass flow rate and the flow of enthalpy, are still unknown. The thermodynamic properties at in- and outlet will later be approximated by the average value of the control volume located upstream. The remaining properties to be determined in this chapter are the mass flow rate $\dot{m}$ and the correction mass flow rate $\dot{m}_{corr}$. The latter is, for known thermodynamic properties, a function of the velocity difference Δw.

6.1 Mass Flow Equation

The mass flow rate in a cross-section is related to the average axial momentum I of a pipe segment

$$I = \int_V \rho w \, dV = \int_{\Delta z} \int_A \rho w \, dA dz = \int_{\Delta z} \dot{m} \, dz \tag{6.1}$$

For an axial range becoming infinitesimal small we obtain

$$\lim_{\Delta z \to dz} I = \dot{m} \Delta z \tag{6.2}$$

while for a finite length Δz the quotient $I/\Delta z$ can be regarded as an average mass flow rate through a pipe segment. The time derivative of this average mass flow rate is then

$$\Delta z \frac{d\dot{m}}{dt} = \frac{dI}{dt} \tag{6.3}$$

Substitution of the right hand side of eq. (6.3) with the momentum balance eq. (4.26) gives a differential equation for the average mass flow rate

$$\Delta z \frac{d\dot{m}}{dt} = \dot{I}_1 - \dot{I}_2 + \rho \boldsymbol{g} \boldsymbol{e}_z V + (p_1 - p_2) A + F_w \tag{6.4}$$

where the gravity and pressure force terms from section 4.2 have been inserted. The momentum flow was found to be

$$\dot{I} = \dot{m} w + \dot{m}_{corr} \Delta w \tag{6.5}$$

where the second term on the right hand side accounts for the effect of slip-flow.

Wall Friction Force

The wall friction force can be expressed as follows

$$F_w = \int_{A_w} \tau dA = \tau_w A_w = \tau_w \kappa_w A \tag{6.6}$$

where τ_w denotes the average sheer stress and κ_w denotes the wall area per cross-sectional area, which for a pipe segment of length Δz is

$$\kappa_w = \frac{A_w}{A} = \frac{\pi D \Delta z}{\pi \frac{D^2}{4}} = \frac{4\Delta z}{D} \tag{6.7}$$

The average shear stress τ_w is usually expressed in terms of a friction factor ξ, which relates the shear stress to the dynamic pressure $\rho w^2/2$. To make sure that τ_w is directed inverse to the flow direction, it is written as follows

$$\tau_w = -\frac{\xi}{8} \rho w |w| \tag{6.8}$$

Inserting κ_w and τ_w into eq. (6.6) yields

$$F_w = -\xi \frac{\Delta z}{2D} \rho w |w| A \tag{6.9}$$

Division by $V = A\Delta z$ yields the pressure drop due to wall friction

$$\Delta p_w = -\xi \frac{\Delta z}{D} \rho \frac{w|w|}{2} \tag{6.10}$$

Correlations for ξ in the one- and two-phase regions are found in appendix B. The wall friction force in eq. (6.9) can also be written as follows

$$F_w = -\xi \frac{\Delta z}{2D} \dot{m} |w| \tag{6.11}$$

6.2 Static Slip-Flow Equation

In a homogeneous flow, the correction mass flow rate $\dot{m}_{corr}$ appearing in the convection terms for momentum and enthalpy equals zero, and eq. (6.4) provides sufficient information to close the system of equations. In a heterogeneous flow, an additional equation is required to determine the mass flow rate of each phase. Empirical approaches usually correlate two parameters among $\dot{x}$, S and γ. A correlation containing $\dot{x}$ or S as independent parameter would require a numerical solution. For that reason a correlation by Levy, cited by Wang [19],

$$\dot{x} = \frac{\gamma(1-2\gamma) + \gamma\sqrt{(1-2\gamma)^2 + \gamma[2\frac{\rho'}{\rho''}(1-\gamma)^2 + \gamma(1-2\gamma)]}}{2\frac{\rho'}{\rho''}(1-\gamma)^2 + \gamma(1-2\gamma)} \tag{6.12}$$

is favourable, because γ is known from the thermodynamic state via eq. (5.47). Moreover the equation contains no empirical variables, and no flow regimes have to be considered. The equation is therefore easier to handle than more detailed approaches such as listed in [10]. In the root term of eq. (6.12) the term $(1-\gamma)^2$ can be factored out

$$\dot{x} = \frac{\gamma(1-2\gamma) + \gamma(1-\gamma)\sqrt{(1-2\gamma) + 2\gamma\frac{\rho'}{\rho''}}}{2\frac{\rho'}{\rho''}(1-\gamma)^2 + \gamma(1-2\gamma)} \tag{6.13}$$

In fig. 6.1 $\dot{x}$ from eq. (6.13) and $x = \gamma\rho''/\rho$ are plotted against the void fraction for R22 at $p = 5\,\mathrm{bar}$.

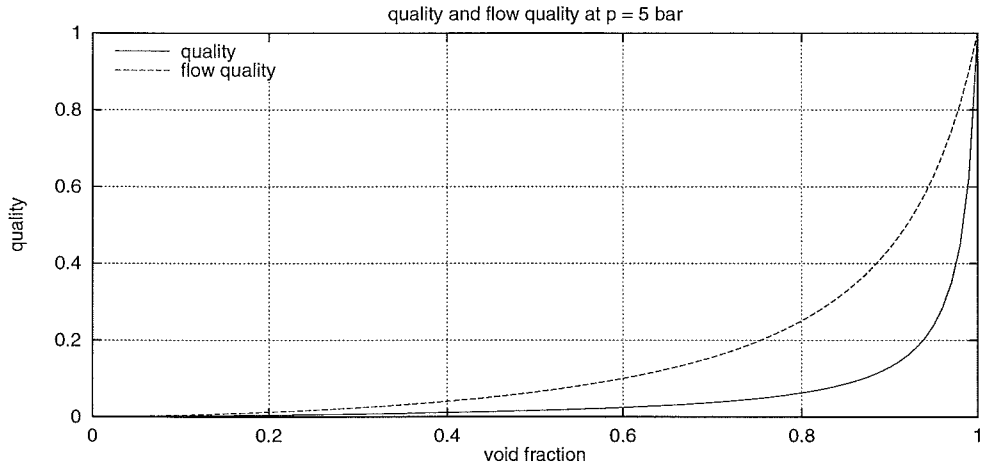

Figure 6.1 Flow quality and quality as functions of the void fraction

It can be seen that for a given void fraction the quality is always smaller than the flow quality $x < \dot{x}$. In a steady state the flow quality is determined by the energy balance eq. (5.4)

$$\dot{H} = \dot{m}\left[\dot{x}h'' + (1-\dot{x})h'\right] = \dot{H}_1 + \dot{Q} \tag{6.14}$$

For a given heat flux $\dot{Q}$ and inlet enthalpy flux $\dot{H}_1$ the equation can be solved for $\dot{x}$

$$\dot{x} = \frac{\dot{H}_1 + \dot{Q}}{\dot{m}(h'' - h')} - \frac{h'}{h'' - h'} \tag{6.15}$$

Therefore, $\dot{x}$ and thus $\dot{m}'$ and $\dot{m}''$ at the outlet are determined. Since $\dot{m}'' = \gamma\rho''w''A$ a higher vapour velocity enforces a lower void fraction and thus a lower quality. From eq. (3.51) follows that the difference between $\dot{x}$ and x is proportional to Δw

$$\dot{x} - x = x(1-x)\frac{\Delta w}{w} \tag{6.16}$$

Eq. (6.16) can be solved for the velocity difference. Employing eq. (3.16) yields

$$\frac{\Delta w}{w} = \frac{\rho}{\gamma(1-\gamma)\rho'\rho''}\left[\dot{x}\rho - \gamma\rho''\right] \tag{6.17}$$

From this equation Δw can also be computed in the limiting cases $\gamma \rightarrow 0$ and $\gamma \rightarrow 1$: Inserting eq. (6.13) and using eq. (3.17) yields

$$\frac{\Delta w}{w} = \frac{\rho}{\gamma(1-\gamma)\rho'\rho''}\left[\frac{\rho\gamma(1-\gamma)\sqrt{(1-2\gamma)+2\gamma\frac{\rho'}{\rho''}} - \gamma(1-\gamma)\rho'}{2\frac{\rho'}{\rho''}(1-\gamma)^2 + \gamma(1-2\gamma)}\right] \tag{6.18}$$

Now $\gamma(1-\gamma)$ can be cancelled down

$$\frac{\Delta w}{w} = \frac{\rho}{\rho'} \cdot \frac{\rho\sqrt{(1-2\gamma)+2\gamma\frac{\rho'}{\rho''}} - \rho'}{2(1-\gamma)^2\rho' + \gamma\rho''(1-2\gamma)} \tag{6.19}$$

From eq. (6.19) the related liquid and vapour velocities are obtained via eq. (3.46) and eq. (3.47). To enable an evaluation independent of the average velocity these equations are divided by w

$$\frac{w''}{w} = 1 + (1-x)\frac{\Delta w}{w} \qquad \frac{w'}{w} = 1 - x\frac{\Delta w}{w} \tag{6.20}$$

Division of these terms yields the slip ratio $S = w''/w'$. The results obtained for $p = 5$ bar are shown in fig. 6.2.

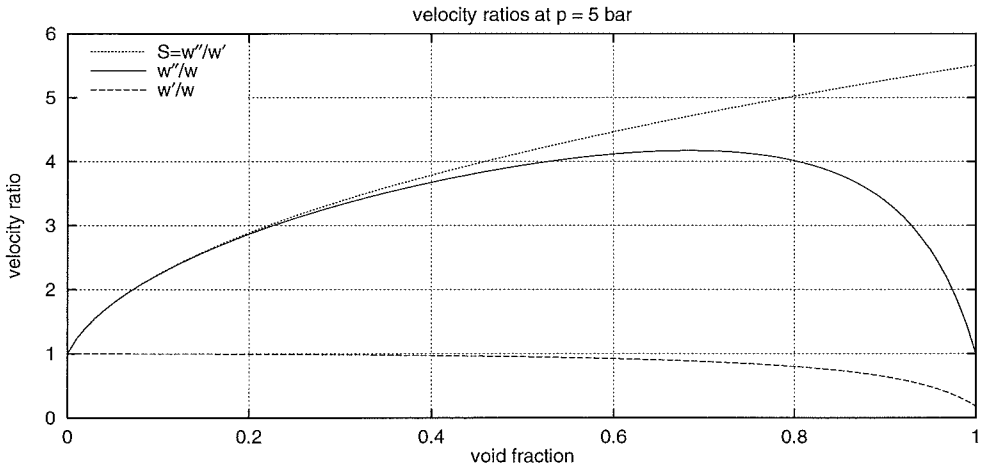

Figure 6.2 Velocity ratios as functions of the void fraction

At $\gamma = 0$ both velocities are equal, while at $\gamma = 1$ the velocity of the last evaporating drops is about 20% of the vapour velocity. The latter result is arguable in a spray flow, where the liquid drops with a vanishing diameter are more likely to be accelerated to the vapour velocity.

6.3 Dynamic Approach

The static slip-flow equation derived in the previous section does not account for acceleration effects. Differential equations containing these effects can be obtained from the separate momentum balances derived in section 4.2. One might use these equations in a similar way as eq. (6.3) to compute the mass flow rates of each phase

$$\Delta z \frac{d\dot{m}''}{dt} = \frac{dI''}{dt} \qquad \Delta z \frac{d\dot{m}'}{dt} = \frac{dI'}{dt} \tag{6.21}$$

The velocities, however, would then have to be computed from

$$w'' = \frac{\dot{m}''}{\gamma \rho'' A} \qquad w' = \frac{\dot{m}'}{\gamma \rho' A} \tag{6.22}$$

which obviously causes computational problems, if γ tends to one or zero, because the velocity of the vanishing phase then tends to 0/0. A numerical evaluation of this term usually leads to a division by zero singularity.

Differential equations for the velocities provide a better basis to avoid singularities. From a differentiation of $I'' = w''M''$ we get

$$M'' \frac{dw''}{dt} = \frac{dI''}{dt} - w'' \frac{dM''}{dt} \tag{6.23}$$

Inserting the vapour mass balance eq. (4.9) and the axial component of the vapour momentum balance eq. (4.42) yields

$$M'' \frac{dw''}{dt} = \dot{m}_1''(w_1'' - w'') - \dot{m}_2''(w_2'' - w'') - w'' \int_{A_{int}} \mu''\, dA + \int_{A_{int}} \mu'' w_{int}''\, dA + \sum F'' \tag{6.24}$$

By replacing $''$ with $'$ we obtain the equation for the liquid velocity

$$M' \frac{dw'}{dt} = \dot{m}_1'(w_1' - w') - \dot{m}_2'(w_2' - w') - w' \int_{A_{int}} \mu'\, dA + \int_{A_{int}} \mu' w_{int}'\, dA + \sum F' \tag{6.25}$$

To solve these equations for the velocity derivatives, they have to be divided by M'' and M' respectively. As pointed out in [7][1], this division is also legitimate for $M'' \rightarrow 0$ and $M' \rightarrow 0$, because the right hand side of the equation for the vanishing phase also tends to zero. However, the limiting value of the velocity derivative cannot be computed numerically; a division by 0 singularity would occur.

The problem can be solved by applying a number of simplifying assumptions to the terms on the right hand side of eq. (6.24) and eq. (6.25). In the following sections these terms will be rearranged to include M'' or M' as a factor, so that the masses can be eliminated from the equations.

[1] referring to the differential form of eq. (6.24) and eq. (6.25)

Convective Momentum Transfer

In the convective term of eq. (6.24) the average velocity inside the control volume w'' and the average mass flow rate $\dot{m}'' = \gamma\rho''w''A$ will be approximated by the arithmetic average values of the related quantities at in- and outlet[2]:

$$\begin{aligned}\dot{m}_1''(w_1'' - w'') - \dot{m}_2''(w_2'' - w'') &= \dot{m}_1''(w_1'' - \frac{w_1'' + w_2''}{2}) - \dot{m}_2''(w_2'' - \frac{w_1'' + w_2''}{2}) \\ &= \dot{m}_1''\frac{w_1'' - w_2''}{2} - \dot{m}_2''\frac{w_2'' - w_1''}{2} \\ &= \frac{\dot{m}_1'' + \dot{m}_2''}{2}(w_1'' - w_2'') \\ &= \gamma\rho''w''A(w_1'' - w_2'')\end{aligned}$$

Inserting $w'' = (w_1'' + w_2'')/2$ and rearranging yields

$$\dot{m}_1''(w_1'' - w'') - \dot{m}_2''(w_2'' - w'') = \gamma\rho''A\frac{w_1''^2 - w_2''^2}{2} \tag{6.26}$$

In a similar manner we can rewrite the convection term in eq. (6.25)

$$\dot{m}_1'(w_1' - w') - \dot{m}_2'(w_2' - w') = (1-\gamma)\rho'A\frac{w_1'^2 - w_2'^2}{2} \tag{6.27}$$

Acceleration Due to Phase Change

The integral in the third terms on the right hand side of eq. (6.24) and eq. (6.25) represent the mass flow rate over the interface. It will be denoted as $\dot{m}_{int}$ and defined positive for a flow towards the vapour. Since $\mu'' = -\mu'$ the following definitions are equivalent

$$\dot{m}_{int} := \int_{A_{int}} \mu''\, dA = -\int_{A_{int}} \mu'\, dA \tag{6.28}$$

Provided $\dot{m}_{int}$ is equally distributed over the interface, then the interfacial mass velocity does not vary spatially, thus

$$\dot{m}_{int} = \mu''A_{int} = -\mu'A_{int} \tag{6.29}$$

Following the premise made, the mass velocity can also be extracted from the integral in the fourth terms of eq. (6.24) and eq. (6.25). The remaining integrals then represent average axial vapour and liquid velocities on the interface. For the vapour we obtain

$$\int_{A_{int}} \mu''w_{int}''\, dA = \dot{m}_{int}\frac{1}{A_{int}}\int_{A_{int}} w_{int}''\, dA = \dot{m}_{int}\bar{w}_{int}'' \tag{6.30}$$

[2]In a finite difference approach these manipulations are obtained directly from $d(\dot{m}w) - wd\dot{m} = \dot{m}dw$, which is, however, only true for an infinitesimal small difference. The control volume approach reveals the assumptions actually made when applying this relation to a finite difference.

The related liquid term can be rewritten in the same way. The third and fourth terms in eq. (6.24) and eq. (6.25) finally take the form

$$-w'' \int_{A_{int}} \mu''\, dA + \int_{A_{int}} \mu'' w''_{int}\, dA = -(w'' - \bar{w}''_{int})\dot{m}_{int} \quad (6.31)$$

$$-w' \int_{A_{int}} \mu'\, dA + \int_{A_{int}} \mu' w'_{int}\, dA = -(\bar{w}'_{int} - w')\dot{m}_{int} \quad (6.32)$$

For a flow where the interfacial mass flow is primarily perpendicular to the flow direction eq. (4.17) can be used, which after averageing over the interface turns to

$$\bar{w}''_{int} \approx \bar{w}'_{int} \approx \bar{w}_{int} \quad (6.33)$$

where $\bar{w}_{int}$ is the average interfacial velocity (the velocity of displacement of the interfacial area). During an evaporation a particle passing through the interface accelerates from the average liquid velocity w' to the average vapour velocity w''. The evaporating mass flow causes a reaction force

$$F_{evap} = -(w'' - w')\dot{m}_{int} \quad (6.34)$$

From eq. (6.31) and eq. (6.32) we can conclude that each phase is slowed down by a fraction of this force, which depends on the value of $\bar{w}_{int}$. Using a factor ε to denote the fraction of the acceleration force that acts upon the vapour we can write

$$F''_{evap} = -\varepsilon(w'' - w')\dot{m}_{int} = -(w'' - \bar{w}_{int})\dot{m}_{int} \quad (6.35)$$

$$F'_{evap} = -(1-\varepsilon)(w'' - w')\dot{m}_{int} = -(\bar{w}_{int} - w')\dot{m}_{int} \quad (6.36)$$

In an isentropic process the force is equally shared by both phases [18], ε then takes the value 0.5. Another assumption is obtained from solving eq. (6.35) for $\bar{w}_{int}$

$$\bar{w}_{int} = \varepsilon w' + (1-\varepsilon)w'' \quad (6.37)$$

For $\varepsilon = 1$ we get $\bar{w}_{int} = w'$, which is the case in spray flows: The velocity on the surface of a small liquid drop hardly differs from the average velocity of the liquid inside the drop. Spray flow appears for high values of the void fraction, $\gamma \to 1$. For $\varepsilon = 0$ the above equation turns to $\bar{w}_{int} = w''$, which can be assumed in bubbly flows appearing at low void fractions $\gamma \to 0$. These considerations show, that ε is related to γ. Thus

$$\varepsilon \approx \gamma \quad (6.38)$$

will be used as a first approach that fulfils the conditions in the limiting cases discussed above.

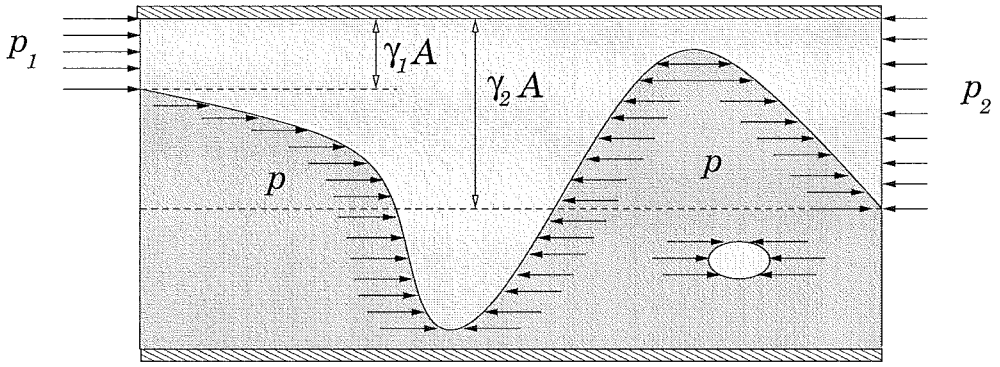

Figure 6.3 Vapour pressure force

Gravity and Pressure Force

The axial components of the gravitational forces, derived in section 4.2, require no further manipulation

$$F_g'' = \gamma\rho''\boldsymbol{g}\boldsymbol{e}_z V \qquad F_g' = (1-\gamma)\rho'\boldsymbol{g}\boldsymbol{e}_z V \tag{6.39}$$

In the equation for the axial pressure force, eq. (4.38), the contribution of the interfacial pressure is not yet modelled

$$F_p'' = p_1 A_1'' - p_2 A_2'' - \int_{A_{int}} p\boldsymbol{n}_{int}''\boldsymbol{e}_z \, dA \tag{6.40}$$

To evaluate the integral we consider the pressure p at the interface to be constant. The resulting force acting from the interface towards the vapour phase in axial direction is obtained from a multiplication of p with the axial projection area of A_{int}. As shown in fig. 6.3 the forces cancel themselves out at waves, bubbles, etc. The force not compensated is $p(A_2'' - A_1')$. Employing the void fraction in a cross sectional area eq. (3.15) yields

$$F_p'' = (\gamma_1 p_1 - \gamma_2 p_2)A + p(\gamma_2 - \gamma_1)A \tag{6.41}$$

The average pressure p will approximated by the arithmetic average of the pressures at in- and outlet, which yields

$$\begin{aligned} F_p'' &= (\gamma_1 p_1 - \gamma_2 p_2)A + \frac{p_1 + p_2}{2}(\gamma_2 - \gamma_1)A \\ &= (p_1 - p_2)\frac{\gamma_1 + \gamma_2}{2}A \end{aligned}$$

Applying the same approximation to the void fraction yields

$$F_p'' = (p_1 - p_2)\gamma A \tag{6.42}$$

Since the liquid and the vapour pressure force must sum up to $F_p = (p_1 - p_2)A$, the liquid pressure force is

$$F_p' = (p_1 - p_2)(1-\gamma)A \tag{6.43}$$

Friction Force

The friction force acting on a phase is the sum of the wall friction and the interfacial friction.

Wall Friction The wall friction force acting upon each phase depends on the fraction of the wall area in contact with the phase and the shear stress at the wall

$$F''_w = \int_{A''_w} \tau''_z \, dA \qquad F'_w = \int_{A'_w} \tau'_z \, dA \tag{6.44}$$

the sum of these yields the overall wall friction force

$$F_w = F''_w + F'_w \tag{6.45}$$

which in section 6.1 has been expressed as follows

$$F_w = -\xi \frac{\Delta z}{2D} \rho w|w| A \tag{6.46}$$

The fraction of F_w acting upon the liquid phase rises with the wetted fraction of the pipe wall. In most flow regimes the wall can be considered as completely wetted, and the entire friction force acts upon the liquid, $F'_w \approx F_w$. In horizontal pipes, however, the wall gets partially dry as the void fraction increases, and for $\gamma \rightarrow 1$ the condition $F''_w \rightarrow F_w$ must be fulfilled in any case.

The vapour fraction of the wall friction should therefore rise from almost zero up to one when the void fraction tends to one. This can qualitatively be achieved by resolving the density $\rho = \gamma\rho'' + (1-\gamma)\rho'$ into the sum of the partial densities

$$F''_w = -\xi \frac{\Delta z}{2D} \gamma\rho'' w|w| A \tag{6.47}$$

$$F'_w = -\xi \frac{\Delta z}{2D} (1-\gamma)\rho' w|w| A \tag{6.48}$$

With eq. (3.16) this is equivalent to

$$F''_w = xF_w \qquad F'_w = (1-x)F_w \tag{6.49}$$

The quality thus serves as a parameter denoting the fraction of the wall force acting upon the vapour. As fig. 6.1 shows, it provides a qualitatively correct dependence on the void fraction.

Interfacial Friction Due to the condition of equilibrium of tangential forces at the interface, eq. (4.50), the interfacial friction forces must sum up to zero

$$F''_{int} + F'_{int} = 0 \tag{6.50}$$

The axial vapour wall friction can be written as follows

$$F''_{int} = \int_{A_{int}} \tau''_{int}\, dA = \bar{\tau}''_{int} A_{int} = \bar{\tau}''_{int} \kappa_{int} A \tag{6.51}$$

where κ_{int} is the interfacial area divided by the cross-sectional area. Empirical approaches for the interfacial shear stress $\bar{\tau}''_{int}$ usually have the same form as the one for the shear stress at the wall eq. (6.8). The relevant velocity is the velocity difference $\Delta w = w'' - w'$. If it is positive, the vapour is decelerated, thus

$$\bar{\tau}''_{int} = -\frac{\zeta}{8} \rho_{ref} \Delta w |\Delta w| \tag{6.52}$$

which gives

$$F''_{int} = -\frac{\zeta}{8} \rho_{ref} \Delta w |\Delta w| \kappa_{int} A \tag{6.53}$$

To make a proper choice for the reference density eq. (6.53) is rewritten similar to eq. (6.11)

$$F''_{int} = -\frac{\zeta}{8} \dot{m}_{ref} |\Delta w| \kappa_{int} \tag{6.54}$$

with $\dot{m}_{ref} = \rho_{ref} \Delta w A$. No mass actually moves with the velocity Δw. Viewed from an observer moving with the liquid, it is the velocity of the vapour and vice versa, leaving it to the point of view, which density is to be considered as relevant.

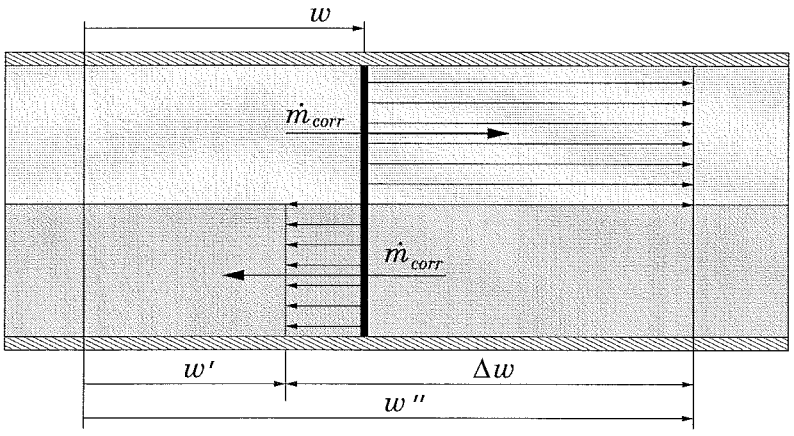

Figure 6.4 Relative mass flow rates

A mass flow that is related to both phases is the correction mass flow, defined in eq. (3.50). As explained in section 3.3, for an observer moving at average velocity w both phases have the same mass flow rate $\dot{m}_{corr}$, but opposite flow directions, fig. 6.4. Applying the wall friction force analogy for the vapour in fig. 6.4 yields $F''_{int} \sim \dot{m}_{corr} \Delta w$. For the liquid we find $F'_{int} \sim -\dot{m}_{corr} \Delta w$. The

approach is in accord with the condition eq. (6.50). Moreover, since $\dot{m}_{corr} \sim \Delta w$, the resulting force is proportional to the square of the velocity difference, which is consistent with eq. (6.53), thus

$$\dot{m}_{ref} = \dot{m}_{corr} = x(1-x)\rho\Delta w A \tag{6.55}$$

will be used. Now eq. (6.54) gets

$$F''_{int} = -\frac{\zeta}{8}x(1-x)\rho\Delta w A|\Delta w|\kappa_{int}A \tag{6.56}$$

Multiplication with $1 = \kappa_w/\kappa_w$ and employing eq. (6.7) yields

$$F''_{int} = -\zeta\frac{\Delta z}{2D}x(1-x)\rho\Delta w|\Delta w|\frac{\kappa_{int}}{\kappa_w}A \tag{6.57}$$

Due to the difficulty of predicting the interfacial area, the term κ_{int}/κ_w will be included in the friction factor

$$F''_{int} = -\zeta^*\frac{\Delta z}{2D}x(1-x)\rho\Delta w|\Delta w|A \tag{6.58}$$

where

$$\zeta^* = \zeta\frac{\kappa_{int}}{\kappa_w} = \zeta\frac{A_{int}}{A_w} = \zeta\frac{A_{int}}{\pi D\Delta z} \tag{6.59}$$

is to be determined empirically. Eq. (6.58) has the advantage that, as a first approach, ζ^* may be approximated by a constant value, since the condition, that the interfacial area disappears for $\gamma\to 0$ and $\gamma\to 1$, is implicitly fulfilled by the factor $x(1-x)$ which after insertion of eq. (3.16) can also be expressed as

$$x(1-x) = x\frac{(1-\gamma)\rho'}{\rho} = (1-x)\frac{\gamma\rho''}{\rho} \tag{6.60}$$

Contrary to eq. (6.53) with the common choice $\rho_{ref} = \rho''$ [18], eq. (6.58) also allows explicit division by γ and $(1-\gamma)$.

6.4 Dynamic Slip-Flow Equation

Inserting the equations for the forces and convection terms derived in the previous section into the differential equation for the vapour velocity eq. (6.24) yields with $M'' = \gamma\rho''\Delta z A$ and eq. (6.60)

$$\begin{aligned}\gamma\rho''\Delta z A\frac{dw''}{dt} &= \gamma\rho'' A\frac{w_1''^2 - w_2''^2}{2} - \gamma(w'' - w')\dot{m}_{int} \\ &\quad +\gamma\rho''\boldsymbol{g}\boldsymbol{e}_z\Delta z A + (p_1 - p_2)\gamma A \\ &\quad -\frac{\Delta z}{2D}\gamma\rho'' A\left[\xi w|w| + \zeta^*(1-x)\Delta w|\Delta w|\right]\end{aligned} \tag{6.61}$$

The same procedure carried out for the average liquid velocity yields with $F''_{int} = -F'_{int}$

$$\begin{aligned}(1-\gamma)\rho' \Delta z A \frac{dw'}{dt} &= (1-\gamma)\rho' A \frac{{w'_1}^2 - {w'_2}^2}{2} - (1-\gamma)(w'' - w')\dot{m}_{int} \\ &+(1-\gamma)\rho' \boldsymbol{g} e_z \Delta z A + (p_1 - p_2)(1-\gamma)A \\ &-\frac{\Delta z}{2D}(1-\gamma)\rho' A \left[\xi w|w| - \zeta^* x \Delta w|\Delta w|\right] \end{aligned} \tag{6.62}$$

These equations can now be divided by $\gamma\rho'' A$ and $(1-\gamma)\rho' A$ respectively. Using a specific interfacial mass flow rate ν

$$\nu := \frac{\dot{m}_{int}}{A} = \frac{1}{A}\int_{A_{int}} \mu''\, dA \tag{6.63}$$

we obtain

$$\begin{aligned}\Delta z \frac{dw''}{dt} &= \frac{{w''_1}^2 - {w''_2}^2}{2} + \frac{1}{\rho''}(p_1 - p_2 - \Delta w \nu) + \boldsymbol{g} e_z \Delta z \\ &-\frac{\Delta z}{2D}\left[\xi w|w| + \zeta^*(1-x)\Delta w|\Delta w|\right] \end{aligned} \tag{6.64}$$

and

$$\begin{aligned}\Delta z \frac{dw'}{dt} &= \frac{{w'_1}^2 - {w'_2}^2}{2} + \frac{1}{\rho'}(p_1 - p_2 - \Delta w \nu) + \boldsymbol{g} e_z \Delta z \\ &-\frac{\Delta z}{2D}\left[\xi w|w| - \zeta^* x \Delta w|\Delta w|\right] \end{aligned} \tag{6.65}$$

Numerical integration of these equations yields the velocities w'' and w'. The mass flow rates $\dot{m}''$ and $\dot{m}'$ are then obtained from eq. (3.35) and eq. (3.36). In that case the differential equation for the overall mass flow rate eq. (6.4) is not needed. The equations for the velocity difference are, however, applicable only in the two-phase region. In the one-phase region the equation for the mass flow rate eq. (6.4) must be used instead.

To avoid a switching of differential equations, it is desirable to use the equation for the mass flow rate eq. (6.4) also in the two-phase region. As a second equation either eq. (6.64) or eq. (6.65) can be applied, but the choice is difficult. Therefore, a combination of both will be used: Subtraction of eq. (6.65) from eq. (6.64) yields a differential equation for the velocity difference, a dynamic slip-flow equation

$$\begin{aligned}\Delta z \frac{d\Delta w}{dt} &= \frac{{w''_1}^2 - {w''_2}^2 - {w'_1}^2 + {w'_2}^2}{2} + \left[\frac{1}{\rho''} - \frac{1}{\rho'}\right][p_1 - p_2 - \Delta w \nu] \\ &-\zeta^* \frac{\Delta z}{2D}\Delta w|\Delta w| \end{aligned} \tag{6.66}$$

As can be seen, the gravitational force and the wall friction terms have vanished; the latter result follows from the modelling approach made in eq. (6.49).

The interfacial friction in eq. (6.66) appears in the form of wall friction term. The pressure gradient is reduced by the acceleration force.

From the mass flow rate and the velocity difference the vapour and liquid velocities can be computed from eq. (3.46) and eq. (3.47). Since the average velocity w is defined via $\dot{m} = \rho w A$ this gives

$$w'' = \frac{\dot{m}}{\rho A} + (1 - x)\Delta w \tag{6.67}$$

$$w' = \frac{\dot{m}}{\rho A} - x\Delta w \tag{6.68}$$

Using an average velocity

$$\bar{w} = \frac{w'' + w'}{2} \tag{6.69}$$

eq. (6.66) can be rewritten in a more compact way

$$\Delta z \frac{d\Delta w}{dt} = \bar{w}_1 \Delta w_1 - \bar{w}_2 \Delta w_2 + \left[\frac{1}{\rho''} - \frac{1}{\rho'}\right][p_1 - p_2 - \Delta w \nu] - \zeta^* \frac{\Delta z}{2D} |\Delta w| \Delta w \tag{6.70}$$

A similar equation for Δw has been derived by Kolev [10] on the basis of the differential form of the balance equations. However, the terms for the interfacial mass transfer and friction therein are not modelled and the equation cannot be applied in the limiting cases $\gamma \to 0$ and $\gamma \to 1$. Contrary to this, the above equation has the advantage that no singularities appear at the one/two-phase boundary. The equation can easily be replaced by the static slip-flow equation eq. (6.19) or the homogeneous model $\Delta w = 0$ to switch between different modelling approaches.

Interfacial Mass Transfer

The specific interfacial mass flow rate $\nu = \dot{m}_{int}/A$ is not yet determined. Under the assumption of two-phase equilibrium $\dot{m}_{int}$ can be expressed as a function of the rate of change of mass and pressure. The interfacial mass flow rate appears as the last term in the vapour mass balance eq. (4.9)

$$\frac{dM''}{dt} = \dot{m}_1'' - \dot{m}_2'' + \dot{m}_{int} \tag{6.71}$$

To compute $\dot{m}_{int}$ from this equation, the derivative on the left hand side must be determined from another condition: The volume of the control volume adds up from the fractions of both phases.

$$V = V' + V'' = \frac{M''}{\rho''} + \frac{M'}{\rho'} \tag{6.72}$$

Differentiating this equation by the time leads to

$$\frac{dV}{dt} = \frac{1}{\rho''}\frac{dM''}{dt} + \frac{1}{\rho'}\frac{dM'}{dt} - \frac{M''}{\rho''^2}\frac{d\rho''}{dt} - \frac{M'}{\rho'^2}\frac{d\rho'}{dt} \tag{6.73}$$

Inserting $dM' = dM - dM''$ and $M'' = \gamma\rho''V$ and $M' = (1-\gamma)\rho'V$ yields

$$\frac{dV}{dt} = \left[\frac{1}{\rho''} - \frac{1}{\rho'}\right]\frac{dM''}{dt} + \frac{1}{\rho'}\frac{dM}{dt} - \frac{\gamma}{\rho''}V\frac{d\rho''}{dt} - \frac{1-\gamma}{\rho'}V\frac{d\rho'}{dt} \tag{6.74}$$

At saturation equilibrium the densities are dependent on the pressure only, thus

$$\frac{dV}{dt} = \frac{\rho' - \rho''}{\rho''\rho'}\frac{dM''}{dt} + \frac{1}{\rho'}\frac{dM}{dt} - V\left[\frac{\gamma}{\rho''}\frac{d\rho''}{dp} + \frac{1-\gamma}{\rho'}\frac{d\rho'}{dp}\right]\frac{dp}{dt} \tag{6.75}$$

Solving for the vapour mass derivative yields with $V = \text{const}$

$$(\rho' - \rho'')\frac{dM''}{dt} = -\rho''\frac{dM}{dt} + V\left[\gamma\rho'\frac{d\rho''}{dp} + (1-\gamma)\rho''\frac{d\rho'}{dp}\right]\frac{dp}{dt} \tag{6.76}$$

where dM/dt and dp/dt are known from eq. (5.3) and eq. (5.20). The interfacial mass flow rate can now be computed from the vapour mass balance

$$\dot{m}_{int} = \frac{dM''}{dt} + \dot{m}_2'' - \dot{m}_1'' \tag{6.77}$$

Interfacial Friction Factor

The modified interfacial friction factor ζ^* in eq. (6.70) is considered to be determined empirically. It includes the influence of the interfacial friction friction factor ζ and the interfacial area A_{int}

$$\zeta^* = \zeta\frac{A_{int}}{A_w} \tag{6.78}$$

With the help of the static slip-flow equation eq. (6.19) it is possible to obtain a first guess in case of a stationary adiabatic two-phase flow. In that case the left hand side of eq. (6.70) equals zero. In an adiabatic process evaporation occurs only due to the pressure loss. The related interfacial mass velocity ν is negligible. Moreover, the change of density is small and thus the velocities remain almost constant. The dynamic slip-flow equation then reads

$$0 = \left[\frac{1}{\rho''} - \frac{1}{\rho'}\right][p_1 - p_2] - \zeta^*\frac{\Delta z}{2D}\Delta w|\Delta w| \tag{6.79}$$

Applying the same simplifications to the mass flow equation eq. (6.4) gives with eq. (6.9)

$$0 = \rho g e_z V + (p_1 - p_2)A - \xi\frac{\Delta z}{2D}\rho w|w|A \tag{6.80}$$

Eliminating the pressure difference from both equations yields

$$\zeta^*\frac{\Delta z}{2D}|\Delta w|\Delta w = \left[\frac{1}{\rho''} - \frac{1}{\rho'}\right]\left[\xi\frac{\Delta z}{2D}\rho w|w| - \rho g e_z \Delta z\right] \tag{6.81}$$

In a horizontal pipe the gravity term vanishes

$$\zeta^* = \xi \left[\frac{\rho}{\rho''} - \frac{\rho}{\rho'} \right] \frac{w}{\Delta w} \left| \frac{w}{\Delta w} \right| \tag{6.82}$$

From this equation it becomes obvious that a homogeneous model $\Delta w = 0$ is equivalent to an infinite interfacial friction. In a heterogeneous flow, the velocity ratio can be computed from eq. (6.19) and is thus a function of the pressure and the void fraction. Fig 6.5 shows the result obtained for ζ^*/ξ as a function of the void fraction.

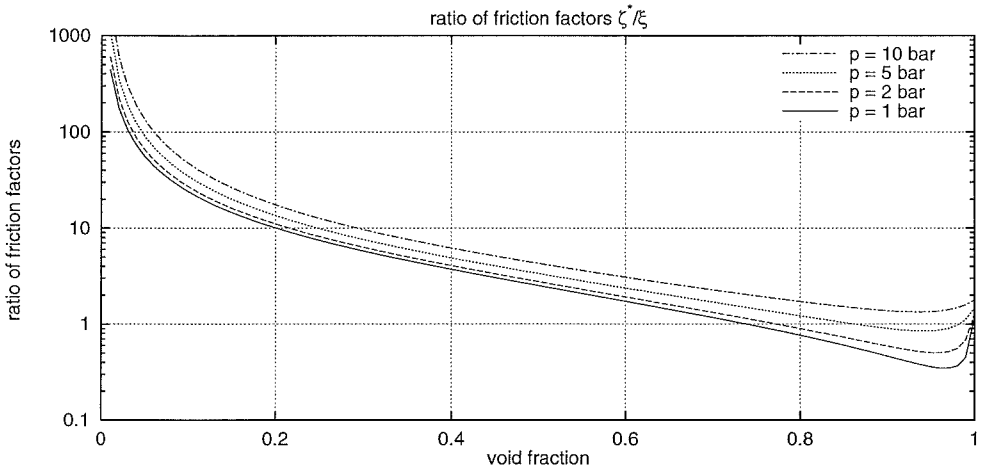

Figure 6.5 Interfacial friction factor

At low qualities, ζ^* exceeds ξ by several orders of magnitude; this is due to eq. (6.19), which yields $\Delta w = 0$ for $x = 0$. The result is in accord with the large surface area appearing in bubble flow. At higher qualities we find

$$\zeta^* = (0.3..2)\,\xi \qquad \text{for } \gamma > 0.8 \text{ and } p = 1..10 \text{ bar}; \tag{6.83}$$

Annular flow is most likely to occur in that region: The liquid forms a film covering the entire pipe wall. As the liquid mass fraction decreases the film becomes thinner and thus the interfacial area tends to the wall area $A_{int} \rightarrow A_w$. The liquid is more and more restrained and the velocity difference becomes $\Delta w \approx w$, while $\rho \rightarrow \rho'' \ll \rho'$ and thus eq. (6.82) turns to

$$\zeta^* \approx \xi \tag{6.84}$$

Depending on the pressure, ζ^* is in times even lower than ξ, which reveals that, due to the low viscosity of the vapour, the interfacial shear stress is actually small. The interfacial friction is thus dominated by the size of the interfacial area.

After passing through a minimum value at $\gamma \approx 0.95$ the curves rise again and arrive at $\zeta^* \approx 1.5\,\xi$ for $x = 1$. This is in accord with the appearance of spray flow, where the interfacial area is increased, but the actual value should rise almost as rapid as for $\gamma \rightarrow 0$. The relatively low value of ζ^* at $\gamma = 1$ is a result of the static slip flow equation, which produces a remaining velocity difference. The above function for ζ^* is thus restricted to a separated flow.

7. Discretized Model Equations

The differential equations derived in the previous chapters are now used to create a model that allows prediction of the outlet conditions of the flow through a heated or cooled straight pipe. The general approach which is taken is known as the finite volume method.

7.1 The Finite Volume Method

The main characteristic of the finite volume method, that distinguishes it from the finite difference and the finite element method, is the use of balance equations in integral form. In principle the entire pipe could be treated as one single control volume, but the results would be inaccurate, since the influence of the spatial distribution of the properties is neglected. Increased accuracy is achieved by subdividing the pipe into a number of non-overlapping control volumes, each of which is small enough to justify its representation by average properties.

If the diameter of the pipe is small compared to the length, $D \ll L$, an axial subdivision is sufficient; the control volumes are thus pipe segments. The related one-dimensional model equations have been derived in chapter 5 and 6. The outlet conditions of each pipe segment equals the inlet condition of its neighbour, but the actual interface condition is not known. Therefore, the application of the control volume method requires two preparations:

- The determination of the size and location of the control volumes,
  i.e. the grid structure
- A relation for the approximation of properties between the control volumes,
  i.e. the interface conditions

The technique chosen was first described by Patankar [13].

Grid Structure

Two different grid structures are applied: The basic grid structure serves to determine the thermodynamic state. It will be referred to as the thermal grid. The pipe is divided into n numbered cells of equal length $\Delta z = L/n$ as shown in fig. 7.1. An average state variable inside cell number i is denoted as ψ_i, while $\hat{\psi}_i$ denotes the state at the inlet of the cell. ψ_0 and ψ_{n+1} denote the state of the flow before the inlet and behind the outlet of the pipe.

To compute the mass flow rates at the interface of the thermal cells, a staggered grid is used, which will be called the flow grid. As fig. 7.2 illustrates, each thermal cell overlaps two flow cells. The entering mass flow rate of the thermal cell i is computed as the average mass flow rate of the flow cell i. The pressure between the flow cells i and $i+1$ is approximated by the average pressure in

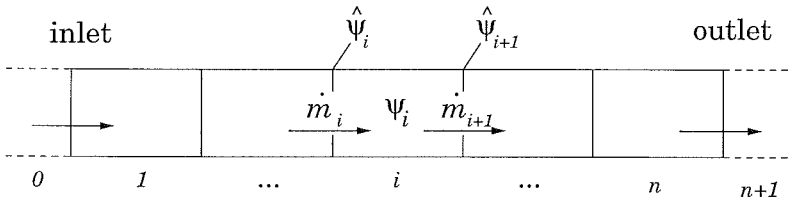

Figure 7.1 Thermal grid

the thermal cell i. The average thermodynamic properties of the flow cell i equals the state at the inlet of the thermal cell i.

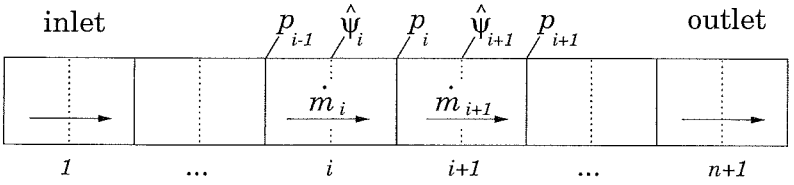

Figure 7.2 Flow grid

Interface Conditions

The thermodynamic state at the interface $\hat{\psi}_i$ is approximated by the state of the thermal cell located upstream, thus

$$\hat{\psi}_i = \delta_i \psi_i + (1 - \delta_i)\psi_{i-1} \qquad i = 1..n+1 \tag{7.1}$$

where δ_i is an indicator function denoting direction of the the mass flow

$$\delta_i = \begin{cases} 0 & \dot{m}_i \geq 0 \\ 1 & \dot{m}_i < 0 \end{cases} \tag{7.2}$$

The following interface variables are needed

$$\hat{\psi}_i = \left\{ \hat{h}_i, \hat{h}''_i, \hat{h}'_i, \hat{\rho}_i, \hat{\rho}''_i, \hat{\rho}'_i, \hat{x}_i, \hat{\gamma}_i, \hat{\nu}_i \right\} \tag{7.3}$$

The upwind method described here is recommended for convection-dominated problems. Compared to other approaches it is more stable and yields reasonable results even for a small number of cells n [13].

7.2 Pipe Model

Thermal Grid

Mass and energy balance are applied to each thermal cell. Using the numbering shown in fig. 7.2 we obtain

$$\frac{dM_i}{dt} = \dot{m}_i - \dot{m}_{i+1} \tag{7.4}$$

$$\frac{dU_i}{dt} = \dot{H}_i - \dot{H}_{i+1} + \dot{Q}_i \tag{7.5}$$

The computation of the heat flux $\dot{Q}_i$ is part of the wall model described in the next chapter. The enthalpy flow is

$$\dot{H}_i = \dot{m}_i \hat{h}_i + \dot{m}_{corr} \left(\hat{h}_i'' - \hat{h}_i' \right) \tag{7.6}$$

with a correction mass flow rate

$$\dot{m}_{corr} = \hat{x}_i (1 - \hat{x}_i) \hat{\rho}_i \Delta w_i A \tag{7.7}$$

The equations above are inserted into eq. (5.20) and eq. (5.21) to obtain differential equations for enthalpy and pressure

$$V \frac{\rho_i}{a_i^2} \frac{dp_i}{dt} = \left(\rho_i + h_i \left. \frac{\partial \rho_i}{\partial h} \right|_p \right) \frac{dM_i}{dt} - \left. \frac{\partial \rho_i}{\partial h} \right|_p \frac{dU_i}{dt} \tag{7.8}$$

$$V \frac{\rho_i}{a_i^2} \frac{dh_i}{dt} = \left(1 - h_i \left. \frac{\partial \rho_i}{\partial p} \right|_h \right) \frac{dM_i}{dt} + \left. \frac{\partial \rho_i}{\partial p} \right|_h \frac{dU_i}{dt} \tag{7.9}$$

where a_i is the velocity of sound, which is a function of the density derivatives

$$\frac{1}{a_i^2} = \left. \frac{\partial \rho_i}{\partial p} \right|_h + \frac{1}{\rho_i} \left. \frac{\partial \rho_i}{\partial h} \right|_p \tag{7.10}$$

Numerical integration of eq. (7.8) and eq. (7.9) yields the values of p_i and h_i. The related properties are computed from the equation of state described in section 5.2

$$\psi_i = \psi(p_i, h_i) \qquad \psi_i = \left\{ x_i, \gamma_i, T_i, \rho_i, \left. \frac{\partial \rho_i}{\partial p} \right|_h, \left. \frac{\partial \rho_i}{\partial h} \right|_p, \frac{d\rho_i'}{dp}, \frac{d\rho_i''}{dp} \right\} \tag{7.11}$$

The derivatives of the equilibrium liquid and vapour densities are needed to compute the interfacial mass flow rate: The vapour mass balance eq. (6.77) gives

$$\nu_i = \frac{\dot{m}_{int}}{A} = \frac{1}{A} \left[\frac{dM_i''}{dt} + \dot{m}_{i+1}'' - \dot{m}_i'' \right] \tag{7.12}$$

The unsteady term therein is obtained from

$$(\rho_i' - \rho_i'') \frac{dM_i''}{dt} = -\rho_i'' \frac{dM_i}{dt} + V \left[\gamma_i \rho_i' \frac{d\rho_i''}{dp} + (1 - \gamma_i) \rho_i'' \frac{d\rho_i'}{dp} \right] \frac{dp_i}{dt} \tag{7.13}$$

Flow Grid

The mass flow rates and velocities are calculated as average values of the flow cells. The momentum balance in the form of eq. (6.4) applied to the flow cell i in fig. 7.2 reads

$$\Delta z \frac{d\dot{m}_i}{dt} = \Delta(\dot{I})_i + \hat{\rho}_i |\boldsymbol{g}| \cos\varphi V + (p_{i-1} - p_i) A - \xi_i \frac{\Delta z}{2D} \dot{m}_i |w_i| \tag{7.14}$$

Where φ is the angle between the axial unit vector $\boldsymbol{e}_z$ and $\boldsymbol{g}$. The difference of the momentum of the entering and leaving mass in a flow cell $\Delta(\dot{I})_i$ is approximated by the average difference of the momentum flows of the overlapping thermal cells

$$\Delta(\dot{I})_i \approx \frac{\left(\dot{I}_{i-1} - \dot{I}_i\right) + \left(\dot{I}_i - \dot{I}_{i+1}\right)}{2} = \frac{1}{2}\left(\dot{I}_{i-1} - \dot{I}_{i+1}\right) \qquad i = 2..n \quad (7.15)$$

This central difference approach serves to avoid discontinuities in the momentum balance. In the entering and leaving cross section, the momentum of the cell located outside the pipe is approximated by the momentum of the first and last flow cell respectively

$$\Delta(\dot{I})_1 \approx \dot{I}_1 - \dot{I}_2 \quad (7.16)$$

$$\Delta(\dot{I})_{n+1} \approx \dot{I}_n - \dot{I}_{n+1} \quad (7.17)$$

The momentum flow is computed from

$$\dot{I}_i = \dot{m}_i w_i + \dot{m}_{corr} \Delta w_i \quad (7.18)$$

where w_i is the average velocity

$$w_i = \frac{\dot{m}_i}{\hat{\rho}_i A} \quad (7.19)$$

The velocity difference may either be neglected, which gives the homogeneous model,

$$\Delta w_i = 0 \quad (7.20)$$

or be computed from the static slip-flow equation eq. (6.19)

$$\Delta w_i = w_i \frac{\hat{\rho}_i}{\hat{\rho}'_i} \cdot \frac{\hat{\rho}_i \sqrt{(1 - 2\hat{\gamma}_i) + 2\hat{\gamma}_i \frac{\hat{\rho}'_i}{\hat{\rho}''_i}} - \hat{\rho}'_i}{2(1 - \hat{\gamma}_i)^2 \hat{\rho}'_i + \hat{\gamma}_i \hat{\rho}''_i (1 - 2\hat{\gamma}_i)} \quad (7.21)$$

or from integration of the dynamic slip-flow equation eq. (6.70)

$$\Delta z \frac{d\Delta w_i}{dt} = \Delta(\bar{w}\Delta w)_i + \left[\frac{1}{\hat{\rho}''_i} - \frac{1}{\hat{\rho}'_i}\right](p_{i-1} - p_i - \Delta w_i \hat{\nu}_i) - \zeta_i^* \frac{\Delta z}{2D} \Delta w_i |\Delta w_i| \quad (7.22)$$

where the convective term is modelled analogously to eq. (7.15)

$$\Delta(\bar{w}\Delta w)_i \approx \frac{1}{2}(\bar{w}_{i-1}\Delta w_{i-1} - \bar{w}_{i+1}\Delta w_{i+1}) \qquad i = 2..n \quad (7.23)$$

The interfacial mass flow rate per cross-sectional area $\hat{\nu}_i$ is obtained from application of the indicator function eq. (7.1), and $\bar{w}$ is an arithmetic average

$$\bar{w}_i = \frac{w_i'' + w_i'}{2} \tag{7.24}$$

In every case the velocities and mass flow rates are computed as follows

$$\begin{aligned} w_i'' &= w_i + (1 - \hat{x}_i)\Delta w_i && (7.25)\\ w_i' &= w_i - \hat{x}_i \Delta w_i && (7.26)\\ \dot{m}_i'' &= \hat{x}_i \dot{m}_i + \dot{m}_{corr} && (7.27)\\ \dot{m}_i' &= (1 - \hat{x}_i)\dot{m}_i - \dot{m}_{corr} && (7.28) \end{aligned}$$

At in- and outlet the velocity difference will be set equal to zero

$$\Delta w_1 = \Delta w_{n+1} = 0 \tag{7.29}$$

to avoid inconsistencies with other models, which are usually based on the assumption of homogeneous flow.

Closure of the System of Equations

The model contains four differential equations, i.e. the ones for p, h, $\dot{m}$ and Δw. The remaining differentials appearing in the equations above are computed from algebraic equations.

In the basic form of the model, the mass flow equations at in- and outlet are not included. The following boundary conditions are then required to close the system of equations

- pressure and enthalpy on the upstream side
- mass flow rate $\dot{m}_i$ at inlet $i = 1$ and outlet $i = n + 1$
- heat flux $\dot{Q}_i$ for every thermal cell $i = 1..n$
- heat transfer coefficient α_i for every thermal cell $i = 1..n$
- friction factors ξ_i, ζ_i^* for every flow cell $i = 1..n + 1$

This basic model is extended by submodels containing the differential equations for $\dot{m}$ at in- and/or outlet. The pressure on the related side of the pipe is then a boundary condition, regardless of the flow direction.

The heat transfer coefficients are needed in case $\dot{Q}_i$ is not known and must thus be computed from the temperature difference between pipe wall and fluid. For a known heat flux distribution, however, α may be used to compute the wall temperature. The interfacial friction factor ζ^* is only used in the dynamic heterogeneous model. The computation of α and ξ depends on the direction of the heat flux and the incline of the pipe. The case of a horizontal heated pipe is considered in the next chapter.

8. Modelling of an Evaporator

The two-phase flow model is applied to simulate an evaporator in a test refrigeration plant described in [1]. The evaporator pipe is placed inside a second pipe, fig. 8.1, where a mixture of ethanol and water flows, which will be referred to as "the fluid" (subscript f). The refrigerant R22 in the inner pipe and the fluid in the ring slot have opposite flow directions (counter-flow heat exchanger). The pipe dimensions are shown in fig. 8.2

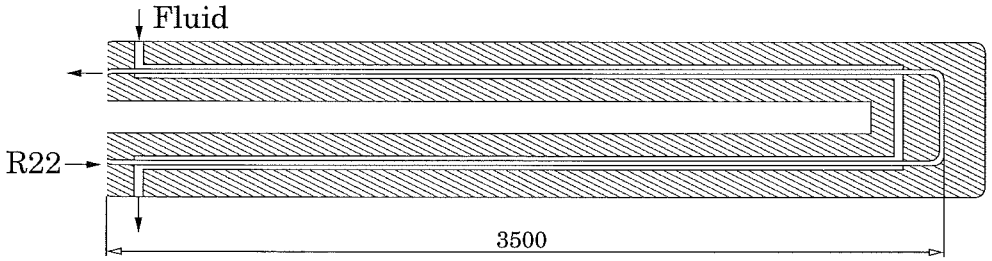

Figure 8.1 Test evaporator

8.1 Model Equations

The effect of the pipe elbows will be neglected. Two concentric straight pipes of length $L = 7\,\mathrm{m}$ form the basis of the model. Since the pipe diameter is small compared to the length of the pipe, the one-dimensional two-phase flow model from chapter 7 can be applied. Complementary models are required to compute the distribution of heat fluxes towards the refrigerant, i.e. a model for the fluid in the ring slot, which will be treated as incompressible, and a model for the heat transfer through the wall of the inner pipe.

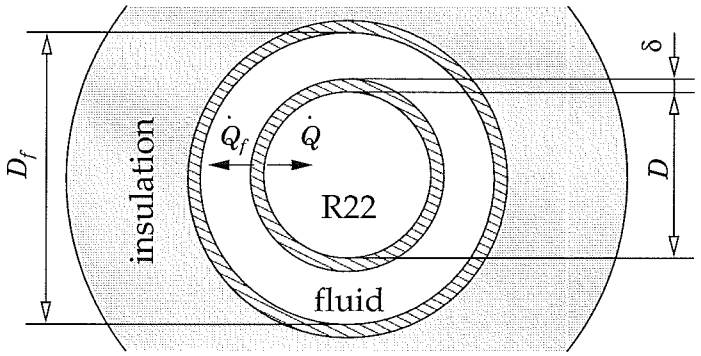

Figure 8.2 Pipe dimensions

$$D = 12.7\,\mathrm{mm} \qquad \delta = 0.8\,\mathrm{mm} \qquad D_f = 22.2\,\mathrm{mm}$$

Wall Model

The pipe consists of copper; the related properties at $T = 0\,°\mathrm{C}$ are [17]

$$\begin{aligned} \rho_w &= 8960\,\mathrm{kg/m^3} \\ c_w &= 381\,\mathrm{J/(kgK)} \\ \lambda_w &= 401\,\mathrm{W/(mK)} \end{aligned}$$

The pipe wall is separated into n elements corresponding to the number of thermal cells in the two-phase flow model, fig. 7.1. The internal energy balance eq. (4.57) is applied: Since no movement takes place within the wall, $\boldsymbol{w} = 0$, and the pressure is spatially constant, it simplifies to

$$\frac{dU_{w,i}}{dt} = \dot{Q}_{w,i} \tag{8.1}$$

with $U_w = u_w \rho_w V_w$. The specific internal energy is approximated by $u_w = c_w T_w$, where c_w is the heat capacity of the wall and T_w is the average temperature of a wall segment. The volume of the pipe wall segment is

$$V_w = \pi \frac{(D+2\delta)^2 - D^2}{4} \Delta z = \pi (D+\delta)\delta \Delta z \tag{8.2}$$

The internal energy decreases due to the heat flux towards the refrigerant on the inside

$$\dot{Q}_i = \alpha_i A_{int} \left(T_{w,i} - T_i\right) \tag{8.3}$$

and the heat flux towards the fluid on the outside

$$\dot{Q}_{f,i} = \alpha_{f,i} A_{ext} \left(T_{w,i} - T_{f,i}\right) \tag{8.4}$$

where the wall surface temperature has been approximated by the average temperature, which is justified due to the high ratio λ_w/δ. The surface areas are $A_{int} = \pi D \Delta z$ and $A_{ext} = \pi(D+2\delta)\Delta z$. The energy balance now reads with $c_w \approx$ const

$$\rho_w c_w V_w \frac{dT_{w,i}}{dt} = -\left(\dot{Q}_i + \dot{Q}_{f,i}\right) \tag{8.5}$$

The heat transfer coefficients are computed within the models for the refrigerant and the fluid.

Incompressible Fluid Model

The liquid flowing through the ring slot is ethanol with $x_{\mathrm{H2O}} = 10\,\%$ mass content water. The mixture will be treated as incompressible, the mass flow rate is therefore spatially constant and the internal energy balance eq. (4.57) reads

$$\frac{dU_{f,i}}{dt} = \dot{m}_f \left(\hat{h}_{f,i} - \hat{h}_{f,i+1}\right) + \dot{Q}_{f,i} \tag{8.6}$$

The heat loss through the insulation is neglected. With $c_f = c_p \approx c_v \approx$ const we obtain

$$\rho_f c_f V_f \frac{dT_{f,i}}{dt} = \dot{m}_f c_f \left(\hat{T}_{f,i} - \hat{T}_{f,i+1}\right) + \dot{Q}_{f,i} \tag{8.7}$$

with a volume

$$V_f = \pi \frac{(D_f^2 - D^2)}{4} \Delta z - V_w \tag{8.8}$$

The temperature on the boundary of a cell is determined by the flow direction (upwind method):

$$\hat{T}_{f,i} = \begin{cases} T_{f,i-1} & \dot{m}_f \geq 0 \\ T_{f,i} & \dot{m}_f < 0 \end{cases} \tag{8.9}$$

Since fluid and refrigerant have opposite flow directions and the numbering of cells refers to the thermal grid in the refrigerant model, the fluid mass flow rate is negative.

The properties of the fluid will be approximated by constants. From the densities at $T = 0\,^\circ\mathrm{C}$, $\rho_{H_2O} = 999.8\,\mathrm{kg/m^3}$ and $\rho_{C_2H_6O} = 807\,\mathrm{kg/m^3}$ [17], the mixture density is obtained in the same way as the density of a one-component two-phase fluid, eq. (5.46)

$$\rho_f = \frac{1}{x_{H_2O}/\rho_{H_2O} + (1 - x_{H_2O})/\rho_{C_2H_6O}} = 823\,\frac{\mathrm{kg}}{\mathrm{m^3}} \tag{8.10}$$

With $c_{H_2O} = 4217\,\mathrm{J/(kgK)}$ and $c_{C_2H_6O} = 2232\,\mathrm{J/(kgK)}$ [17] the mixture heat capacity at $T = 0\,^\circ\mathrm{C}$ gets

$$c_f = x_{H_2O} c_{H_2O} + (1 - x_{H_2O}) c_{C_2H_6O} = 2430\,\frac{\mathrm{J}}{\mathrm{kgK}} \tag{8.11}$$

Data of the thermal conductivity and dynamic viscosity of ethanol/water mixtures are listed in [15] as functions of the mole fraction of water. With the molecular weights $M_{H_2O} = 18.02\,\mathrm{kg/kmol}$ and $M_{C_2H_6O} = 46.07\,\mathrm{kg/kmol}$ the mole fraction of water is obtained via [16]

$$n_{H_2O} = x_{H_2O} \frac{M_{C_2H_6O}/M_{H_2O}}{1 + x_{H_2O}\,(M_{C_2H_6O}/M_{H_2O} - 1)} = 0.22\,\frac{\mathrm{kmol_{H_2O}}}{\mathrm{kmol}} \tag{8.12}$$

Using this value, linear interpolations of the data from [15] at $p = 1\,\mathrm{bar}$ and $T = 275\,\mathrm{K}$ give

$$\lambda_f = 196 \cdot 10^{-3}\,\mathrm{W/mK} \qquad \eta_f = 2566 \cdot 10^{-6}\,\mathrm{Pa\,s} \tag{8.13}$$

Application of eq. (B.4) yields the average fluid heat transfer coefficient. The result obtained for a cell of length $\Delta z = 1.4\,\mathrm{m}$ can be approximated by

$$\alpha_f = 4820 \cdot \dot{m}_f[\mathrm{kg/s}] - 170 \qquad \text{in } \mathrm{W/m^2K} \tag{8.14}$$

which is valid for $\dot{m}_f = 0.22\,..\,0.5\,\mathrm{kg/s}$. The deviation from eq. (B.4) is less than 1%.

Pipe Model

The model equations for a two-phase flow have been derived in chapter 7. For computation of the properties of R22 the approximation functions described in section 5.2 will be used. The transport properties are approximated by the values of the saturated vapour and liquid, which are expressed as polynomial functions.

The one-phase heat transfer coefficients can be computed from eq. (B.1). It was evaluated for the range of mass flow rates and pressures appearing in the measurement data. Fig. 8.3 shows the results for a cell length $\Delta z = 1.4\,\mathrm{m}$. The actual value of the heat transfer coefficient often shows a large deviation from a theoretical value. Therefore, the results from eq. (B.1) are multiplied with correction factors k_1, k_2 that will be determined empirically

$$\alpha' = k_1 \cdot \alpha'_{th} \qquad \alpha'' = k_2 \cdot \alpha''_{th} \tag{8.15}$$

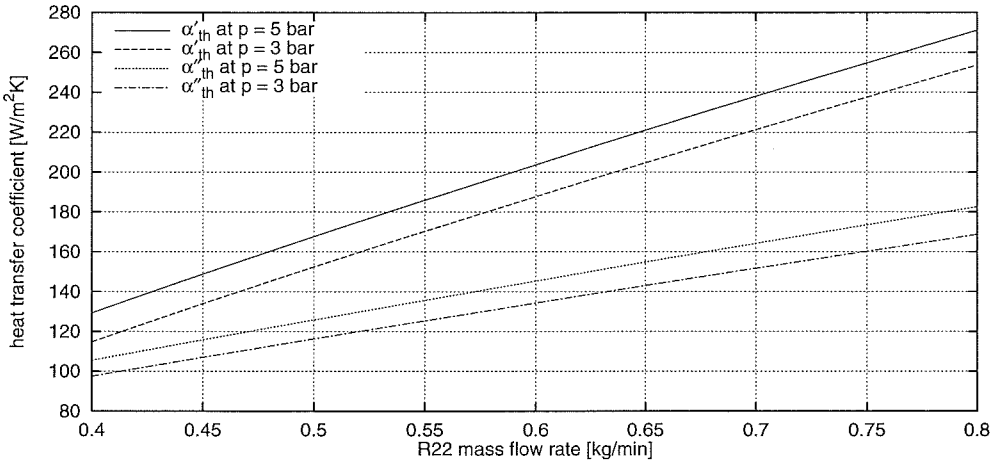

Figure 8.3 Theoretical heat transfer coefficients for R22

The one-phase friction factors obtained from the Blasius equation eq. (B.10) barely varied, $\xi'_{th} = 0.036\,..\,0.044$, $\xi''_{th} = 0.017\,..\,0.02$; thus constant values will be used

$$\xi'_{th} = 0.04 \qquad \xi''_{th} = 0.02 \tag{8.16}$$

These values are valid for a hydraulic smooth pipe, which is an ideal assumption. Moreover an additional pressure loss is likely to occur due to 12 thermometers, which are placed inside the pipe in a distance of 20 cm starting at the outlet. To account for these installations and the actual roughness of the pipe, ξ' and ξ'' will be adapted to the measured pressure loss.

In the two-phase region empirical correlations for α and ξ are used, which are based on the values for a one-phase flow with the same mass flow rate, i.e. the values computed above. In appendix B these correlations are rearranged into the following form for the heat transfer coefficient

$$\alpha = \frac{\alpha'\alpha''}{\sqrt{(\alpha'')^2(1-\dot{x})^{0.01}\phi_1^{-2.2} + (\alpha')^2\dot{x}^{0.01}\phi_2^{-2}}} \tag{8.17}$$

and the friction factor

$$\frac{\xi}{\rho} = \dot{x}^2 \frac{\xi''}{\rho''} + (1-\dot{x})^2 \frac{\xi'}{\rho'} + \dot{x}^{0.685}(1-\dot{x})^{0.24}\phi_3 \tag{8.18}$$

These equations provide a continuous transition into the one-phase values at $\dot{x} = 0$ and $\dot{x} = 1$. The functions ϕ_1, ϕ_2 and ϕ_3 are listed in section B.1 and B.2, which also contain plots of the above equations.

In the dynamic heterogeneous model, the interfacial friction factor ζ^* is an additional parameter that will be approximated by a constant. As shown in section 6.4, it can also be expressed as a function of ξ.

8.2 Implementation

The model described above is implemented in the object-oriented modelling language **Modelica** [5]. Fig. 8.4 gives an overview over the code structure. The arrows indicate where the equation is placed that provides the information required to compute the related variable.

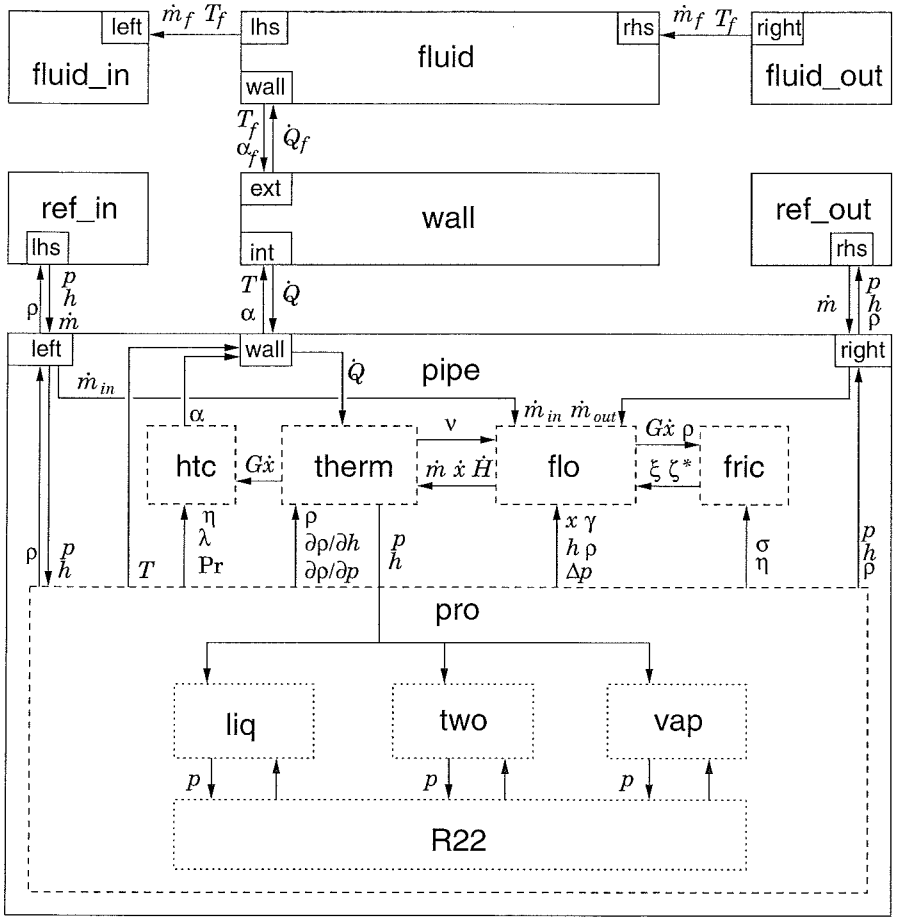

Figure 8.4 Evaporator model

The evaporator model contains the models for the fluid, the wall and the pipe. Additional models are used for the boundary conditions of the flows at in-

and outlet. The naming refers to the design flow direction of the refrigerant; a counter-flow heat exchanger is obtained by assigning a negative fluid mass flow rate to fluid_out.

The pipe model contains the thermodynamic model therm (computed in the thermal grid) and the hydrodynamic model flo (computed in the flow grid). The analytical equations for friction factors and heat transfer coefficients are placed within fric and htc. The model pro serves to compute thermodynamic properties including inlet and outlet; the related vector has thus $n + 2$ components, where n is the number of thermal cells.

9. Simulation of an Evaporator

The simulation program **Dymola** is used to evaluate the evaporator model. Version 4.0, released in July 1999, is the first that supports the **Modelica** language. The simulation results will be compared with data obtained from measurements carried out by Antonius [1] at Danfoss, Denmark. Fig. 9.1 shows a simplified diagram of the refrigeration test plant and the data obtained from measurements.

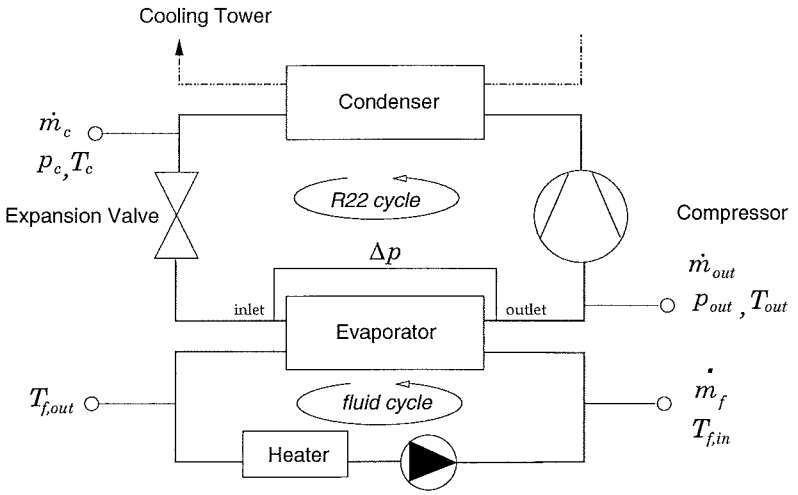

Figure 9.1 Refrigeration test plant

Some of the measured variables will be selected to serve as boundary conditions for the simulation. Steady state measurement results are used to identify heat transfer coefficients and friction factors. The model is finally applied to simulate a transient process. The measurement data will be presented at first to give an overview over the thermohydraulic behaviour of the test plant.

9.1 Measurement Data

A part of a measurement recording of $t = 400\,\mathrm{s}$ duration was selected. During this period the compressor speed is changed four times between certain levels. It regulates the mass flow in the refrigerant cycle and thus the removal of heat from the fluid cycle.

Hydraulic Behaviour

For a given compressor speed a certain volume of refrigerant per unit time is removed from the evaporator. As the speed is reduced at $t = 25\,\mathrm{s}$, the outlet mass flow rate instantly drops, fig. 9.2. Since the entering mass now exceeds the leaving mass, the amount of mass inside the evaporator increases and thus the pressure rises, fig. 9.3.

While the evaporator pressure rises, the condenser pressure decreases due to the reduced entering mass, fig. 9.3. As a result of the decreasing pressure dif-

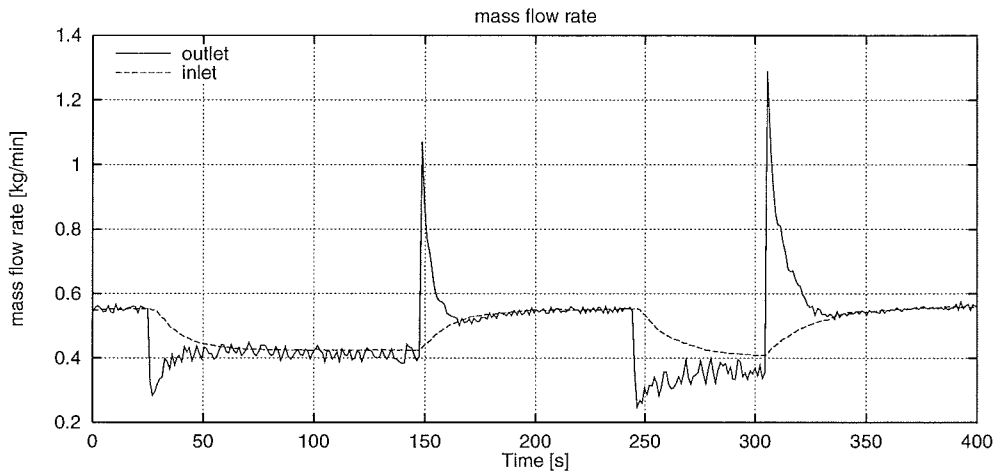

Figure 9.2 Measured entering and leaving mass flow rates

ference at the expansion valve, $\dot{m}_{in}$ is reduced. At the same time $\dot{m}_{out}$ begins to rise again, which is due to the increasing density at the evaporator outlet. The mass flow rates finally agree on a reduced level at $t \approx 60\,\mathrm{s}$. The evaporator pressure has then reached a maximum value and begins to decrease again, because of a lowering heat flux towards the refrigerant.

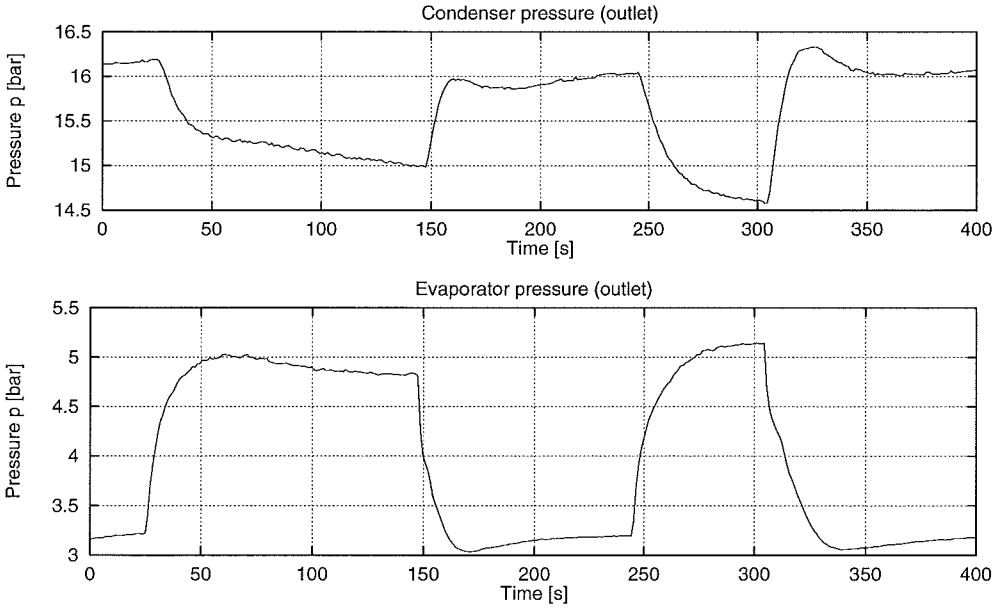

Figure 9.3 Measured condenser and evaporator pressure

When the compressor speed is increased at $t = 147\,\mathrm{s}$, the same process takes place with reversed signs. Now the evaporator pressure drops due to the removal of mass at the outlet, while the condenser pressure rises due to the added mass. After adaption of the mass flow rates at $t \approx 170\,\mathrm{s}$, the evaporator pressure rises due to the increased heat flux towards the refrigerant.

Thermal Behaviour

The driving force for the heat flux towards the refrigerant is the temperature difference between the refrigerant and the fluid. Since the entering refrigerant is a two-phase mixture with $x \approx 0.2$ mass content vapour, its temperature is determined by the pressure $T = T_{sat}(p)$. The saturation temperature related to the outlet pressure is shown in fig. 9.4. It also includes the refrigerant outlet temperature T_{out} and the fluid inlet temperature $T_{f,in}$.

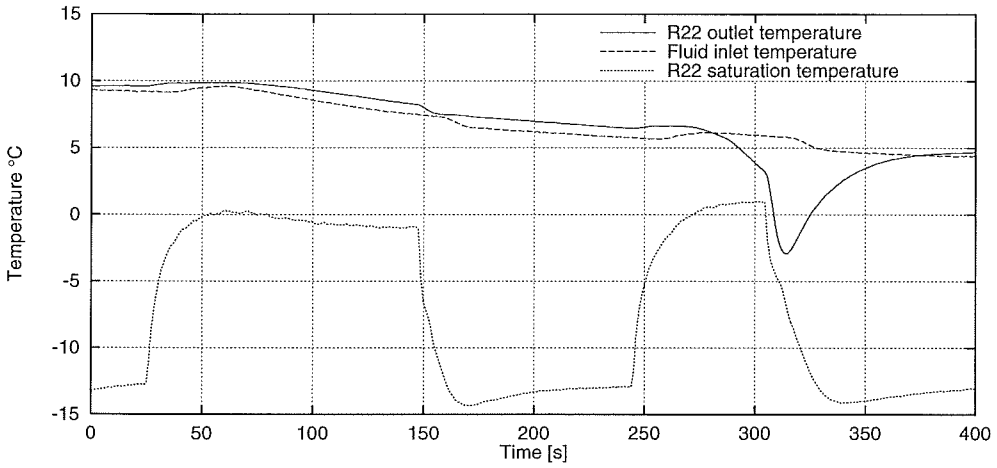

Figure 9.4 Measured refrigerant and fluid temperatures

The heat flux towards the refrigerant rises with the difference between the fluid temperature and the saturation temperature of the refrigerant $\Delta T = T_{f,in} - T_{sat}(p)$. Therefore, a reduced evaporator pressure, caused by a high compressor speed, leads to an increased removal of heat from the fluid cycle. It also provides an increased refrigerant mass flow rate, which is necessary to remove the heat from the evaporator.

After the refrigerant is evaporated, the vapour is superheated up to a temperature T_{out} close to the fluid inlet temperature. Most of the time, the measured outlet temperature exceeds the fluid temperature by 1 K, which is actually impossible and must be due to a warming of the refrigerant at the outlet or a measurement error.

When the compressor speed is reduced at $t = 245\,\mathrm{s}$, the saturation pressure rises. Since $T_{f,in}$ has decreased, the temperature difference ΔT is now just about sufficient to enable a complete evaporation of the refrigerant, and thus the superheat begins to decrease. As the compressor speed is increased again at $t = 305\,\mathrm{s}$, the superheat has finally reduced to 3 K. Now the refrigerant in the pipe is almost completely in state of saturation and thus T_{out} initially drops even more due to the reduction of the pressure. As the temperature difference gets larger, the heat flux is increased; the fraction of the pipe required for evaporation gets smaller and T_{out} rises again.

9.2 Steady-State Simulation

A steady state simulation is used to identify the empirical parameters, i.e. the one-phase friction factors ξ', ξ'' and the correction factors for the one-phase

heat transfer coefficients k_1,k_2. The number of cells is $n = 5$; a higher number of cells does not give a noticeable change of simulation results.

Boundary Conditions

The boundary conditions chosen are

- R22 inlet enthalpy h_{in}
- R22 inlet pressure $p_{in} = p_{out} + \Delta p$
- R22 inlet mass flow rate $\dot{m}_{in} = \dot{m}_c$
- R22 outlet volume flow rate $\dot{V}_{out}$
- fluid inlet temperature $T_{f,in}$
- fluid mass flow rate $\dot{m}_f$

The inlet mass flow rate $\dot{m}_{in}$ is set equal to the measured mass flow rate at the outlet of the condenser, because the throttling process can be considered as stationary. The inlet enthalpy h_{in} is obtained from an energy balance for the expansion valve. For a stationary, adiabatic, homogeneous flow eq. (4.51) gets, after division by $\dot{m}$,

$$h_{in} = h_c + \frac{w_c^2}{2} - \frac{w_{in}^2}{2} + \boldsymbol{g}\,(\boldsymbol{z}_c - \boldsymbol{z}_{in}) \tag{9.1}$$

where $\boldsymbol{z}$ is the position vector. The last term is negligible. During the throttling process the refrigerant evaporates partially, which causes a decrease of the density and thus an increase of the velocity. The reduction of enthalpy due to this effect will, however, be neglected for simplicity, thus

$$h_{in} \approx h_c = h(T_c, p_c) \tag{9.2}$$

The pressure at the inlet p_{in} is required to compute the saturation densities and the void fraction of the entering refrigerant. It does not determine the pressure inside the pipe, which is a simulation result and may differ from p_{in}.

In agreement with [1] the outlet volume flow rate is chosen as a boundary condition, since the compressor removes a certain volume per unit time, regardless of the density. The data are computed from

$$\dot{V}_{out} = \frac{\dot{m}_{out}}{\rho(p_{out}, T_{out})} \tag{9.3}$$

The following steady-state data [1] are used as boundary conditions

Table 9.2 shows the measured pressure drop and outlet conditions. It also contains results of the simulation program SINDA FLUINT [1] including the charge M.

No.	$\dot{m}_{in}$	$\dot{V}_{out}$	$\dot{m}_f$	$T_{f,in}$	T_c	p_c	p_{in}	h_{in}
	kg/min	m^3/min	kg/min	°C	°C	bar	bar	kJ/kg
1	0.60	0.044	0.22	0.7	26.6	15.9	3.39	232.3
2	0.69	0.045	0.28	4.2	28.5	17.1	3.91	234.7
3	0.48	0.042	0.28	-1.8	25.9	15.0	2.88	231.4
4	0.72	0.046	0.33	9.4	30.0	18.0	4.12	236.6

Table 9.1 Boundary conditions for stationary simulation

No.	source	p_{out}	Δp	T_{out}	$T_{f,out}$	M
		bar	bar	°C	°C	g
1	measured	3.29	0.090	-2.50	-2.30	–
	homogeneous	3.20	0.045	-13.70	-2.28	17
	heterogeneous	3.20	0.050	-13.70	-2.29	61
2	measured	3.77	0.110	2.30	1.50	–
	homogeneous	3.66	0.055	-3.40	1.40	18
	heterogeneous	3.66	0.060	-4.10	1.37	62
3	measured	2.79	0.080	-1.40	-3.80	–
	homogeneous	2.75	0.035	-3.96	-3.84	12
	heterogeneous	2.75	0.038	-4.05	-3.87	32
4	measured	3.98	0.120	9.30	7.00	–
	homogeneous	3.95	0.058	7.74	6.85	16
	heterogeneous	3.96	0.063	7.70	6.84	41

Table 9.2 Simulation results of SINDA FLUINT [1]

Simulation Results

In table 9.3 the simulation results of the homogeneous and static heterogeneous model are compared with measurement data. The theoretical one-phase friction factors and heat transfer coefficients were used, i.e. $\xi'_{th} = 0.04$, $\xi''_{th} = 0.02$ and α'_{th}, α''_{th} from fig. 8.3. Both models yield almost identical results concerning the intensive variables. Compared to the measurements, p_{out} and $T_{f,out}$ show reasonable good agreement. However, the refrigerant outlet temperature is up to 8 K below the measured value and the pressure drop is too low by a factor 4. The result is thus similar to the one of SINDA FLUINT, table 9.2, where the pressure loss is too low by a factor 2 and the superheat is too low by 1.5 .. 11 K.

The low simulated pressure loss is a result of the ideal assumption of a hydraulic smooth pipe and the neglect of the pressure loss due to the pipe elbows and the thermometers placed inside the pipe. Further pressure losses may occur in the space between the measuring point and the in- and outlet of the pipe. From the measured pressure drop the actual friction factors can be identified as $\xi' = 0.1$ and $\xi'' = 0.1$.

No.	source	p_{out}	Δp	T_{out}	$T_{f,out}$	M
		bar	bar	°C	°C	g
1	measured	3.29	0.090	-2.50	-2.30	–
	homogeneous	3.20	0.026	-10.29	-2.47	20.8
	heterogeneous	3.20	0.026	-10.30	-2.47	64.6
2	measured	3.77	0.110	2.30	1.50	–
	homogeneous	3.66	0.032	-3.66	1.31	22.9
	heterogeneous	3.66	0.032	-3.67	1.32	65.4
3	measured	2.79	0.080	-1.40	-3.80	–
	homogeneous	2.78	0.020	-4.07	-3.86	14.4
	heterogeneous	2.78	0.020	-4.07	-3.86	36.4
4	measured	3.98	0.120	9.30	7.00	–
	homogeneous	3.92	0.033	6.00	6.78	20.4
	heterogeneous	3.92	0.033	6.00	6.78	46.9

Table 9.3 Simulation results of Dymola

The low simulated superheat may be due to the application of eq. (8.17) in the two-phase region, which is valid for convective evaporation and does not account for nucleate boiling, which intensifies the heat transfer and may appear at low void fractions. Moreover, liquid drops are still present when the vapour is superheated and thus a higher heat transfer coefficient may be present in the region where due to $h > h''(p)$ the value for pure vapour is used. Measurements on boiling nitrogen, cited in [14], show that for a value of $\dot{x} = 1$, computed from eq. (6.15), the actual flow quality is 0.6..0.8. From fig. B.1 it can be seen that the heat transfer coefficient is then approximately six times as high as the related value for pure vapour.

Considering the influences discussed above and the general uncertainty concerning the prediction of heat transfer coefficients in boiling two-phase flows, it appears to be justified to apply correction factors k_1, k_2, as proposed in eq. (8.15), to achieve better agreement with the measured superheat. Table 9.4 shows the simulation results obtained for $k_1 = 2$ and $k_2 = 2$. The friction factors are $\xi' = 0.1$ and $\xi'' = 0.1$.

The deviation from the measured outlet temperature is reduced to less than 2 K. The error of the pressure loss is less than 10%. The above values for the correction parameters are thus kept for further simulations.

From the tables it is already apparent that the mass inside the evaporator is up to three times bigger in the heterogeneous model. This is due to the lower void fraction γ in a heterogeneous flow, which has been discussed in section 6.2. From $\rho = \gamma\rho'' + (1 - \gamma)\rho'$ follows that for a given pressure the density is higher in a heterogeneous flow. The charge has a huge effect on the transient behaviour, as the following section will show.

No.	source	p_{out}	Δp	T_{out}	$T_{f,out}$	M
		bar	bar	°C	°C	g
1	measured	3.29	0.090	-2.50	-2.30	–
	homogeneous	3.30	0.084	-3.59	-2.55	20.3
	heterogeneous	3.30	0.085	-3.60	-2.55	58.3
2	measured	3.77	0.110	2.30	1.50	–
	homogeneous	3.72	0.099	0.50	1.27	21.4
	heterogeneous	3.72	0.099	0.50	1.27	55.0
3	measured	2.79	0.080	-1.40	-3.80	–
	homogeneous	2.80	0.072	-2.61	-3.88	13.0
	heterogeneous	2.80	0.072	-2.61	-3.88	27.0
4	measured	3.98	0.120	9.30	7.00	–
	homogeneous	3.95	0.114	8.02	6.76	18.7
	heterogeneous	3.95	0.114	8.02	6.76	36.9

Table 9.4 Simulation results of Dymola - fitted parameters

9.3 Transient Simulation

Boundary Conditions

The measurement data have been presented in section 9.1. The data used as boundary conditions, i.e. time-dependent data for the variables in table 9.1, were computed from linear interpolation

$$\psi(t) = \psi(t_i) + \frac{t - t_i}{t_{i+1} - t_i} [\psi(t_{i+1}) - \psi(t_i)] \quad \text{for} \quad t_i \leq t \leq t_{i+1} \tag{9.4}$$

C-code was created to apply this interpolation automatically to data tables. The above method was not used for the outlet volume flow rate. As fig. 9.5 shows, heavy oscillations appear, which are obviously due to statistical measurement errors. To provide physically realistic boundary conditions, $\dot{V}_{out}$ is approximated by piecewise constant functions, except at fast transients, where third order polynomial functions are used. The result is shown in fig. 9.5.

The fluid mass flow rate is constant $\dot{m}_f = 0.33\,\mathrm{kg/s}$. The inlet enthalpy is almost constant, $h_{in} = 233..234\,\mathrm{kJ/kg}$. The number of pipe segments is $n = 5$.

Simulation Results

Fig. 9.6 compares the measured pressure loss with the simulation results of the homogeneous and the heterogeneous model. A large pressure loss occurs when the pressure is low, which is due to the low related vapour density causing a high velocity at the outlet. The resulting reaction force is particularly high due to the large mass flow rate present at the same time, which also increases the friction force.

Both models yield good agreement with the measured pressure loss, except when the compressor speed is increased at $t = 147\,\mathrm{s}$ and $t = 305\,\mathrm{s}$, where

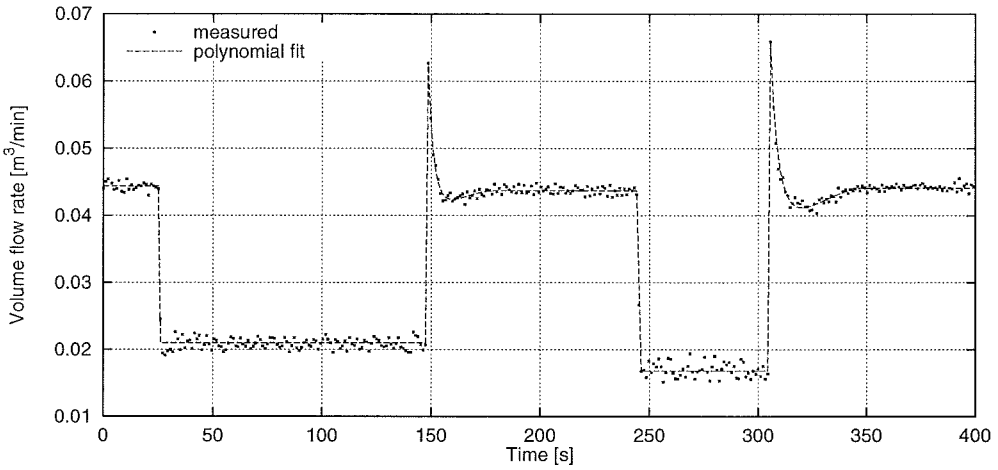

Figure 9.5 Outlet volume flow rate

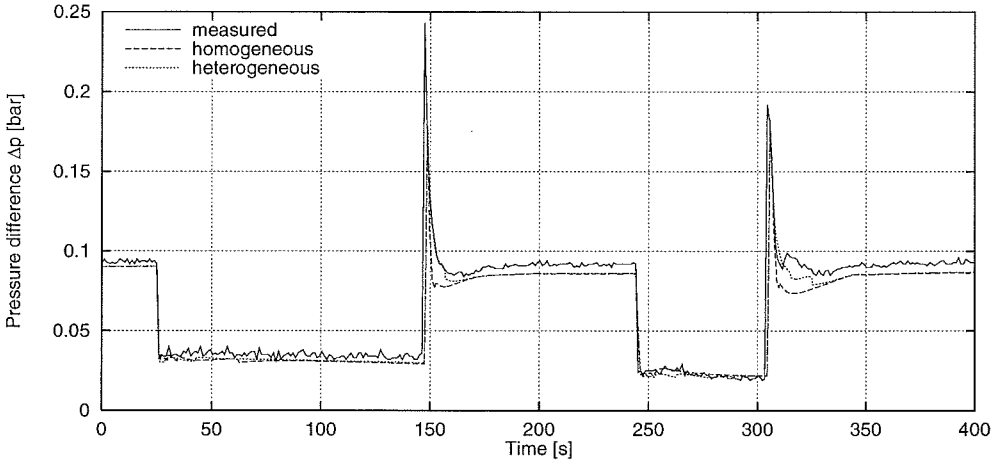

Figure 9.6 Simulated pressure drop in the evaporator

the homogeneous model produces a too quick decrease from an initial peak. The same effect is obvious from fig. 9.7, which shows the simulated outlet pressure. The homogeneous model produces large overshoots as the pressure changes. Application of the heterogeneous model yields a qualitatively better agreement with the measured value. The error is less than 10% during the whole measurement recording.

The improved accuracy of the heterogeneous model is caused by the higher simulated charge, fig. 9.8: Due to the lower void fraction, more liquid mass is present. As the compressor speed is increased, the pressure drops and the liquid evaporates. As a result, the outlet mass flow rate suddenly rises and then slowly decreases as the amount of liquid is reduced, fig. 9.9. In the homogeneous model, the amount of liquid is lower and thus the outlet mass flow rate adapts too quickly to the given inlet mass flow rate (fig. 9.2).

Due to the increased accuracy of the pressure, a qualitatively better result is also obtained for the outlet temperature. At $t = 40\,\mathrm{s}$ and $t = 250\,\mathrm{s}$ the homogeneous model produces too high pressures, causing a low temperature

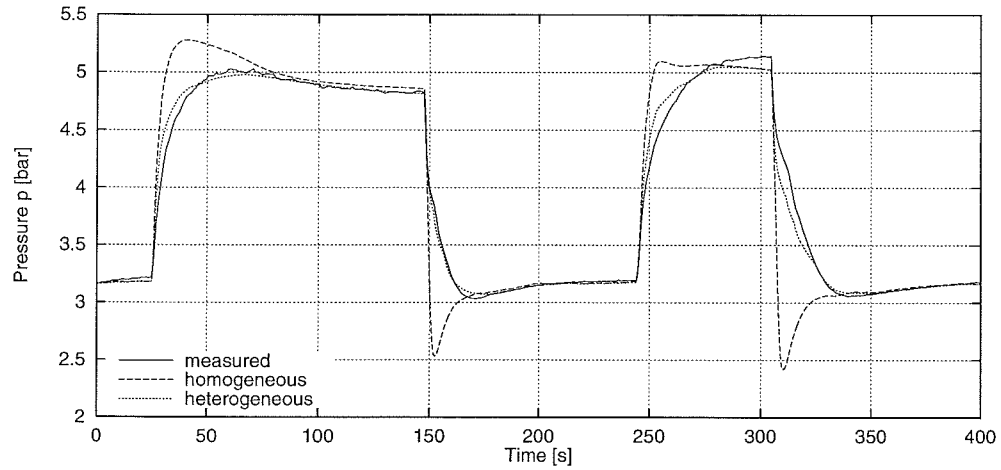

Figure 9.7 Simulated outlet pressure

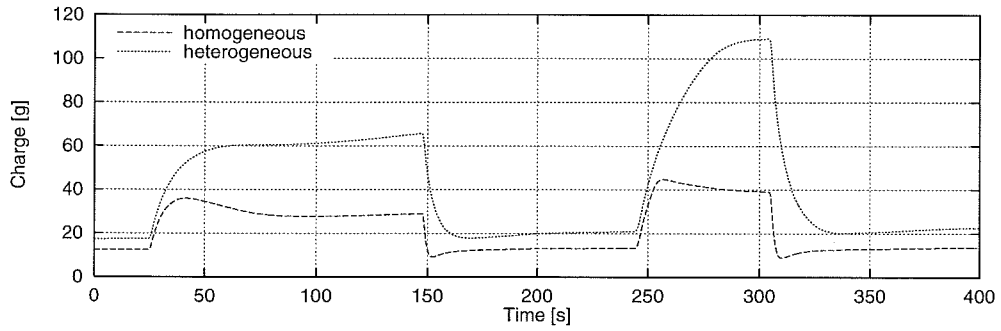

Figure 9.8 Simulated evaporator charge

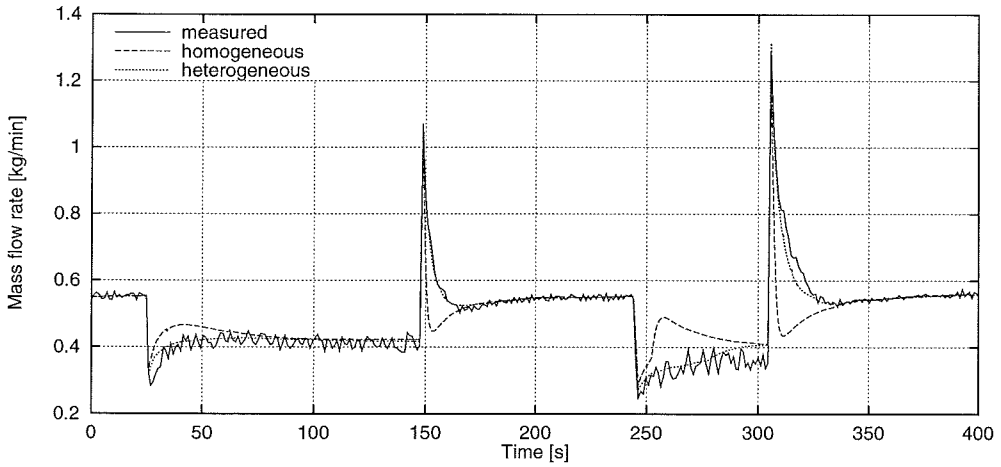

Figure 9.9 Simulated evaporator outlet mass flow rate

difference ΔT between the saturated refrigerant and the fluid. The simulated heat flux is therefore too low and the superheat drops. At $t = 250\,\mathrm{s}$ the superheat reduces to zero in the homogeneous model, while the heterogeneous model gives a better picture of the decreasing superheat.

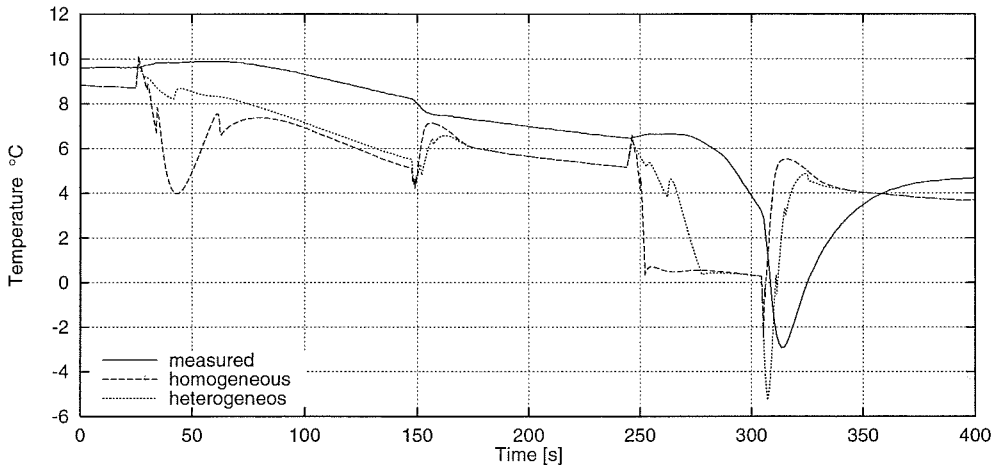

Figure 9.10 Simulated outlet temperature

As explained in section 9.1, the sudden temperature drop at $t = 305\,\mathrm{s}$ is caused by the decrease of the pressure and the related saturation temperature. The simulation produces a similar effect, but there is a large deviation from the measurement recording. The deviation is partially due to the high time constant of the thermometer, causing a delayed notice of sudden changes: At $t = 147\,\mathrm{s}$ the measured value only changes its slope, while the simulations show a temperature drop similar to the one at $t = 305\,\mathrm{s}$.

The above results of the heterogeneous model are based on the static slip-flow equation eq. (7.21). To apply the dynamic slip-flow equation eq. (7.22), the factor ζ^* must be determined. From fig. 6.5 we can read off a first guess: Since the void fraction in the measured data is $\gamma > 0.8$ we obtain $\zeta^* \approx \xi$. Using this relation the dynamic slip-flow model gives nearly the same results as the static slip-flow model. In the scaling used in the plots above no difference would be visible. Fig. 9.11 gives a closer look at the outlet pressure: The dynamic equation yields only a slight improvement.

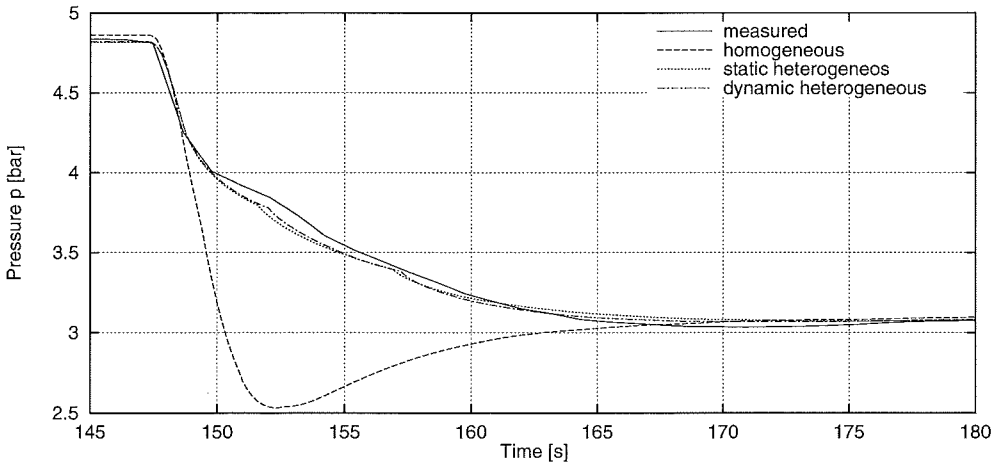

Figure 9.11 Simulated outlet pressure

The interfacial friction factor was also approximated by a constant value

$\zeta^* = 0.3..0.5$, fig. 9.12. For $\zeta^* > 0.5$ the result tends to the one of the homogeneous model, which is due to the increased interfacial friction, causing an equilibration of the velocities. For $\zeta^* < 0.3$ the simulation gets unstable. While $\zeta^* = 0.3$ turns out to be the appropriate choice for fast transients, $\zeta^* = 0.5$ provides increased accuracy in a steady-state. Application of $\zeta^* = 0.4$ yields the best overall result.

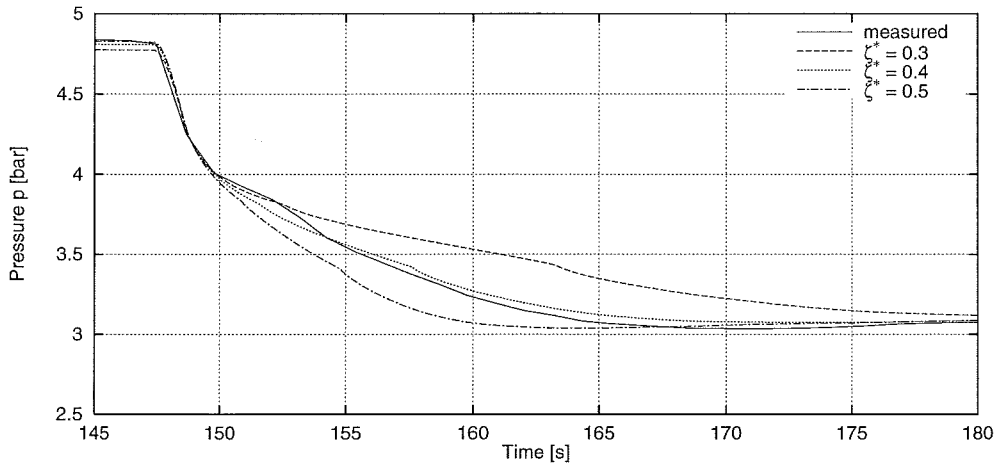

Figure 9.12 Simulated outlet pressure

The results show that a better agreement with measured data can be achieved by variation of ζ^* instead of using a constant value. However, the result depends very much on the values of α' and α'' which have been adapted very roughly. Before determination of a function for ζ^*, the heat transfer coefficients should be computed more precisely.

10. Summary

Among the variables applied to describe two-phase flows, thermodynamic and hydrodynamic properties can be distinguished. For each category a distinct model is created. The thermodynamic model is based on the integral form of the balance equations for mass and energy, which yield differential equations for density ρ and specific internal energy u. To increase the numerical stability, these equations are transformed into differential equations for pressure p and enthalpy h by symbolic inversion of the Jacobian matrix.

Simple equations of state are created using p and h as independent parameters. The properties in the two-phase region can be expressed as a linear interpolation between dew- and boiling point. In the one-phase region Taylor expansions at the dew- and boiling point are used, which provide a continuous transition on the phase boundaries. The approach requires solely functions for the properties and certain derivatives of saturated liquid and vapour, which can be approximated by polynomial functions. The technique was applied to the refrigerant R22 on the basis of data computed from the NIST REFPROP database.

A hydrodynamic model is derived in order to determine the convective terms appearing in the thermodynamic model. In the case of homogeneous flow assumption, sufficient information is provided by a differential equation for the mass flow rate which is derived from a momentum balance. In case of a heterogeneous flow an additional equation is required to account for the difference of the average velocities of vapour and liquid Δw. An algebraic equation for Δw is obtained from an empirical equation for the flow quality. As an alternative, a differential equation for Δw is derived from separate momentum balances for each phase.

The separate momentum balances contain terms quantifying momentum exchange and friction forces between the phases. Common approaches cause singularities in the limiting case of a vanishing phase. To ensure a safe transition into the one-phase region, these terms are modelled under the premise that in the limiting cases realistic results are obtained instead of singularities. A relation for the mass flow through the interfacial area follows from a vapour mass balance. The interfacial friction is expressed in terms of a factor ζ^*, which is defined in analogy to the wall friction factor ξ in a one-phase flow.

Thermo- and hydrodynamic model form a system of coupled differential equations. Following the principles of the finite volume method, the equations for each model are discretized to account for the spatial distribution of properties. Thermo- and hydrodynamic equations are applied to different grid structures. The properties on the boundary of a pipe segment are approximated by the average properties of the cell located upstream. Complementary models are required to compute the heat transfer through a heated or cooled pipe wall. For heat transfer coefficients and friction factors empirical correlations are selected that provide a continuous transition on the phase boundaries.

The model is applied to simulate an evaporator in a refrigeration test plant. Measured inlet conditions and outlet volume flow rate are used as boundary

conditions. The simulated pressure loss and superheat temperature are too low compared to the measured values; by increasing the one-phase friction factors and heat transfer coefficients a better agreement is achieved. In steady-state and slow transient simulations the homogeneous and heterogeneous model yield almost identical results, except for the charge, which is several times larger in the heterogeneous model compared to the homogeneous model.

The influence of the different charges becomes evident in fast transient processes: As the evaporator outlet volume flow rate is abruptly increased, the heterogeneous model produces a delayed pressure drop due to the time it takes to evaporate the large amount of liquid mass in the evaporator. Contrary to this, application of the homogeneous model causes overshoots of the pressure that are not in agreement with the measurement recording. The maximum error of the simulated pressure is 45% in the homogenous model compared to 10% in the heterogeneous model.

The simulated superheat temperature is only roughly in accord with measurement data; the deviation is due to the high time-constant of the thermoelement, which thus cannot detect the sudden temperature changes predicted by the simulation. Moreover, the computation of heat transfer coefficients in boiling two-phase flows is still afflicted with a huge inaccuracy, and a precise determination of a function for α in the given evaporator has not been attempted. The heterogeneous model provided only a slight improvement due to the increased accuracy concerning the pressure.

The differential equation for Δw in the heterogeneous model gives almost the same results as the related analytical equation, if the interfacial friction factor ζ^* is set equal to the wall friction factor ξ, which is justified in annular flows. In some cases it is possible to obtain a better agreement between data and simulation by adaption of ζ^*. Due to the strong influence of the heat transfer coefficient, which had been adapted very roughly, a more accurate determination of ζ^* should not be attempted before the heat transfer coefficients are computed more precisely.

The transition from the two-phase region into the vapour region did not cause any numerical problems. The transition into the liquid region is not contained in the measurement recording. Test runs using fictitious boundary conditions show that numerical problems arise when the void fraction in a pipe segment gets zero, which is due to the abruptly decreasing compressibility. This problem can be solved by application of separate energy balances for each phase, but this is beyond the scope of this thesis.

[1] Antonius, Jesper
Distribuerede fordampermodeller på flere detaljeringsniveauer
Danmarks Tekniske Universitet, 1998

[2] Baehr, Hans Dieter; Stephan, Karl
Wärme und Stoffübertragung
3. Auflage, Springer-Verlag, Berlin, Heidelberg, 1998

[3] Bronstein, I.N.; Semendjajew, K.A.
Taschenbuch der Mathematik
14. Auflage, Verlag Harri Deutsch, Thun und Frankfurt/Main, 1989

[4] Carey, Van P.
Liquid-Vapour Phase-Change Phenomena
Hemisphere Publishing Corporation, 1992

[5] Elmqvist, H. et al.
Modelica Tutorial and Rationale
http://www.modelica.org

[6] Guyon, Etienne; Hulin, Jean-Pierre; Petit, Luc
Hydrodynamik
Verlag Vieweg, Braunschweig/Wiesbaden, 1997

[7] Hetsroni, Gad
Handbook of Multiphase Systems
Hemisphere Publishing Corporation, 1982

[8] Heusser, Peter Andreas
Modelling and Simulation of Boiling Channels with a General Front Tracking Approach
SCS - Society for Computer Simulation International, Ghent, 1996

[9] Köhler, Jürgen
Wärme- und Stoffübertragung in Zweiphasenströmungen
Verlag Vieweg, Braunschweig/Wiesbaden, 1996

[10] Kolev, Nikolay Ivanov
Transiente Zweiphasenströmung
Springer-Verlag, Berlin, Heidelberg, 1986

[11] Mayinger, Franz
Strömung und Wärmeübergang in Gas-Flüssigkeits-Gemischen
Springer-Verlag, Wien, New York, 1982

[12] NIST REFPROP Database
National Institute of Standards and Technology, Version 6.0

[13] Patankar, Suhas, V.
Numerical Heat Transfer and Fluid Flow
Hemisphere Publishing Corporation, 1980

[14] Stephan, Karl
Wärmeübergang beim Kondensieren und beim Sieden
Springer-Verlag, Berlin, Heidelberg, 1988

[15] Stephan, Karl; Heckenberger, Thomas
Thermal Conductivity and Viscosity Data of Fluid Mixtures
Chemistry Data Series 10, Frankfurt am Main, 1988

[16] Stephan, Karl; Mayinger, Franz
Thermodynamik, Band 2: Mehrstoffsysteme und chemische Reaktionen
14. Auflage, Springer-Verlag, Berlin, Heidelberg, 1999

[17] VDI-Wärmeatlas
8. Auflage, Springer-Verlag Berlin, Heidelberg, 1997

[18] Wallis, Graham, B.
One-Dimensional Two-Phase Flow
McGraw-Hill, New York, 1969

[19] WANG, HONGWEI
Modelling of a Refrigerating System Coupled with a Refrigerated Room
Delft University of Technology, 1991

A. Balance Equations for Kinetic and Internal Energy

An infinitesimal small cubical fluid particle with lateral length dz is considered. The edges of the cube are parallel to a system of coordinates, whose directions are numbered $j = 1, 2, 3$. The velocity is counted positive in direction of the coordinates.

A.1 Mass Balance

The mass within the cube $dM = \rho dV$ changes due to the entering and leaving mass in all three coordinates. Using a Taylor series approximation this gives

$$dV\frac{\partial \rho}{\partial t} = \rho w_j dA - \left[\rho w_j + \frac{\partial(\rho w_j)}{\partial z_j}dz\right] dA \tag{A.1}$$

where the subscript j implies summation over $j = 1, 2, 3$ (Einsteins' summation convention). Division by dV yields

$$\frac{\partial \rho}{\partial t} + \frac{\partial(\rho w_j)}{\partial z_j} = 0 \tag{A.2}$$

Eq. (A.2) will be used to simplify the derivative of a quantity $\rho\psi$, which can be expanded as follows

$$\frac{\partial(\rho\psi)}{\partial t} + \frac{\partial(\rho w_j \psi)}{\partial z_j} = \rho\frac{\partial \psi}{\partial t} + \rho w_j \frac{\partial \psi}{\partial z_j} + \psi\left[\frac{\partial \rho}{\partial t} + \frac{\partial(\rho w_j)}{\partial z_j}\right] \tag{A.3}$$

According to eq. (A.2) the last term equals zero, therefore

$$\frac{\partial(\rho\psi)}{\partial t} + \frac{\partial(\rho w_j \psi)}{\partial z_j} = \rho\frac{\partial \psi}{\partial t} + \rho w_j \frac{\partial \psi}{\partial z_j} \tag{A.4}$$

A.2 Momentum Balance

The change of momentum in direction of a coordinate i

$$dV\frac{\partial(\rho w_i)}{\partial t} \tag{A.5}$$

equals the sum of the momentums in direction i transfered with the entering and leaving mass in all directions $j = 1, 2, 3$

$$\rho w_i w_j dA - \left[\rho w_i w_j + \frac{\partial(\rho w_i w_j)}{\partial z_j}dz\right] dA = -\frac{\partial(\rho w_i w_j)}{\partial z_j}dzdA \tag{A.6}$$

plus the gravity force

$$\rho g_i dV \tag{A.7}$$

plus the pressure force

$$pdA - \left[p + \frac{\partial p}{\partial z_i} dz\right] dA = -\frac{\partial p}{\partial z_i} dz dA \tag{A.8}$$

minus the forces due to shear stresses

$$-\left\{\tau_{ji} dA - \left[\tau_{ji} + \frac{\partial \tau_{ji}}{\partial z_j} dz\right] dA\right\} = \frac{\partial \tau_{ji}}{\partial z_j} dz dA \tag{A.9}$$

where τ_{ji} is the shear stress on a surface j = const in direction of i. Summing up and dividing by dV yields

$$\frac{\partial(\rho w_i)}{\partial t} + \frac{\partial(\rho w_i w_j)}{\partial z_j} = -\frac{\partial p}{\partial z_i} + \frac{\partial \tau_{ji}}{\partial z_j} + \rho g_i \tag{A.10}$$

According to eq. (A.4) this is equivalent to

$$\rho \frac{\partial w_i}{\partial t} + \rho w_j \frac{\partial w_i}{\partial z_j} = -\frac{\partial p}{\partial z_i} + \frac{\partial \tau_{ji}}{\partial z_j} + \rho g_i \tag{A.11}$$

A.3 Energy Balance

The energy stored within the cube is

$$dE = \rho e dV \tag{A.12}$$

where e is the specific energy, i.e. the sum of internal and kinetic energy

$$e = u + \frac{w_i^2}{2} \tag{A.13}$$

The convective transport of energy into the volume is

$$\rho e w_j dA - \left[\rho e w_j + \frac{\partial(\rho e w_j)}{\partial z_j} dz\right] dA = -\frac{\partial(\rho e w_j)}{\partial z_j} dz dA \tag{A.14}$$

The power due to the forces is obtained from multiplication of the forces introduced in the previous section with the related velocity component in all three directions

$$-\frac{\partial(p w_i)}{\partial z_i} dz dA + \frac{\partial(\tau_{ji} w_i)}{\partial z_j} dz dA + \rho g_i w_i dV \tag{A.15}$$

The energy also increases due to convective transfer of heat into the volume

$$\dot{q}_i - \left[\dot{q}_i + \frac{\partial \dot{q}_i}{\partial z_i}\right] = -\frac{\partial \dot{q}_i}{\partial z_i} \tag{A.16}$$

Altogether this gives

$$\frac{\partial(\rho e)}{\partial t} + \frac{\partial(\rho e w_j)}{\partial z_j} = -\frac{\partial p w_i}{\partial z_i} + \frac{\partial(\tau_{ji} w_i)}{\partial z_j} + \rho g_i w_i - \frac{\partial \dot{q}_i}{\partial z_i} \tag{A.17}$$

Kinetic Energy Balance

Multiplication of eq. (A.11) with w_i and summation over $i = 1, 2, 3$ yields

$$\rho \frac{\partial}{\partial t}\left(\frac{w_i^2}{2}\right) + \rho w_j \frac{\partial}{\partial z_j}\left(\frac{w_i^2}{2}\right) = -w_i \frac{\partial p}{\partial z_i} + w_i \frac{\partial \tau_{ji}}{\partial z_j} + w_i \rho g_i \tag{A.18}$$

which by application of eq. (A.4) turns into the kinetic energy balance

$$\frac{\partial}{\partial t}\left(\rho \frac{w_i^2}{2}\right) + \frac{\partial}{\partial z_j}\left(\rho w_j \frac{w_i^2}{2}\right) = -w_i \frac{\partial p}{\partial z_i} + w_i \frac{\partial \tau_{ji}}{\partial z_j} + w_i \rho g_i \tag{A.19}$$

The second term on the left side can be expressed with the divergence operator $\mathrm{div}\psi = \partial \psi_j / \partial z_j$, while the last term on the right side equals the scalar product $\rho \boldsymbol{g} \boldsymbol{w}$. Integration over a control volume V gives

$$\int_V \frac{\partial}{\partial t}\left(\rho \frac{w_i^2}{2}\right) dV + \int_V \mathrm{div}\left[\rho \boldsymbol{w} \frac{w_i^2}{2}\right] dV = \int_V \rho \boldsymbol{g} \boldsymbol{w}\, dV + \int_V \left[-w_i \frac{\partial p}{\partial z_i} + w_i \frac{\partial \tau_{ji}}{\partial z_j}\right] dV \tag{A.20}$$

For a fixed control volume, the derivative operator in the first term can be put before the integral. The second term can be transformed into a surface integral by use of the Gauß theorem. This gives

$$\frac{d}{dt}\int_V \rho \frac{w_i^2}{2}\, dV + \int_A \rho \frac{w_i^2}{2} \boldsymbol{w} \boldsymbol{n}\, dA = \int_V \rho \boldsymbol{g} \boldsymbol{w}\, dV + \int_V \left[-w_i \frac{\partial p}{\partial z_i} + w_i \frac{\partial \tau_{ji}}{\partial z_j}\right] dV \tag{A.21}$$

or

$$\frac{dE_{kin}}{dt} = -\int_A \rho e_{kin} \boldsymbol{w} \boldsymbol{n}\, dA + P_g + \int_V \left[-w_i \frac{\partial p}{\partial z_i} + w_i \frac{\partial \tau_{ji}}{\partial z_j}\right] dV \tag{A.22}$$

where P_g is the power due to gravity forces.

Internal Energy Balance

Separating the internal and kinetic energy on the left side of eq. (A.17) yields

$$\frac{\partial(\rho u)}{\partial t} + \frac{\partial(\rho u w_j)}{\partial z_j} = \frac{\partial(\rho e)}{\partial t} + \frac{\partial(\rho e w_j)}{\partial z_j} - \left[\frac{\partial}{\partial t}\left(\rho\frac{w_i^2}{2}\right) + \frac{\partial}{\partial z_j}\left(\rho\frac{w_i^2}{2}w_j\right)\right] \tag{A.23}$$

The terms on the right side can be replaced by eq. (A.19) and eq. (A.17)

$$\begin{aligned}\frac{\partial(\rho u)}{\partial t} + \frac{\partial(\rho u w_j)}{\partial z_j} &= -\frac{\partial(p w_i)}{\partial z_i} + \frac{\partial(\tau_{ji} w_i)}{\partial z_j} + \rho g_i w_i - \frac{\partial \dot{q}_i}{\partial z_i} && \text{(A.24)}\\ &\quad - \left[-w_i\frac{\partial p}{\partial z_i} + w_i\frac{\partial \tau_{ji}}{\partial z_j} + w_i\rho g_i\right] && \text{(A.25)}\end{aligned}$$

rearrangement yields

$$\frac{\partial(\rho u)}{\partial t} + \frac{\partial(\rho u w_j)}{\partial z_j} = -\frac{\partial(p w_i)}{\partial z_i} + w_i\frac{\partial p}{\partial z_i} + \tau_{ji}\frac{\partial w_i}{\partial z_j} - \frac{\partial \dot{q}_i}{\partial z_i} \tag{A.26}$$

Integration over a control volume gives

$$\begin{aligned}\int_V \frac{\partial(\rho u)}{\partial t}\,dV + \int_V \operatorname{div}(\rho u \boldsymbol{w})\,dV &= -\int_V \operatorname{div}(p\boldsymbol{w})\,dV - \int_V \operatorname{div}\dot{\boldsymbol{q}}\,dV \\ &\quad + \int_V \left[w_i\frac{\partial p}{\partial z_i} + \tau_{ji}\frac{\partial w_i}{\partial z_j}\right] dV \qquad \text{(A.27)}\end{aligned}$$

For a fixed control volume after applying the Gauß theorem we get

$$\frac{d}{dt}\int_V \rho u\,dV = -\int_A \rho u \boldsymbol{w}\boldsymbol{n}\,dA - \int_A p\boldsymbol{w}\boldsymbol{n}\,dV - \int_A \dot{\boldsymbol{q}}\boldsymbol{n}\,dA + \int_V \left[w_i\frac{\partial p}{\partial z_i} + \tau_{ji}\frac{\partial w_i}{\partial z_j}\right] dV \tag{A.28}$$

Using P_p and $\dot{Q}$ to denote the power due to pressure forces and the heat flux we obtain

$$\frac{dU}{dt} = -\int_A \rho u \boldsymbol{w}\boldsymbol{n}\,dA + P_p + \dot{Q} + \int_V \left[w_i\frac{\partial p}{\partial z_i} + \tau_{ji}\frac{\partial w_i}{\partial z_j}\right] dV \tag{A.29}$$

In eq. (A.26) the pressure terms may be simplified analogously to the terms containing the shear stresses. This leads to an equivalent equation

$$\frac{dU}{dt} = -\int_A \rho u \boldsymbol{w}\boldsymbol{n}\,dA + \dot{Q} + \int_V \left[-p\frac{\partial w_i}{\partial z_i} + \tau_{ji}\frac{\partial w_i}{\partial z_j}\right] dV \tag{A.30}$$

B. Correlations for heat transfer coefficients and friction factors

B.1 Heat Transfer Coefficient

One-Phase Region

The heat transfer coefficient for turbulent one-phase flow inside a horizontal pipe of length Δz is obtained from [2]

$$\mathrm{Nu} = \frac{(\xi/8)\,(\mathrm{Re} - 1000)\mathrm{Pr}}{1 + 12.7\sqrt{\xi/8}\left(\mathrm{Pr}^{2/3} - 1\right)}\left[1 + \left(\frac{D}{\Delta z}\right)^{2/3}\right] \tag{B.1}$$

where ξ is the friction factor

$$\xi = (0.79\ln\mathrm{Re} - 1.64)^{-2} \tag{B.2}$$

The equation is applicable for $2300 \leq \mathrm{Re} \leq 5 \cdot 10^6$, $0.5 \leq \mathrm{Pr} \leq 2000$, $\Delta z/D > 1$. The Nusselt, Prandtl and Reynolds number are defined as follows

$$\mathrm{Nu} = \frac{\alpha D}{\lambda} \qquad \mathrm{Pr} = \frac{\eta c_p}{\lambda} \qquad \mathrm{Re} = \frac{\rho w D}{\eta} = \frac{\dot{m}}{A}\frac{D}{\eta} \tag{B.3}$$

Therein λ denotes the thermal conductivity, η denotes the dynamic viscosity and c_p denotes the specific isobaric heat capacity.

In an isolated ring slot the heat transfer coefficient for the heat transfer towards the inner wall can be estimated from [2]

$$\frac{\mathrm{Nu}_{\mathrm{slot}}}{\mathrm{Nu}} = 0.86\left(\frac{D_{int}}{D_{ext}}\right)^{-0.16} \tag{B.4}$$

where Nu is computed from eq. (B.1) with the diameter D replaced by a hydraulic diameter $D_h = D_{ext} - D_{int}$.

Two-Phase Region

The heat transfer coefficient in a horizontal pipe in the case of convective evaporation can be expressed as a function of the related values α' and α'' for

a liquid and vapour flow with the same mass velocity $G = \rho w$ [17]

$$\frac{\alpha}{\alpha'} = \left\{ (1-\dot{x})^{0.01} \left[(1-\dot{x}) + 1.2\dot{x}^{0.4} \left(\frac{\rho'}{\rho''} \right)^{0.37} \right]^{-2.2} + \dot{x}^{0.01} \left[\frac{\alpha''}{\alpha'} \left\{ 1 + 8(1-\dot{x})^{0.7} \left(\frac{\rho'}{\rho''} \right)^{0.67} \right\} \right]^{-2} \right\}^{-0.5} \tag{B.5}$$

Eq. (B.5) can be written in a more compressed form

$$\alpha = \frac{\alpha' \alpha''}{\sqrt{(\alpha'')^2 (1-\dot{x})^{0.01} \phi_1^{-2.2} + (\alpha')^2 \dot{x}^{0.01} \phi_2^{-2}}} \tag{B.6}$$

with

$$\phi_1 = 1 - \dot{x} + 1.2\,\dot{x}^{0.4} \left(\frac{\rho'}{\rho''} \right)^{0.37} \tag{B.7}$$

$$\phi_2 = 1 + 8(1-\dot{x})^{0.7} \left(\frac{\rho'}{\rho''} \right)^{0.67} \tag{B.8}$$

Fig. B.1 shows the result obtained for R22 with $\alpha' = 150$ and $\alpha'' = 120\,\mathrm{W/m^2K}$.

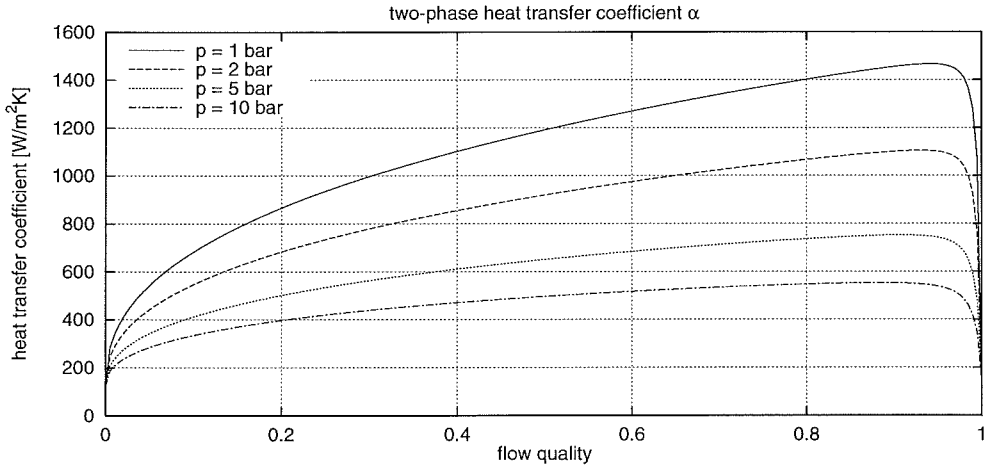

Figure B.1 Two-phase heat transfer coefficient

B.2 Friction Factor

One-Phase Region

In a one-phase flow, the frictional pressure drop in a pipe is written as

$$\frac{dp}{dz} = -\xi \frac{1}{D} \frac{\rho w |w|}{2} \tag{B.9}$$

The friction factor ξ may be obtained from the Blasius equation

$$\xi = \frac{C}{\mathrm{Re}^n} \tag{B.10}$$

where Re is the Reynolds number, see eq. (B.3). The values of C and n depend on the state of the flow and the roughness of the pipe. For laminar flows is $C = 64$ and $n = 1$. For turbulent flows in smooth pipes the exponent gets $n = 0.2..0.25$. The constant is $C = 0.184$ for $n = 0.2$ and $C = 0.3164$ for $n = 0.25$ [9].

Two-Phase Region

The frictional pressure drop in a two-phase flow is usually expressed as a multiple of the one-phase pressure drop, e.g.

$$\frac{dp}{dz} = \Phi_0^2 \left.\frac{dp}{dz}\right|_0' \tag{B.11}$$

where Φ_0^2 is a modified two-phase multiplier and the liquid pressure drop is computed for a liquid flow with the same mass velocity $G = \rho w$ [2]

$$\left.\frac{dp}{dz}\right|_0' = -\xi' \frac{1}{D} \frac{G|G|}{2\rho'} = -\xi' \frac{1}{D} \frac{\rho}{\rho'} \frac{\rho w|w|}{2} \tag{B.12}$$

Inserting the last expression into eq. (B.11) yields

$$\frac{dp}{dz} = -\xi \frac{1}{D} \frac{\rho w|w|}{2} \tag{B.13}$$

which is identical with eq. (B.9), but ξ gets

$$\xi = \Phi_0^2 \rho \frac{\xi'}{\rho'} \tag{B.14}$$

The factor Φ_0^2 can be obtained from an empirical correlation [11]

$$\begin{aligned} \Phi_0^2 \;=\; & (1-\dot{x})^2 + \dot{x}^2 \frac{\xi''}{\xi'} \frac{\rho'}{\rho''} + 3.43\, \dot{x}^{0.685} (1-\dot{x})^{0.24} \left(\frac{\rho'}{\rho''}\right)^{0.8} \\ & \cdot \left(\frac{\eta''}{\eta'}\right)^{0.22} \left(1 - \frac{\eta''}{\eta'}\right)^{0.89} \mathrm{Fr}^{-0.047} \mathrm{We}^{-0.0334} \end{aligned} \tag{B.15}$$

The Froude and Weber numbers are computed for a liquid flow with the same mass velocity

$$\mathrm{Fr} = \frac{G^2}{|\boldsymbol{g}|(\rho')^2 D} \qquad \mathrm{We} = \frac{G^2 D}{\sigma \rho'} \tag{B.16}$$

where σ is the surface tension. Inserting eq. (B.15) into eq. (B.14) gives

$$\frac{\xi}{\rho} = \dot{x}^2 \frac{\xi''}{\rho''} + (1-\dot{x})^2 \frac{\xi'}{\rho'} + \dot{x}^{0.685}(1-\dot{x})^{0.24}\phi_3 \tag{B.17}$$

with

$$\phi_3 = 3.43 \left(\frac{\rho'}{\rho''}\right)^{0.8} \left(\frac{\eta''}{\eta'}\right)^{0.22} \left(1 - \frac{\eta''}{\eta'}\right)^{0.89} \mathrm{Fr}^{-0.047}\mathrm{We}^{-0.0334} \tag{B.18}$$

For $\dot{x} = 0$ and $\dot{x} = 1$ the above equation yields $\xi = \xi'$ and $\xi = \xi''$ respectively. Fig. B.2 shows the two-phase friction factor as a function of the void fraction $\gamma = x\rho/\rho''$ for the homogeneous model $\dot{x} = x$ and for the static heterogeneous model with $\dot{x} = \dot{x}(p, x)$ computed from eq. (6.12) for a pressure $p = 5\,\mathrm{bar}$, a mass velocity $G = 60\,\mathrm{kg/m^2s}$, a pipe diameter $D = 12.7\,\mathrm{mm}$ and constant one-phase friction factors $\xi' = 0.04$, $\xi'' = 0.02$.

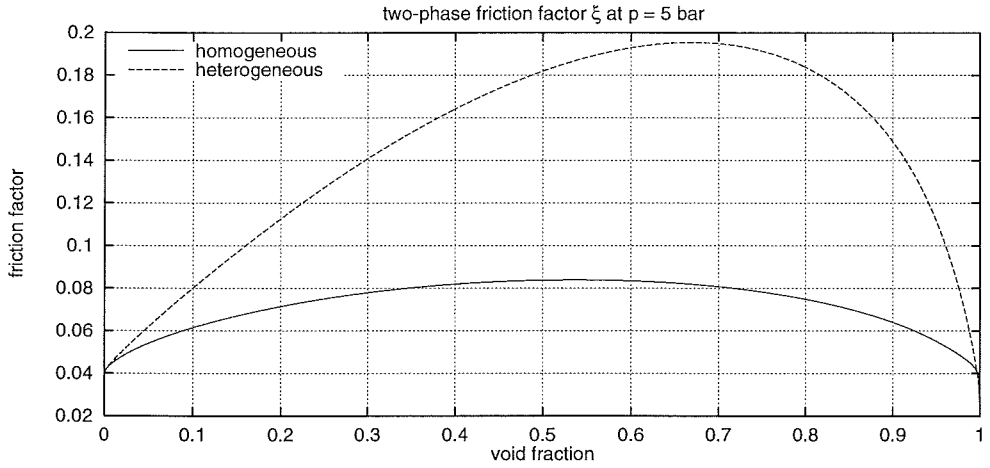

Figure B.2 Two-phase friction factor

ξ is higher in a heterogeneous flow, because for a given flow quality $\dot{x}$ the void fraction is lower, fig. 6.1, and thus the density is higher. The maximum ratio ξ/ρ is the same in both models.

C. Thermodynamic Properties and Derivatives

The approximation functions described in section 5.2 are based on data from the NIST REFPROP database, which applies fundamental equations to compute thermodynamic properties and derivatives.

C.1 Fundamental Equations

This section gives a short overview over fundamental equations in general. The purpose is the derivation of some equations, which will be used later.

Basic Form

Comparison of the first law of thermodynamics

$$du = Tds - pdv \tag{C.1}$$

with the total differential of a function $u = u(s, v)$

$$du = \left.\frac{\partial u}{\partial s}\right|_v ds + \left.\frac{\partial u}{\partial v}\right|_s dv \tag{C.2}$$

shows

$$T = \left.\frac{\partial u}{\partial s}\right|_v \qquad\qquad p = -\left.\frac{\partial u}{\partial v}\right|_s \tag{C.3}$$

Therefore, an equation of state $u = u(s, v)$ does not only serve to compute the internal energy, but also yields temperature end pressure when being differentiated symbolically. The enthalpy is then obtained from $h = u + pv$. An equation of state, that allows all thermodynamic functions to be computed from two independent variables, is called a fundamental equation.

Secondary Forms

The independent variables in $u(s, v)$ may be changed and still the thermodynamic state is determined, but the related equation may not contain sufficient information to allow computation of all properties by differentiation. Loss of information is avoided, when applying the Legendre transformation [14].

The Legendre transformation serves to create secondary forms of a fundamental equation $\phi(x, y)$. In its simplest form, one independent variable is replaced by the partial derivative with respect to that variable.

$$\phi(x, y) \rightarrow \psi\left(\left.\frac{\partial \psi}{\partial x}\right|_y, y\right) \tag{C.4}$$

The derivative represents a tangent on a curve $y = \text{const}$ in a $\phi(x)$ diagram. To determine that tangent, its crossing point with the ordinate is required,

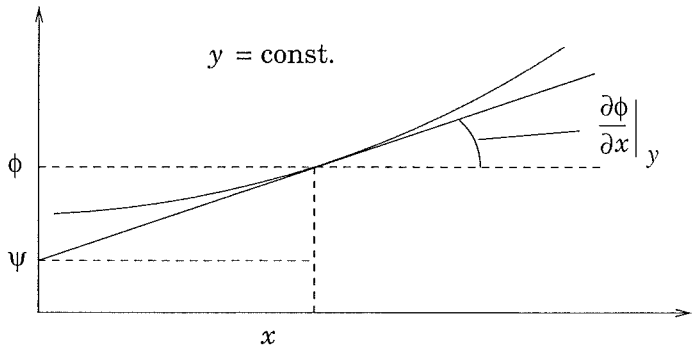

Figure C.1 Legendre transformation

which gives the definition of the new function ψ. This definition makes sure, that the new function ψ contains the same information as the original ϕ. This transformation is possible as long as $\partial\psi/\partial x \neq 0$, in other words, $\psi(x, y = const)$ is convex or concave for all y.

$$\phi(x,y) \rightarrow \psi = \phi - \left.\frac{\partial\phi}{\partial x}\right|_y x \tag{C.5}$$

Free Energy The function obtained from replacing the entropy in $u(s,v)$ with the related derivative is called the free energy f. Together with eq. (C.3) the Legendre transformation yields

$$u(s,v) \rightarrow f\left(\left.\frac{\partial u}{\partial s}\right|_v, v\right) = f(T,v) \tag{C.6}$$

And the definition of f is found to be

$$u(s,v) \rightarrow f = u - \left.\frac{\partial u}{\partial s}\right|_v s = u - Ts \tag{C.7}$$

Differentiation of the last expression gives, after replacing du with eq. (C.1),

$$df = du - Tds - sdT = -pdv - sdT \tag{C.8}$$

Comparison with the total differential of $f(T,v)$, similar to eq. (C.2), shows

$$p = -\left.\frac{\partial f}{\partial v}\right|_T \qquad s = -\left.\frac{\partial f}{\partial T}\right|_v \tag{C.9}$$

Internal energy and enthalpy are obtained from $u = f + Ts$ and $h = u + pv$.

Often v is replaced by $\rho = 1/v$ to give a fundamental function $f(T,\rho)$. In that case the pressure is obtained from

$$p = -\frac{d\rho}{dv}\left.\frac{\partial f}{\partial \rho}\right|_T = \rho^2 \left.\frac{\partial f}{\partial \rho}\right|_T \tag{C.10}$$

Free Enthalpy The fundamental equation for the free enthalpy g is obtained from replacing the specific volume in $f(T, v)$ with the related derivative

$$f(T,v) \rightarrow g\left(T, \left.\frac{\partial f}{\partial v}\right|_T\right) = g(T,p) \tag{C.11}$$

The definition of g is found to be

$$f(T,v) \rightarrow g = f - \left.\frac{\partial f}{\partial v}\right|_T v = f + pv \tag{C.12}$$

Differentiation of the last expression yields with df from eq. (C.8)

$$dg = df + pdv + vdp = -sdT + vdp \tag{C.13}$$

Comparison with the total differential of $g(T,p)$ shows

$$s = -\left.\frac{\partial g}{\partial T}\right|_p \qquad\qquad v = \left.\frac{\partial g}{\partial p}\right|_T \tag{C.14}$$

Enthalpy and internal energy are obtained from and $h = g + Ts$ and $u = h - pv$

Enthalpy If the temperature in $g(T,p)$ is replaced by the derivative of g with respect to T we obtain the fundamental equation for the enthalpy h

$$g(T,p) \rightarrow h\left(\left.\frac{\partial g}{\partial T}\right|_p, p\right) = h(s,p) \tag{C.15}$$

defined by

$$g(T,p) \rightarrow h = g - \left.\frac{\partial g}{\partial T}\right|_p T = g + sT \tag{C.16}$$

The last term is differentiated and rearranged by use of eq. (C.13)

$$dh = dg + sdT + Tds = vdp + Tds \tag{C.17}$$

Comparison with the total differential of $h(s,p)$ shows

$$v = \left.\frac{\partial h}{\partial p}\right|_s \qquad\qquad T = \left.\frac{\partial h}{\partial s}\right|_p \tag{C.18}$$

The internal energy is obtained from $u = h - pv$. Replacing the pressure in $h(s,p)$ with $\partial h/\partial p|_s$ yields $u(s,v)$, which brings us back to the starting point of eq. (C.1).

C.2 Transformation of Partial Derivatives

From a fundamental equation $\phi(x, y)$ derivatives of thermodynamic functions with respect to x and y can easily be obtained from symbolic differentiation, but a derivative

$$\left.\frac{\partial a}{\partial b}\right|_c \tag{C.19}$$

where b and/or c differs from x and/or y appears to require numerical approaches. As will be shown in this section, it can be reduced to derivatives with respect to x and y.

First Derivatives

Let a and another variable β be functions of b and c.

$$\begin{aligned} a &= a(b, c) \\ \beta &= \beta(b, c) \end{aligned}$$

The related Jacobian matrix contains the partial derivatives of a and β

$$\mathbf{J} = \begin{pmatrix} \left.\frac{\partial a}{\partial b}\right|_c & \left.\frac{\partial a}{\partial c}\right|_b \\ \left.\frac{\partial \beta}{\partial b}\right|_c & \left.\frac{\partial \beta}{\partial c}\right|_b \end{pmatrix} \tag{C.20}$$

Its determinant is computed as follows

$$\det \mathbf{J} = \frac{\partial(a, \beta)}{\partial(b, c)} = \left.\frac{\partial a}{\partial b}\right|_c \left.\frac{\partial \beta}{\partial c}\right|_b - \left.\frac{\partial a}{\partial c}\right|_b \left.\frac{\partial \beta}{\partial b}\right|_c \tag{C.21}$$

In the special case β=c we obtain, since $\partial c/\partial c|_b = 1$ and $\partial c/\partial b|_c = 0$,

$$\left.\frac{\partial a}{\partial b}\right|_c = \frac{\partial(a, c)}{\partial(b, c)} \tag{C.22}$$

which is the derivative to be determined. The right side is expanded by application of the multiplication theorem for functional determinants [3]

$$\left.\frac{\partial a}{\partial b}\right|_c = \frac{\partial(a, c)}{\partial(x, y)} \frac{\partial(x, y)}{\partial(b, c)} = \frac{\partial(a, c)/\partial(x, y)}{\partial(b, c)/\partial(x, y)} \tag{C.23}$$

which is equivalent to

$$\left.\frac{\partial a}{\partial b}\right|_c = \frac{\partial a/\partial x|_y \, \partial c/\partial y|_x - \partial a/\partial y|_x \, \partial c/\partial x|_y}{\partial b/\partial x|_y \, \partial c/\partial y|_x - \partial b/\partial y|_x \, \partial c/\partial x|_y} \tag{C.24}$$

This equation allows the derivative on the left side to be written in terms of derivatives with respect to x and y. Further simplification is possible, if a,b and/or c agrees with x and/or y, because

$$\left.\frac{\partial x}{\partial x}\right|_y = \left.\frac{\partial y}{\partial y}\right|_x = 1 \qquad \left.\frac{\partial x}{\partial y}\right|_x = \left.\frac{\partial y}{\partial x}\right|_y = 0 \tag{C.25}$$

which gives

$$\left.\frac{\partial a}{\partial b}\right|_x = \frac{\partial a/\partial y|_x}{\partial b/\partial y|_x} \tag{C.26}$$

$$\left.\frac{\partial x}{\partial y}\right|_a = -\frac{\partial a/\partial y|_x}{\partial a/\partial x|_y} \tag{C.27}$$

$$\left.\frac{\partial a}{\partial x}\right|_b = \left.\frac{\partial a}{\partial x}\right|_y - \left.\frac{\partial b}{\partial x}\right|_y \frac{\partial a/\partial y|_x}{\partial b/\partial y|_x} \tag{C.28}$$

Example: Velocity of Sound As an example from this thesis, eq. (5.16) will be proved: The velocity of sound a is

$$a = \sqrt{\left.\frac{\partial p}{\partial \rho}\right|_s} \tag{C.29}$$

therefore

$$\frac{1}{a^2} = \left.\frac{\partial \rho}{\partial p}\right|_s \tag{C.30}$$

Application of eq. (C.28) to the right side yields with $(x, y) = (p, h)$

$$\left.\frac{\partial \rho}{\partial p}\right|_s = \left.\frac{\partial \rho}{\partial p}\right|_h - \frac{\partial s/\partial p|_h}{\partial s/\partial h|_p} \left.\frac{\partial \rho}{\partial h}\right|_p \tag{C.31}$$

From eq. (C.27) and eq. (C.18) we find

$$\frac{\partial s/\partial p|_h}{\partial s/\partial h|_p} = -\left.\frac{\partial h}{\partial p}\right|_s = -v = -\frac{1}{\rho} \tag{C.32}$$

Therefore

$$\frac{1}{a^2} = \left.\frac{\partial \rho}{\partial p}\right|_h + \frac{1}{\rho} \left.\frac{\partial \rho}{\partial h}\right|_p \tag{C.33}$$

which is eq. (5.16). More applications are found in section C.3

Second Derivatives

The equations above can easily be used to form second derivatives, which may be written as follows

$$\left.\frac{\partial A}{\partial B}\right|_C \qquad \text{with} \qquad A = \left.\frac{\partial a}{\partial b}\right|_c \tag{C.34}$$

The derivative $\partial A/\partial B|_C$ can be reduced to derivatives of A, B, C with respect to x or y. Therein, the derivatives $\partial A/\partial x|_y$ and/or $\partial A/\partial y|_x$ will appear. To compute these, A is reduced to derivatives of a, b, c with respect to x or y. Then A can be differentiated by x and/or y, which gives the required derivatives. In the same way derivatives of any desired order can be formed.

The above relations were implemented in **Maple**. The resulting program **deriv** reduces any first or second derivative of the thermodynamic functions T, p, v, h, u, s, f, g, x to derivatives of the fundamental equations $f(T,v)$, $g(T,p)$ or $h(s,p)$. The fundamental equation for the free energy is also included in the form of $f(T,\rho)$.

For every fundamental equation several basic properties and derivatives are used as an option to substitute for the derivatives of the fundamental equation. In the fundamental equation $f(T,\rho)$ these are

$$\begin{aligned}
p &= \rho^2 f_\rho \\
s &= -f_T \\
p_T &= \rho^2 f_{T\rho} \\
p_\rho &= 2\rho f_\rho + \rho^2 f_{\rho\rho} \\
c_v &= -T f_{TT} \\
p_{TT} &= \rho^2 f_{TT\rho} \\
p_{\rho\rho} &= 2f_\rho + 4\rho f_{\rho\rho} + \rho^2 f_{\rho\rho\rho} \\
p_{T\rho} &= 2\rho f_{T\rho} + \rho^2 f_{T\rho\rho} \\
c_{vT} &= -f_{TT} - T f_{TTT}
\end{aligned}$$

where c_v is the specific isochoric heat capacity. Except for this quantity, subscripts denote derivatives, e.g. p_T denotes $\partial p/\partial T|_\rho$ and $p_{T\rho}$ denotes $\partial p_T/\partial \rho|_T$. Examples for the output of **deriv**:

$$\left.\frac{\partial \rho}{\partial p}\right|_h = \frac{\rho\,(c_v\rho + p_T)}{\rho^2 p_\rho c_v + T p_T^2} \qquad \left.\frac{\partial \rho}{\partial h}\right|_p = -\frac{\rho^2 p_T}{\rho^2 p_\rho c_v + T p_T^2} \tag{C.35}$$

C.3 Derivatives in the Two-Phase Region

In the two-phase region the derivatives cannot be obtained from differentiation of the fundamental equation. The two-phase equilibrium conditions have to be considered.

Density Derivatives

With $(x, y) = (v, T)$ eq. (C.28) gives

$$\left.\frac{\partial v}{\partial h}\right|_p = \left[\left.\frac{\partial h}{\partial v}\right|_p\right]^{-1} = \frac{\partial p/\partial T|_v}{\partial h/\partial v|_T \, \partial p/\partial T|_v - \partial h/\partial T|_v \, \partial p/\partial v|_T} \tag{C.36}$$

$$\left.\frac{\partial v}{\partial p}\right|_h = \left[\left.\frac{\partial p}{\partial v}\right|_h\right]^{-1} = \frac{\partial h/\partial T|_v}{\partial p/\partial v|_T \, \partial h/\partial T|_v - \partial p/\partial T|_v \, \partial h/\partial v|_T} \tag{C.37}$$

Since $h = u + pv$ the enthalpy derivatives are

$$\left.\frac{\partial h}{\partial T}\right|_v = \left.\frac{\partial u}{\partial T}\right|_v + v \left.\frac{\partial p}{\partial T}\right|_v \tag{C.38}$$

$$\left.\frac{\partial h}{\partial v}\right|_T = \left.\frac{\partial u}{\partial v}\right|_T + v \left.\frac{\partial p}{\partial v}\right|_T + p \tag{C.39}$$

where $\partial u/\partial T|_v$ is the specific isochoric heat capacity

$$\left.\frac{\partial u}{\partial T}\right|_v =: c_v \tag{C.40}$$

and $\partial u/\partial v|_T$ can be obtained from differentiation of $u = f + Ts$. Employing eq. (C.9) yields

$$\left.\frac{\partial u}{\partial v}\right|_T = \frac{\partial f}{\partial v} + T \left.\frac{\partial s}{\partial v}\right|_T = -p - T\frac{\partial^2 f}{\partial T \partial v} = -p + T \left.\frac{\partial p}{\partial T}\right|_v \tag{C.41}$$

Therefore

$$\left.\frac{\partial h}{\partial T}\right|_v = c_v + v \left.\frac{\partial p}{\partial T}\right|_v \tag{C.42}$$

$$\left.\frac{\partial h}{\partial v}\right|_T = T \left.\frac{\partial p}{\partial T}\right|_v + v \left.\frac{\partial p}{\partial v}\right|_T \tag{C.43}$$

Now eq. (C.36)and eq. (C.37) get

$$\left.\frac{\partial v}{\partial h}\right|_p = \frac{\partial p/\partial T|_v}{T(\partial p/\partial T|_v)^2 - c_v \, \partial p/\partial v|_T} \tag{C.44}$$

$$\left.\frac{\partial v}{\partial p}\right|_h = \frac{c_v + v \, \partial p/\partial T|_v}{c_v \, \partial p/\partial v|_T - T(\partial p/\partial T|_v)^2} \tag{C.45}$$

In case of two-phase equilibrium the pressure is a function of the temperature only, thus

$$\left.\frac{\partial p}{\partial v}\right|_T = 0 \qquad \left.\frac{\partial p}{\partial T}\right|_v = \frac{dp}{dT} \tag{C.46}$$

The gradient of the saturation pressure is obtained from the Clausius-Clapeyron relation

$$\frac{dp}{dT} = \frac{s'' - s'}{v'' - v'} = \frac{1}{T}\frac{h'' - h'}{v'' - v'} \tag{C.47}$$

The equations now simplify to

$$\left.\frac{\partial v}{\partial h}\right|_p = \frac{1}{T}\frac{dT}{dp} = \frac{v'' - v'}{s'' - s'} \tag{C.48}$$

$$\left.\frac{\partial v}{\partial p}\right|_h = -\frac{c_v + v(dp/dT)}{T(dp/dT)^2} = -\frac{c_v}{T}\left(\frac{dT}{dp}\right)^2 - \frac{v}{T}\frac{dT}{dp} \tag{C.49}$$

And for the density derivatives we find

$$\left.\frac{\partial \rho}{\partial h}\right|_p = -\rho^2 \left.\frac{\partial v}{\partial h}\right|_p = -\frac{\rho^2}{T}\frac{dT}{dp} \tag{C.50}$$

$$\left.\frac{\partial \rho}{\partial p}\right|_h = -\rho^2 \left.\frac{\partial v}{\partial p}\right|_h = \frac{\rho^2 c_v}{T}\left(\frac{dT}{dp}\right)^2 + \frac{\rho}{T}\frac{dT}{dp} \tag{C.51}$$

Heat Capacity

To compute the isochoric heat capacity in the two-phase region eq. (C.28) is applied with (T, x) as independent parameters

$$c_v = \left.\frac{\partial u}{\partial T}\right|_x - \left.\frac{\partial v}{\partial T}\right|_x \frac{\partial u/\partial x|_T}{\partial v/\partial x|_T} \tag{C.52}$$

In the last term, x can be cancelled down:

$$c_v = \left.\frac{\partial u}{\partial T}\right|_x - \left.\frac{\partial v}{\partial T}\right|_x \left.\frac{\partial u}{\partial v}\right|_T \tag{C.53}$$

From eq. (C.43) and eq. (C.46) we find

$$\left.\frac{\partial u}{\partial v}\right|_T = T\frac{dp}{dT} - p \tag{C.54}$$

Differentiation of $u = xu'' + (1-x)u'$ and $v = xv'' + (1-x)v'$ yields, since the liquid and vapour properties are a function of T only,

$$\left.\frac{\partial u}{\partial T}\right|_x = x\frac{du''}{dT} + (1-x)\frac{du'}{dT} \tag{C.55}$$

$$\left.\frac{\partial v}{\partial T}\right|_x = x\frac{dv''}{dT} + (1-x)\frac{dv'}{dT} \tag{C.56}$$

The total differentials of u and v can be written as

$$\frac{du}{dT} = \left.\frac{\partial u}{\partial T}\right|_p + \left.\frac{\partial u}{\partial p}\right|_T \frac{dp}{dT} \tag{C.57}$$

$$\frac{dv}{dT} = \left.\frac{\partial v}{\partial T}\right|_p + \left.\frac{\partial v}{\partial p}\right|_T \frac{dp}{dT} \tag{C.58}$$

Application of eq. (C.26) yields

$$\left.\frac{\partial u}{\partial T}\right|_p = -\frac{\partial u/\partial T|_v}{\partial u/\partial v|_T} \qquad \left.\frac{\partial v}{\partial T}\right|_p = -\frac{\partial p/\partial T|_v}{\partial p/\partial v|_T} \tag{C.59}$$

and from eq. (C.28) we find

$$\left.\frac{\partial u}{\partial p}\right|_T = \left.\frac{\partial u}{\partial v}\right|_T - \left.\frac{\partial u}{\partial T}\right|_v \frac{\partial p/\partial T|_v}{\partial p/\partial v|_T} \tag{C.60}$$

Therein $\partial u/\partial T|_v$ and $\partial u/\partial v|_T$ are known from eq. (C.40) and eq. (C.41). Altogether we obtain

$$c_v = x\tilde{c}_v'' + (1-x)\tilde{c}_v' \tag{C.61}$$

where $\tilde{c}_v''$ and $\tilde{c}_v'$ are the limiting isochoric heat capacities on the dew and boiling point when approached from the two-phase region

$$\tilde{c}_v'' = c_v'' - \frac{T}{\partial p/\partial v|_T''}\left(\frac{dp}{dT} - \left.\frac{\partial p}{\partial T}\right|_\rho''\right)^2 \tag{C.62}$$

$$\tilde{c}_v' = c_v' - \frac{T}{\partial p/\partial v|_T'}\left(\frac{dp}{dT} - \left.\frac{\partial p}{\partial T}\right|_\rho'\right)^2 \tag{C.63}$$